SAPIENZA
Università di Roma
Facoltà di Scienze Matematiche Fisiche Naturali

DOTTORATO DI RICERCA IN BIOLOGIA CELLULARE E DELLO SVILUPPO

XXVII Ciclo
(A.A. 2013/2014)

Carbon nanotube and graphene cellular impact towards their possible use as nanovectors for anticancer therapy and cell targeting

Dottoranda:
Laura Muzi

Docente guida :

Dr. Gianfranco Scarsella

Tutori :

Dr. Gianfranco Risuleo

Dr. Alberto Bianco

Coordinatore :

Prof. Rosa Sorrentino

Acknowledgements

I would like to thank Dr. Gianfranco Scarsella for the opportunity he gave me to develop my PhD and to have supervised my Thesis, together with Dr. Gianfranco Risuleo.

A special thank goes to GiRi, because of the help and the encouragement he always gave me over these years, but also for the friendship he always demonstrated to me as well as to all his students, I really appreciated that.

I would like to thank in a special way Dr. Alberto Bianco who gave me the great opportunity to perform a part of my PhD Thesis in its group in Strasbourg in a multidisciplinary context and in a laboratory of excellence where I could learn a lot of new things in an international stimulating environment.

I wish to thank the Dr. Sylviane Muller for having accepted me in the laboratory of Strasbourg.

Thanks to the graduate school of Biology and Molecular Medicine, to Prof. Rodolfo Negri and Prof. Rosa Sorrentino for giving me the important possibility to develop my work, and also in a foreign institution.

I would like to thank all the jury members to read and judge my work.

I would like to thank all the collaborators and colleagues who were involved in the development of this Thesis: Prof. Camillo La Mesa and Dr. Franco Tardani from the chemistry department of Sapienza Univesity, Prof. Adalberto Bonincontro and Dr. Simona Sennato from the physics department of the same University, Dr. Anna Rita Stringaro and Dr. Marisa Colone from Istituto Superiore di Sanità in Rome.

If I could do a nice job in Strasbourg it was especially thanks to my dear colleague Dr. Julie Russier, who introduced me in the new laboratory. Thank you for helping me with all the techniques and for the fundamental discussions. We could work seriously but also in a relaxed, agreeable and funny ambiance. This is something for me primary to perform a good job in all the contexts.

I wish to thank Dr. Cécilia Ménard-Moyon for her important help with the chemical compounds I used during my period of researches in Strasbourg. Thanks for the help with the platin-nanotubes project and for teaching me how to do a bit “the chemist” during the lysozyme conjugation and for the characterizations.

I would like to thank Dr. Helene Dumortier for kindly giving me the cells for the targeting experiments and Cecile Seifert for her suggestions in performing the test.

Thanks to Monique Duval and Delphine Lamon for the primary macrophages and to Jean-Daniel Fauny for its help with the confocal microscopy.

Finally I would like to thank all the people I met during this adventure. A special thank goes to Franceschina for the funny moment we had together at the beginning of my PhD and for her friendship. We really supported each other and this was fundamental for me at the beginning in the new laboratory. Thanks also to the other members of the group, Mariangelo who always made us laugh and Laura. Thanks a lot to Anna Ce, for her support, for the nice times spent together and for the coffee breaks!

Thanks a lot to ALL the people of our unit in Strasbourg (I will not write all your names, but if you are reading this, yes, I'm speaking also about you!). To work with you it was really a great pleasure. All the people were able to create a très agreeable atmosphere both during working but also outside of the laboratory. Thanks for accepting my noisy presence!

A special thank goes to Alessia, for the help and for the friendship she demonstrated to me soon as I arrived in Strasbourg and to Eri, the most enjoyable person in the world! Thanks also to Isabella, even if we do not know each other since lot of time, we spent already nice and funny moments together. A special thank also to Gloria and Cinzia. It was precious to have you as lab-mates in Strasbourg but also as friends. With you I really could feel a bit like at home!!!

I would like to thank in particular my family, always supporting me in my life choices. Without them, I could never get to this point. Thank you.

Thanks to my best friends in the world Cynthia, Silvia and Giulia. Even if in the last years we were always far, our friendship has demonstrated to be too strong and each time I see you again is like the time has never passed. I am very lucky to have you always supporting me.

Thank you Kira! You are a fundamental presence in my life, you are always with me, following me everywhere I go and always waiting for new adventures…

Finally, I would like to thank Maxime for reminding me each day which are the most important things in life.

THANKS TO ALL OF YOU!

Abbreviations

A20	Mouse B lymphoma cell line
A20D1.3	A20 cell line over-expressing a HEL-specific BCR
Ab	Antibody
ABC	ATP-binding cassette
AFM	Atomic force microscopy
ANOVA	Analysis of variance
AnnV	Annexin V
APC	Allophycocyanin
ATP	Adenosine triphosphate
BCR	B cell receptor
BCRP	Breast cancer resistance protein
BSA	Bovine serum albumin
BSA-SWCNT	SWCNT conjugated with BSA
BCSC	Breast cancer stem cell
C	Capacitance
^{13}C	Carbon 13 isotope
CD20	Cluster of differentiation 20
CD86	Cluster of differentiation 86
CD105	Cluster of differentiation 105
CME	Caveolae-mediated endocytosis
CNS	Central nervous system
CNT	Carbon nanotube
CPT	Camptothecin
CT	Computed tomography
Ctr1	Copper transport protein 1
Cy5	Cyanin 5
dUTP	Deoxyuridine triphosphate
DLS	Dynamic light scattering
DMEM	Dulbecco's modified eagle medium
DMSO	Dimethyl sulfoxide
DOX	Doxorubicin
DTPA	Diethylene triamine pentaacetic acid

EDTA	Ethylenediaminetetraacetic acid
EGF	Epidermal growth factor
EGFR	Epidermal growth factor receptor
ELISA	Enzyme-linked immunosorbent assay
EPO	Eosinophil peroxidase
EPR	Enhanced permeability and retention
f-CNT	Functionalized-carbon nanotube
FA	Folic acid
FBS	Fetal bovine serum
f_{c1}	Dielectric relaxation frequency
FDA	Food and drug administration
FITC	Fluorescein isothiocyanate
FLG	Few layer graphene
FLG1	Non-purified FLG
FLG2	Purified FLG
FMDV	Foot and mouth-disease virus
FRET	Fluorescence resonance energy transfer
G	Conductance
GO	Graphene oxide
GO-A	Commercial GO (Antolin Grupo)
GO-HEL	GO conjugated with HEL
GO-N	Commercial GO (NanoInnova)
GFNs	Graphene family nanomaterials
HBrO	Hypobromous acid
HCl	Hydrochloric acid
HClO	Hypochlorous acid
HCT	Human colorectal carcinoma
HEK 293	Embryonic kidney cell line 293
HeLa	Henrietta Lacks cell line
HEL	Hen egg lysozyme
HEPES	4-(2-hydroxyethyl)-1-piperazineethanesulfonic acid
HiPco	Pure high-pressure carbon monoxide
HNSCC	Head and neck squamous cancer cells
HR-TEM	High resolution TEM

HRP	Horseradish peroxidase
^{111}I	Indium 111 isotope
^{125}I	Indium 125 isotope
IC_{50}	Half maximal inhibitory concentration
ICP-OES/AES	Inductively coupled plasma optical emission spectrometry/ atomic emission spectrometry
IFN γ	Interferon γ
IgG	Immunoglobulin G
IL 1β	Interleukin 1β
IL6	Interleukin 6
L-CNT	Large diameter CNT
LDL	Low density lipoproteins
LPS	Lipopolysaccharide
MDR	Multidrug resistance
mIPM	Murine intraperitoneal primary macrophage
MFI	Mean fluorescence intensity
MPO	Myeloperoxidase
MRP	Multidrug resistance protein
mTOR	Mammalian target of rapamycin
MTT	3-(4,5-dimethylthiazol-2-yl)-2,5-diphenyltetrazolium bromide
MWCNT	Multi-walled carbon nanotube
NaCl	Sodium chloride
NAD(P)H	Nicotinamide adenine dinucleotide (phosphate)
NIR	Near infrared radiation
NF-kB	Nuclear factor kappa B
NGS	Nanographene sheets
NO	Nitric oxide
NP	Nanoparticle
NSC	Neural stem cell
PB	Phosphate buffer
PBS	Phosphate buffered saline
PE	Phycoerythrin
PEG	Polyethylene glycol
PET	Positron emission tomography

PI	Propidium iodide
PI3K	Phosphatidylinositol-3-Kinase
PSF	Phagolysosomal simulating fluid
Pt(II)	Platinum II
Pt(II)@CNT	Pt(II) encapsuled inside the inner cavity of CNTs
Pt(IV)	Platinum(IV)
Pt(IV)@CNT	Pt(IV) encapsuled inside the inner cavity of CNTs
PTEN	Phosphatase and tensin homolog
PTX	Paclitaxel
RA	Rheumatoid arthritis
Raf	Rapidly accelerated fibrosarcoma
Ras	Rat sarcoma
RAW 264.7	Murine macrophage cell line
RES	Reticuloendothelial system
RGD	Arginylglycylaspartic acid
rGO	Reduced graphene oxide
RME	Receptor-mediated endocytosis
ROS	Reactive oxygen species
RPMI	Roswell Park Memorial Institute medium
rTdT	Terminal teoxynucleotidyl transferase
RTK	Receptor tyrosine kinase
S-CNT	Small diameter CNT
SDS	Sodium Dodecyl Sulphate
SDS-PAGE	SDS-Polyacrylamide gel electrophoresis
SEM	Standard error of the mean
siRNA	Small interference RNA
SLE	Systemic lupus erythematosus
SPECT	Single photon emission computed tomography
ssDNA	Single stranded DNA
SWCNT	Single-walled carbon nanotube
TEM	Transmission electron microscopy
TGA	Thermogravimetric analysis
T_m	Average time of rotation
TNFα	Tumor necrosis factor α

TUNEL	Terminal deoxynucleotidyl transferase dUTP nick end labeling
UV-Vis	Ultraviolet–visible
VEGF	Vascular permeability growth factor
3T6	Mouse fibroblast cell line

Abstract

In the last two decades, lots of progresses have been made in the application of nanomaterials in biology, giving rise to a new revolutionary field of the biomedical research that is called nanomedicine. Carbon nanotubes (CNTs) and graphene are among the most attractive candidates under investigation in this context. Such carbon-based nanomaterials possess outstanding chemico-physical properties and their high surface area provides multiple attachment sites for almost all the molecules of biological interest. In fact, chemical strategies allow for their conjugation with DNA, proteins, peptides and small drugs. The so-functionalized materials have shown great promises in several biomedical contexts, from diagnosis to tissue regeneration. In addition, the ability of CNTs and graphene to enter and accumulate inside the cells makes them good candidates as nanovectors for drugs. *In vitro* and *in vivo* studies showed how these nanomaterials could enhance the drug accumulation inside the cells and its bioavailability. CNTs and graphene are also able to passively target tumor tissues exploiting the so-called enhanced permeability and retention effect, and actively, following the conjugation with targeting moieties.

On the other hand, the use of these materials in nanomedicine will be approved only after the demonstration of their safety in terms of tissue damage, carcinogenicity and proinflammatory response. Different approaches have been used to make these materials biocompatible and recently, it has been demonstrated that functionalized CNTs and graphene oxide can be degraded by oxidative enzymes. However, the results obtained on CNT and graphene toxicity are often conflicting; thus, further investigations are needed.

In the first introductive chapter of this thesis, an overview of the general features of nanomaterials is given. The focus goes then on CNTs and graphene. First, we will see how their biocompatibility, biodegradability and *in vivo* fate strictly depend on several factors. The mechanisms by which the two nanomaterials are able to enter the cells are also illustrated. In the second part of the introduction, the potential of CNTs and graphene in targeted drug delivery is described, focusing on anticancer therapy.

The three following chapters illustrate the results obtained by three related studies carried out during my PhD internship.

Results described in the second chapter shed more light on the impact of CNTs on living cells. CNTs having single walls (SWCNTs) were dispersed with the biocompatible protein bovine serum albumin (BSA). BSA protein showed to be a good dispersant agent for the CNTs and was able to enhance their biocompatibility. The impact of the protein-coated materials on cell vital parameters, such as viability, activation and interaction/internalization mechanisms, is described. In addition the effect of nanotubes on the plasma membrane dielectric characteristics and ion flux, very poorly

investigated up to date, is presented.

In the following chapter, a cisplatin prodrug was encapsulated within the inner cavity of two types of multi-walled CNTs (MWCNTs) having different diameters, in order to allow a controlled release inside the cells. The efficacy of the complexes was investigated on human cervix cancer cells and compared to murine macrophages. The latter were also used to evaluate the possibility of a proinflammatory effect. Results on cell viability, cell activation and cell uptake show that CNTs are promising nanocarriers to improve the accumulation of a chemotherapeutic drug inside the cells, without inducing a high proinflammatory response. In addition, by tuning CNT diameter it is possible to control the time of release of the drug prolonging its anticancer efficacy.

The fourth chapter gives more insights about the impact of different types of graphene on cells, focusing on macrophages. Results evidenced a specific cytotoxic effect of graphene oxide (GO) towards this cell population among the other murine immune cells. The mechanisms by which macrophages internalize GO are also elucidated. In addition, GO was conjugated with lysozyme protein and was tested for its ability to selectively target a B cell model overexpressing a lysozyme-specific B cell receptor. Results showed that graphene is able to target B cells in a selective manner, thus suggesting its possible application in therapies where the specific elimination of B lymphocytes is required.

Finally, a conclusive chapter summarizes the main findings obtained during my doctoral work, focusing, in particular, on future perspectives.

CHAPTER I

Introduction

I.1 A world at the nanoscale level

The term *nano* originates etymologically from the greek meaning "dwarf" and it indicates physical dimensions that are in the range of one-billionth of a meter: the nanoscale. By comparison, we are speaking about objects five orders of magnitude smaller than the diameter of a human hair.

Several organizations gave a definition for nanomaterials over the last two decades. In particular, in October 2010 the European Commission invited the member States, the Euopean Agencies and industries to define such materials as objects which meet at least one of the following criteria:

- Consist of particles, with one or more external dimensions in the size range of 1 nm to 100 nm for more that 1 % of their number size distribution;
- Have internal or surface structures in one or more dimensions in the size range of 1 nm to 100 nm;
- Have a specific surface area by volume greater than 60 m^2/cm^3, excluding materials consisting of particles with a size lower than 1 nm.

Nanoparticles (NPs) can originate either unintentionally from environmental processes, such as volcanic activities or spontaneous combustions, or can be the result of human actions. The latter are the so-called anthropic NPs, derived, for example, from industrial processes or car pollution. However, in the context of this thesis, we are referring to another type of NPs, which are intentionally synthesized and engineered to be exploited for specific applications. These nano-objects can be composed of various materials. They can be metals (for example gold, zinc or copper), ceramics, polymeric materials (such as polystyrene) and carbon (such as carbon nanotubes and graphene). They can also display various shape, such as tubular, spheres and rods. The interest toward these materials arises from their outstanding physicochemical properties, related to conductivity or reactivity (for example), which differ from the same material in bulk. Such properties are attributable to NP small size, high surface area to volume ratio, chemical composition, surface reactivity, solubility, shape and agglomeration status (*Nel et al. 2006; Bakand et al. 2012*).

By taking advantage of those special characteristics of NPs, a new field that is called nanotechnology has emerged and represents nowadays an area of scientific research and industrial applications in full expansion. Despite this technology has emerged as matter of enormous interest quite recently, the concept was raised over 40 years ago by the physicist Richard Feynman who

delivered its famous talk in 1959 entitled “There's Plenty of Room at the Bottom” (*Feymann 1960*). From that pioneering talk, there have been many revolutionary developments in physics, chemistry and biology which have demonstrated Feynman’s idea of manipulating matter at an extremely small scale. Although the idea had been already introduced, the term nanotechnology was fashioned by Nori Taniguchi in 1974 at the Tokyo International Conference on Production Engineering, where he described how materials could be processed to nanoscale precision (*Taniguchi 1974*). The world of nanotechnology is highly interdisciplinary and it requires knowledge from a variety of scientific and engineering areas which collaborate to create materials with fundamentally new properties and functions. In fact, the researches in this context involve efforts coming from physics, chemistry, engineering and biology, whose work together into an integrated field. Nanomaterials are already an economic reality and they have demonstrated to benefit society in several contexts. In fact, engineered nanomaterials have been exploited in energy technologies, including economic solar cells (*Law et al. 2005*) and high-performance batteries (*Chan et al. 2008*); in electronics, with ultrahigh density data storage (*Vettiger et al. 2002*) and single-atom transistors (*De Franceschi et al. 2002*); but also in food and agriculture technologies, offering smart delivery of nutrients and increased screening for contaminants (*Sozer et al. 2009*).

On the other hand, the size of nanomaterials falls within the same range of biological macromolecules and, therefore, it is compatible with the size of the fundamental components of life that are the cells (Figure 1). In fact, one of the most interesting and promising issues, is the possibility to apply these materials in biology, in a new field named nanomedicine. Nanotechnology has been exploited to improve both diagnosis and therapy of diseases. Relating to the first purpose, their small size enable nanostructures to measure and detect biological entities at the level of single molecules and single cells. This ability is often lost in traditional bulk assays, which usually afford average information about heterogeneous populations pooled from large numbers. One example of this is the use of nanoscale pores that can discriminate between molecules on the basis of size and biochemical characteristics. Taken together, these observations make nanostructures promising candidates for imaging and diagnosis purposes. On the other hand, nanotechnology has been employed in the treatment of diseases. The researches in this field are related to implantable materials, tissue regeneration, and multifunctional drug delivery platforms. Concerning the latter application, nanomaterials can be designed as carriers for the delivery of therapeutic molecules to targeted locations thus enhancing the bioavailability and pharmacokinetics of the drug. This avoids, for example, the complications associated with conventional drug delivery strategies, which are often associated with poor and inconsistent uptake. (*Etheridge et al. 2013; Wong et al. 2013*). The latest observations provide essential implications in diseases, in which the specific depletion of

diseased cells without affecting normal cells is demanded (e.g. cancer or autoimmune diseases). Some examples of nanostructures currently under investigation for biomedical applications are liposomes, micelles, surfactant vescicles, dendrimers, hydrogels, gold NPs, quantum dots, polymeric NPs and carbon nanostructures (Figure 1). In the latter category are included nanodiamonds, fullerene, carbon nanotubes and graphene (*Wong et al. 2013*).

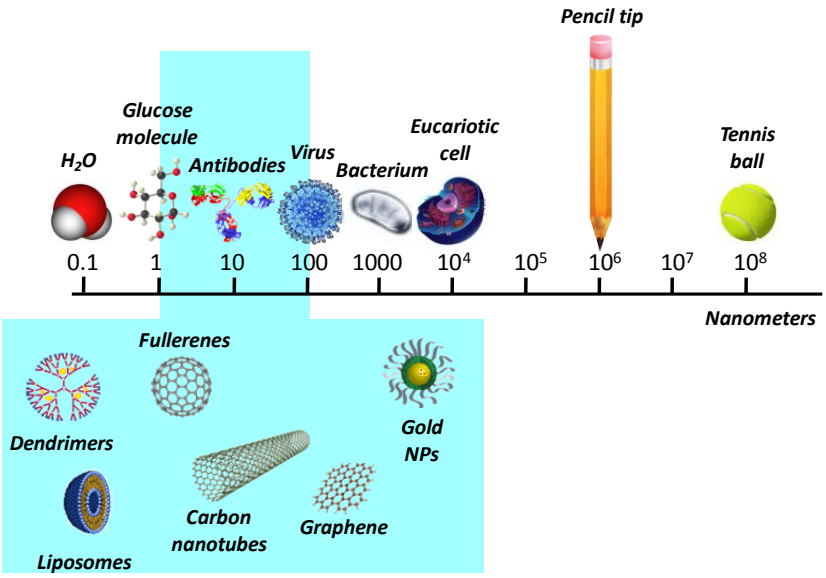

Figure 1. Size of nano-objects. The image underlines nanomaterials similitude to large biological molecules.

On the other hand, in view of the enormous development of nanomaterial-based technologies in the last few decades, a careful assessment of their impact on health and environment is demanded. This applies, first, to professional exposure, since nanomaterials can be inhaled and enter more deeply into the lungs, compared to the same materials of conventional size. Second, the investigation of their cytotoxicity is of fundamental importance in the context of their application in medicine. In fact, secondary side effects of therapies have to be avoided (*Nel et al. 2006; Bakand et al. 2012*).

I.1.1 Carbon nanomaterials

Among all carbon-based nanomaterials, carbon nanotubes (CNTs) and graphene are of particular interest in biological applications as they have shown enormous promises in many important areas of biomedical research (*Cha et al. 2013*).

The unique electronic structure of carbon allows for sp, sp^2 and sp^3 hybridization leading to a large number of stable allotropes. Natural and most common allotropic forms of carbon include amorphous carbon, graphite, which consist of sp^2 hybridized carbon atomic layers stacked together by weak van der Waals forces, and diamond, which display a tridimensional form, with carbons

hybridized sp^3. Graphite is present in nature as an abundant natural mineral and, together with diamond, is well known since antiquity (*Spyrou and Rudolf 2014*). In 1985, a new form of carbon was discovered by the groups of Richard Smalley (*Kroto et al. 1985*). This was the case of fullerene (C_{60}), in which carbon atoms are hybridized sp^2 and organized to form pentagonal and hexagonal structures arranged in a spherical shape, similar to the soccer ball. Afterwards, a large family of other carbon-based nanomaterials has been discovered (Figure 2). In particular, CNTs have been described for the first time at the atomic level in 1991 by Iijima (*Iijima 1991*). CNTs were identified casually during the process of synthesis of fullerene. On the other hand, graphene history is more recent. In fact, the research group guided by Geim and Novoselov, reported for the first time a method for the isolation of single layer graphene from graphite only in 2004 (*Novoselov et al. 2004*).

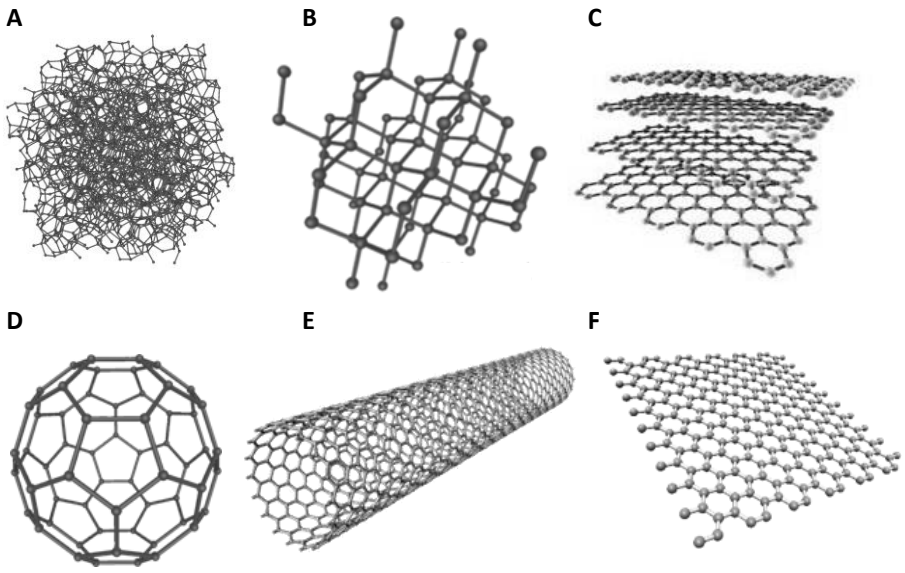

Figure 2. Molecular structure of six forms of carbon: A) amorphous carbon, B) diamond, C) graphite, D) fullerene, E) single-walled carbon nanotube, and F) graphene.

I.2 An introduction to carbon nanotubes and graphene

I.2.1 General features of carbon nanotubes

Carbon nanotubes share graphene and fullerene characteristics. In fact, they can be considered as graphene sheets rolled up to form a cylindrical structure. They can be either single-walled (SWCNTs) or multi-walled (MWCNTs), the latter being formed by two or more cylinder wrapped one inside each other (Figure 3A). SWCNTs have a diameter going from 0.7 to 2.5 nm, while

MWCNTs diameter can be up to 100 nm. Both CNT types have a length ranging from 0.2 to few µm and even mm. According to the way how the graphene sheet is twisted, CNTs can display a chiral, a zig zag, or an armchair form (Figure 3B), which confers to the materials different electronic properties being conductors, semiconductors and metallic, respectively.

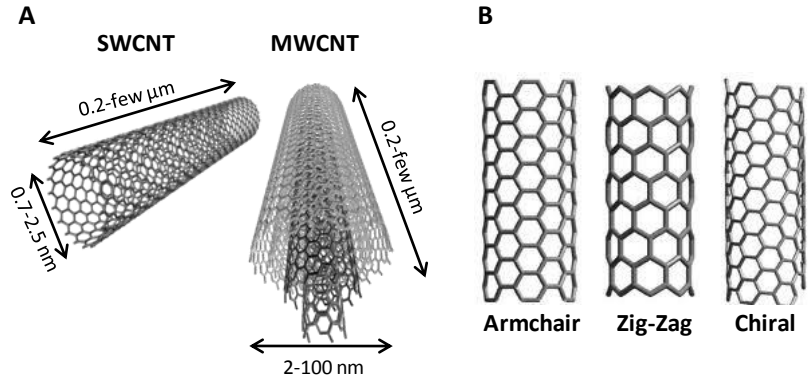

Figure 3. Carbon nanotubes forms (A) and chirality (B).

CNT structure allows the materials to have outstanding physical, chemical and mechanical properties, thermal conductivity and large aspect ratio. Thanks to these properties, CNTs were exploited in several industrial fields. In fact, upon the first industrial synthesis of what are now known as MWCNTs in 1980, a widespread interest in CNT research has begun. During the past decade, worldwide production of CNTs has considerably increased, and the annual number of CNT-related publications and patents continues to grow (*De Volder et al. 2013*). The development of large-scale methods of CNT production, have substantially decreased CNT price. However, the so-produced CNTs are not free of contaminants (*e. g.* metals), which can influence CNT properties (*De Volder et al. 2013*) and also their bio-compatibility (see below).

Thanks to their particular mechanical properties such as high resistance and elasticity, CNTs have been employed in composite materials, in order to enhance material stiffness; they were used as coating materials and films with antibacterial properties; their outstanding electronic properties allow for their use in microelectronics such as transistors and condenser or in energy storage and as components of lithium ion batteries for notebook computers and mobile phones (*De Volder et al. 2013*). On the other hand, one of the most interesting applications of CNTs, which could bring enormous benefits to society, concerns their possible use in the biomedical field (see below).

I.2.2 General features of graphene

Despite being the basic structural element of other allotropes, including carbon nanotubes and fullerenes, graphene history is quite recent (*Novoselov et al. 2004*). Graphene can be described as a one-atom thick single layer of graphite. As well as CNTs, graphene can display different forms which are conventionally put together in the so called graphene family nanomaterials (GFNs). GNFs comprise few-layer graphene (FLG), graphene oxide (GO), reduced graphene oxide (rGO), graphene nanosheets, ultrafine graphite, graphene ribbons and graphene dots. The most common graphene forms are illustrated in Figure 4. FLG is constituted by 2-10 graphene layers, while GO and rGO are normally composed of a single-layer. In particular, GO is the oxidized form of graphene and therefore, it presents numerous oxygenated groups such as carboxyl, hydroxyl and epoxil, on its surface. GO can be reduced upon thermal and chemical treatment becoming rGO (*Bianco 2013*).

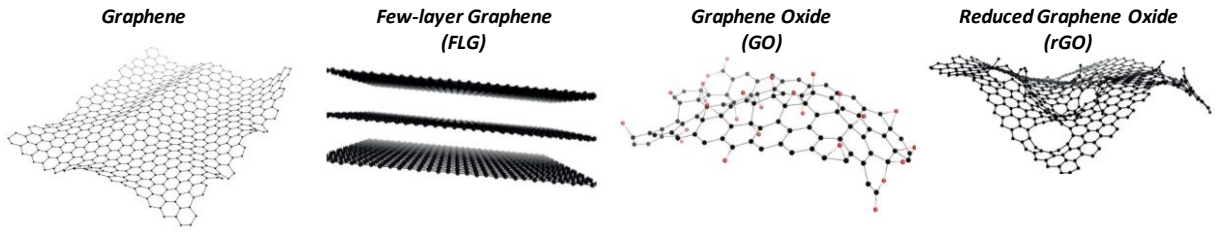

Figure 4. Representative chemical structures of some of the members of the graphene family. (adapted from *Bianco 2013*).

As well as CNTs, and according to its particular shape, graphene displays exceptional properties such as electronic, optical, thermal and mechanical (*Huang et al. 2011 A*). Since its first isolation, graphene has emerged as a new carbon allotrope with great potential for several applications, similar to CNTs. In fact, graphene was firstly exploited in material sciences (*Huang et al. 2011 B*) and very recently it has been proposed to be a good candidate for the development of graphene-based electronics, photonics, composite materials, energy generation, energy storage and sensors. Together with CNTs, graphene is also gaining a lot of interest in the biomedical field (see below). Graphene is commonly isolated from graphite flakes by repeated mechanical exfoliation which provides large amounts of graphene with a high degree of purity, making it suitable for biomedical applications (*Spinato et al. 2014*).

I.3 Carbon nanotube and graphene biocompatibility

As mentioned, CNT and graphene-based nanomaterials have attracted a strong interest toward their application in the biomedical field. Among all, one of the main properties which make the materials good candidate for a large variety of bio-applications is their high surface area which allows for the conjugation with almost all the biological macromolecules such as DNA, proteins, peptides or small drug molecules. In fact, both materials can be conjugated with special moieties which make graphene and nanotubes both dispersible and suitable for their use as biosensors, as scaffold for cell growth and for drug delivery applications. Such applications are strictly dependent on CNT and graphene biocompatibility.

First of all, the material dispersibility is a *conditio sine qua non* the development of nanomaterial-based therapeutic strategies would not be possible. In fact, it has to be noticed that both materials, as well as they are produced, are completely insoluble in most aqueous media. This is related to the strong van der Waals forces that take place among the tubes or graphene sheets leading to their aggregation in large bundles (*Bianco et al. 2011; Spinato et al. 2014*). Moreover, at the beginning, bundled non-purified CNTs have been associated with negative cellular effects (*Kolosnjaj et al. 2007; Holt et al. 2010*). However, several progresses have been made in order to significantly enhance both CNT and graphene dispersibility and biocompatibility. For this purpose, two main strategies are possible. The first one is the non-covalent adsorption of biocompatible molecules on CNT or graphene surfaces, while the second strategy involves the covalent functionalization of their surface by chemical methods.

I.3.1 Non-covalent and covalent functionalization

Non-covalent functionalization of CNTs (*f*-CNTs) is a simple method to disperse the material without perturbing the nanotube structure. These interactions normally occur via π-π stacking and/or van der Waals interactions. Several biocompatible agents are able to disperse CNTs in aqueous media. Some examples are DNA (*Zheng et al. 2003; Tardani and Sennato 2014*), proteins (*Matsuura et al. 2006; Nepal and Geckeler 2006*), polysaccharides (*Piovesan et al. 2010*) polymers (*Rice et al. 2006*) and others. Among them, protein dispersions are of particular interest in the context of CNT bio-applications (Figure 5A). First, proteins have a high affinity with CNTs. This is due to the hydrophobic interactions that occur between the CNT sidewall and the hydrophobic regions of the proteins. Moreover, it has been shown that the interaction of some proteins with CNTs, such as lysozyme or bovine serum albumin, can enhance their biocompatibility with respect to pristine CNTs (*Shim et al. 2002; Ge et al. 2011*). Despite, it is not related to their solubility, another interesting CNT feature is the possibility to fill their inner cavity with diverse molecules (e.

g. drugs) by a chemical method called endohedral functionalization (Figure 5A). This approach permits also to increase the degree of functionalization and the easy release of adsorbed molecules, without perturbing CNT structure, thus having important implications in drug delivery (*Li et al. 2012*).

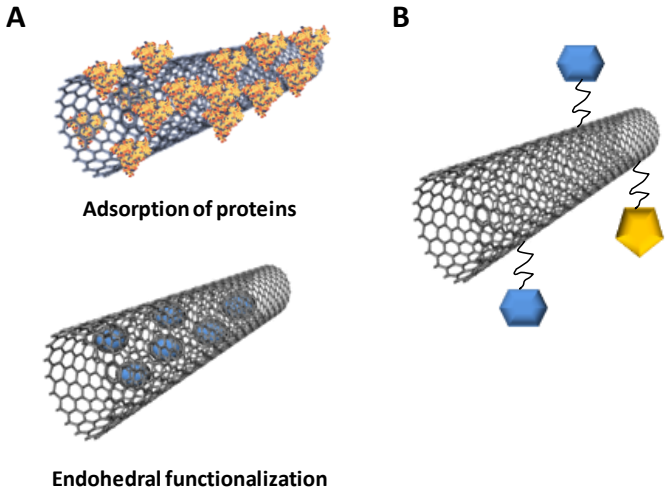

Figure 5. Representative examples of non-covalent (A) and covalent (B) functionalization of CNTs.

On the other hand, CNTs can be covalently functionalized with organic moieties through different reactions, occurring at the sidewall or on the tips of CNTs (Figure 5B). Briefly, CNTs can be firstly oxidized and then, exploiting oxidized defect sites, coupling reactions can be performed such as amidation or esterification. In addition to a remarkable increase in solubility, the so-functionalized CNTs are suitable for further chemical modifications allowing the conjugation with special bioactive molecules for biomedical application purposes (*Bianco et al. 2004; Prato et al. 2007*).
Thanks to the experience gained with CNTs, similar approaches have been developed in the last few years to modify graphene or GO surfaces. In fact, similar strategies have been used to improve graphene and GO solubility and to allow for the conjugation with various molecules. Differently to CNTs, having two free surfaces, the moieties of interest can be stacked onto both graphene faces thus allowing a high density of functionalization. As it was described above for CNTs, both a non-covalent and covalent functionalization is possible. Graphene and graphene oxide can be wrapped with polymers and can be dispersed with surfactants or with biomolecules such as DNA, proteins and peptides, which adsorb on their surfaces. On the other hand, several reactions exist, permitting to covalently functionalize their surfaces with different groups, similarly to CNTs. In particular, the various reactive GO functional groups make this graphene form the most suitable for biological applications in comparison to pristine graphene. Therefore, upon specific chemical reactions, bioactive molecules, such as nucleic acids, peptides antibodies and small drug molecules can be

covalently conjugated to both sides of the graphene sheet (*Spinato et al. 2014*). Noteworthy is the fact that both materials can carry different molecules at the same time. In fact, their surface can also be multifunctionalized. Such possibility has many implications in the context of drug delivery, as it will be described later. Taken together, these characteristic make CNTs and graphene revolutionary materials like no others which could change completely the field of biomedicine.

I.3.2 Toxicity

The cytotoxicity of carbon nanotubes and graphene *in vitro* and *in vivo* is an important issue to be investigated, especially in view of their possible application in the biomedical field. In fact, if these materials have to be used for therapeutic applications, they absolutely do not have to provoke tissue damage or a proinflammatory response. A large variety of studies can be found in literature reporting the cytotoxicity findings on the two material types. Despite this, in most cases the described results are incompatible with each other. Such conflictuality has to be ascribed to variability in the doses, properties, purification level and type and degree of functionalization of the two materials used in the different cytotoxicity studies. The use of diverse cellular models may also be responsible of paradoxical findings. Moreover, in the case of CNTs, common cytotoxicity test such as the Mosmann colorimetric assay may give false results as CNTs are able to bind to the MTT (3-(4,5-dimethylthiazol-2-yl)-2,5-diphenyltetrazolium bromide) die (*Belyanskaya et al. 2007*). Thus, further explorations in this context are certainly needed and a major standardization is required. Despite the variability in the results, an overview can be given on the main characteristics affecting CNT and graphene toxicity.

Concerning CNTs, their cytotoxicity can be first correlated to the effect of the impurities derived from their production process. In fact, metal catalysts are the main source of adverse effects as evidenced by early studies in which poorly purified CNTs were used. For instance, such behavior was evidenced in human HEK 293 cells. Results showed that SWCNTs could inhibit the cell proliferation and decrease HEK 293 cell ability to adhere in a dose- and time-dependent manner (*Cui et al. 2005*). The role of metal catalysts on CNT toxicity was also evidenced by Kagan et al. who investigated the impact of iron-purified or iron-rich SWCNTs in RAW 264.7 murine macrophages in terms of oxidative stress induction (*Kagan et al. 2006*). As SWCNTs are more prone to aggregate into bundles due to their stronger van der Waals forces compared to MWCNTs, the latter seems to be less toxic as the aggregation of CNTs is known to be harmful to the living cells, organs and tissues (*Colvin 2003*). As it was previously described in this thesis, the surface functionalization of CNTs allowed the materials to have an improved biocompatibility. In fact, some publications have demonstrated a significant reduction in the CNT cytotoxicity due to their

high degree of functionalization. For instance, a cytotoxicity study performed on human dermal fibroblasts showed how, as the degree of sidewall functionalization increases, the SWCNT samples become less cytotoxic compared to the underivatized SWCNTs stabilized in 1% Pluronic F108 (*Sayes et al. 2006*). Another study carried out by our laboratories studied the behavior of two types of *f*-CNTs, oxidized and or amidated, on primary immune cells. Both types of *f*-CNTs were uptaken by B and T lymphocytes as well as macrophages in vitro, without affecting cell viability. Although amidated *f*-CNTs provoked the secretion of proinflammatory cytokines by macrophages, any impairment of immune cell functional activity was observed (*Dumortier et al. 2006*). CNT dimensions are also important in determining their cytotoxicity. For instance, the effect of CNT length was assessed by Poland et al. Inflammation was chosen as cytotoxicity readout as it is a key factor in tissue remodeling and carcinogenesis. In a first study, the peritoneal mesothelium was exposed to CNTs in order to determine whether there was asbestos-like, length-dependent cytotoxicity. The authors demonstrated how long fibrous CNTs were able to induce inflammation and fibrosis in the peritoneal cavity, similarly to asbestos fibers. On the other hand, short CNTs caused any significant inflammation (*Poland et al. 2008*). These findings were confirmed by the same group, in another study. In this case, CNTs having different lengths were instilled into the pleural cavity of mice (*Murphy et al. 2011*). Such behavior could be explained first by the fact that long CNTs failed to surpass the diaphragmatic or pleural stomata thus being consequently retained at the vicinity of the diaphragm or the pleural cavity, in contrast to smaller particles. Second, as it was subsequently demonstrated, macrophages could not fully engulf the long CNTs. Such phenomenon is named frustrated phagocytosis (Figure 6A) and promotes the recruitment of inflammatory cells and mesothelial cell damage leading to chronic inflammation and granuloma formation (*Murphy et al. 2012*). The latter studies, give also an example of the CNT toxicity *in vivo*. Few studies also investigated the CNT toxicokinetics upon systemic exposure (*Ali-Boucetta and Kostarelos 2013*). Also in this case, CNT aggregation and impurity seems to be the most responsible factors for toxicity. Again, CNT chemical functionalization dramatically reduces their *in vivo* cytotoxicity (Figure 6B). This could be also due to the fact, that certain types of *f*-CNT can be degraded thus allowing for their better elimination trough the renal system (see session I.3.4).

On the other hand, graphene researches towards their application in nanomedicine started more recently. For this reason, a limited amount of data there are in literature on the impact of graphene on health and the environment (*Bianco 2013*). As well as CNTs, graphene exists in different forms having different chemical-physical characteristics. For this reason its toxicological profile is little understood and more studies are required. Despite this, it is possible also in this case to give an overview of the major findings in this subject. Similarly to CNTs it seems that the nature of the

graphene type used is strictly linked to its behavior in biological environment and that the chemical modification of graphene modulates the toxicity impact. The explanations for such observations could be derived, as in the case of CNTs, from a reduction in their aggregation and from the possibility of modified graphene to be degraded *in vivo*. This issue will be described later in this thesis. The biological response varies also depending on graphene number of layers, lateral size, rigidity, hydrophobocity, dose administered and purity of the material (*Bianco 2013*). As GO and rGO are better soluble in water and consequently more prone to be used in biology, the toxicity of these two graphene types is the most investigated.

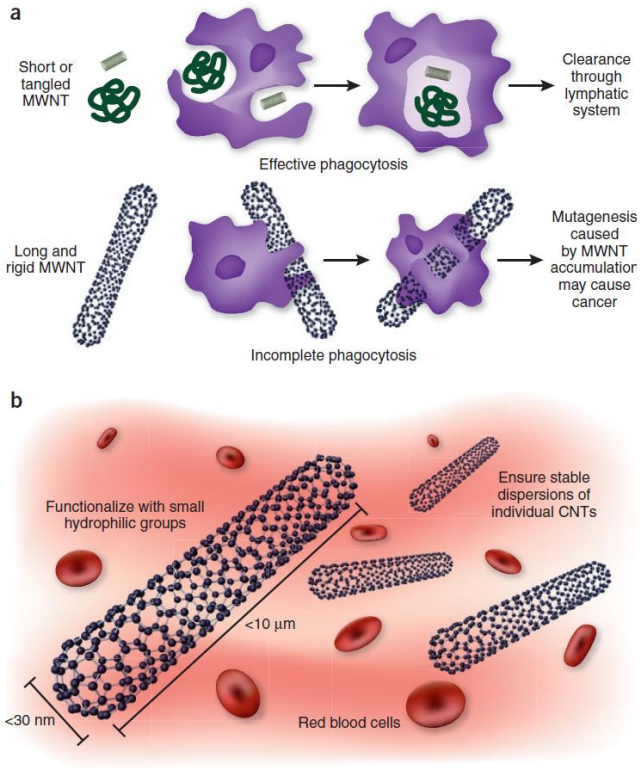

Figure 6. Factors influencing the safety of CNTs *in vivo*. (a) The effect of CNT structure on phagocytosis by macrophages and clearing from tissues. Whereas macrophages can engulf MWNTs with a low aspect ratio (ratio of length to width) before their clearance by draining lymph vessels, MWNTs with a high aspect ratio cannot be cleared and accumulate in tissues. (b) In addition to their dimensions, other considerations relevant to the safety of CNTs include increasing their solubility and preventing their aggregation, to facilitate urinary excretion and thereby prevent tissue accumulation (from *Kostarelos 2008*).

To give some examples, in an initial study, pristine graphene was tested on rat neuronal PC12 cells and it was compared with CNTs. Graphene induced oxidative stress and caspase-3 activation, which was indicative of an apoptotic process, in a larger extent compared to CNTs thus indicating the importance of the material shape (*Zhang et al. 2010*). In another study, GO and carboxylated GO were tested on monkey renal cells. While the first accumulated in the cell membrane and caused

oxidative stress, F-actin destabilization and cell death, carboxylated GO penetrated into the cells and did not induce any cytotoxic effect up to a concentration of 300 µg/ml (*Sasidharan et al. 2011*). Such study suggests that graphene functionalization may reduce the material toxicity. Other studies evidenced that GO cytotoxicity can be also strongly dependent on the type of cell tested and on the purity of the material (*Bianco 2013*). GO behavior towards immune system cells is also of great interest. In an interesting study, different GO layers having different lateral sizes were tested on 6 different cell models among which two were phagocytic (J774A.1 macrophages and primary peritoneal macrophages). While the GO samples were not uptaken by the non-phagocytic cell lines, macrophages were able to internalize the materials. Interestingly, the bigger GO flakes (about 2 µm), triggered a much stronger inflammatory response with high release of key cytokines, contrarily to the nano-sized GO (*Yue et al. 2012*). Another work performed by Russier et al. was again focused on the effect of GO sheet lateral dimension on human primary monocyte-derived macrophages and murine intraperitoneal macrophages (mIPM). Contrarily to the previous findings, the authors have shown that, the more the lateral dimensions of GO were reduced, the higher was the impact on both cellular activation and TNFα production in mIPM (*Russier et al. 2013*).

As well as CNTs, graphene *in vivo* toxicity was evaluated. For instance, significant pathological changes including inflammatory cell infiltration, pulmonary aedema and formation of granulomas were found after intravenous administration of GO into mice and rats (*Wang et al. 2011; Zhang et al. 2011*). It seems that GO is responsible of pulmonary toxicity as compared to pristine graphene dispersed in pluronic surfactant after injection in mice, suggesting that a stable dispersion can improve graphene biocompatibility in the lung (*Duch et al. 2011*). Not surprisingly, pristine graphene having few layers and a big lateral size (about 25 µm) induced an acute pulmonary inflammatory response in mice after inhalation. As well as in the case of CNTs, the accumulation of large graphene sheets and induction of frustrated phagocytosis by macrophages was responsible for the observed toxicity (*Schinwald et al. 2012*). As for CNTs, chemical functionalization can reduce graphene *in vivo* toxicity. It is likely that, tuning the graphene sheet lateral size and its surface functionalization, it will be possible to create a material that can be easily cleared from the body also trough degradation.

I.3.3 Biodistribution

Strictly related to their toxicity it is also the CNT and graphene biodistribution *in vivo*. In fact, having particular properties, they can exhibit new and unexpected metabolism kinetics. As mentioned, such objects can enter the human body both unintentionally and this concerns the occupational exposure, but can they be also voluntary administrated in the case of therapeutic

applications. According to the context, nanomaterials can enter the blood stream upon inhalation, ingestion, injection or dermal exposure (*Wang et al. 2013; Ali-Boucetta et al. 2013* A).

In the context of biomedical applications, a good therapeutic molecule has to display a correct balance between its retention into the blood, its biodistribution and ability to reach its target tissue (bioavailability) and finally its clearance from the tissues and its excretion. A special field of pharmacology named pharmacokinetics is interested in such investigations (*Ruiz-Garcia et al. 2008*). Once in the blood system, nanomaterials are distributed in various tissues. In particular, they have the tendency to accumulate in the reticuloendothelial system (RES) organs (*Wang et al. 2013*). RES is the common name given to phagocytic cells as monocytes and macrophages which are located throughout the body in various organs and tissues. They are present, for istance, in the connective tissues, having the name of histiocytes, in the lungs (alveolar macrophages), in the lymphonodes, in the in liver (Kupffer cells), in the spleen and in the central nervous system where they are component of microglia. Being an important part of the immune system their function is to filter out dead and toxic particles and to identify foreign substances, thus maintaining the body homeostasis (*Wynn et al. 2013*).

The rapid blood clearance followed by an overaccumulation of nanomaterials in non target organs such as liver and spleen is considered one of the main causes of their *in vivo* side effects and, in the context of therapeutic applications, a major challenge in the delivery of nanomaterials to the organs of interest (*Wang et al. 2013*). On the other hand, the tissue accumulation and clearance of nanomaterials is highly dependent to the tissue-specific properties of endothelial cells (Figure 7).

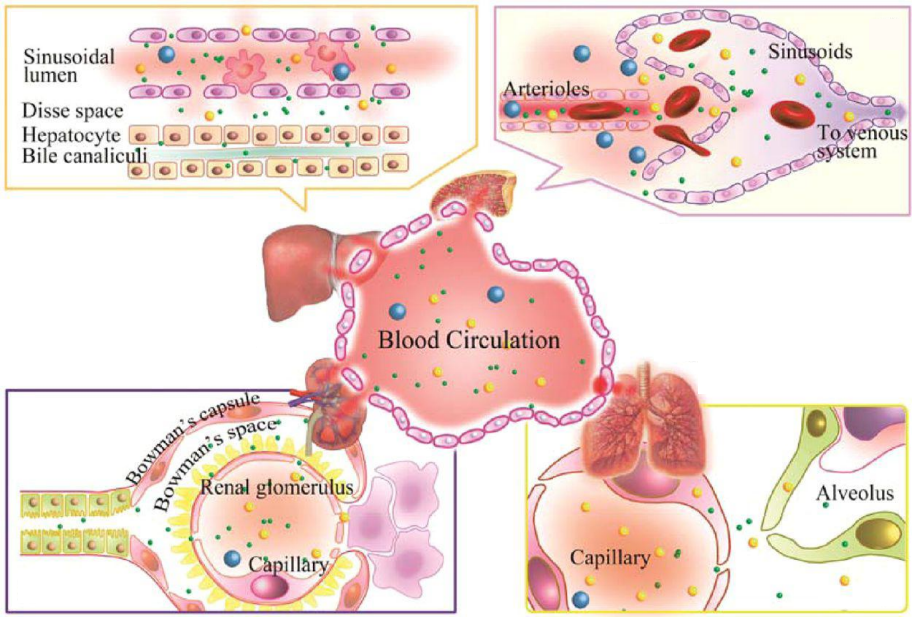

Figure 7. The tissue-specific extravasation of nanomaterials (adapted from *Wang et al. 2013*).

Liver capillaries, named sinusoids, possess endothelial cells with fenestrations sized 100-200 nm which facilitate the extravasation of nanomaterials. Thus, it is assumed that small nanomaterials (10-20 nm) can be cleared from the blood via rapid hepatocyte uptake or via the lymphatic circulation. On the contrary, larger ones (> 200 nm), as in the case of CNTs and graphene, are cleared by Kuppfer cells upon phagocytosis being too big to cross the sinusoidal endothelium. In the case of spleen, blood flows through the discontinuous capillary into the splenic venous system. The dimension of spleen cellular fenestrations, could allow nanomaterials bigger than 100 nm to be cleared from the blood by splenic filtration via the lymphatic circulation or they could be uptaken by the RES cells resident in the organ. Concerning renal clearance, glomeruli are the filtration units of the kidney. Their endotheliums, which interact with a basal membrane, have fenestrations of 80-100 nm. In contact to the basal membrane, glomeruli possess a layer of special cells named podocytes which form a structure called slit diaphragm having pores of 4-5 nm. Glomeruli structure makes the glomerular barrier highly selective. CNTs and graphene have a much bigger size compared to glomeruli pores. Despite this, renal elimination of functionalized CNTs has been reported (*Ali-Boucetta and Kostarelos 2013*). This could be due to metabolic modifications of CNTs by phagocytic cells (see next session) or to a special perpendicular orientation of the material toward endothelial fenestrations (*Ruggero et al. 2010*). Finally a special issue concerns the lungs. In fact, these organs are the first point of entry of inhaled nanomaterials into the body. Moreover, CNT- and graphene-induced pulmonary toxicity has been reported (see previous session). The lung endothelium is characterized by a continuous morphology that allows only small particles (having a size below 3 nm) to cross the interendothelial fenestrations. For these reasons, once graphene or CNTs arrive in the lung, they are likely to be cleared by alveolar macrophages which can be recruited to the site upon nanomaterial exposure. Upon being phagocytosized, the materials could be eliminated by mucociliary movement or could be exocytated in the interstices. Afterwards, some particles could be further transported into the blood circulation (*Wang et al. 2010*). On the other hand, the interstitial biopersistence of the the nanomaterials in the lungs could enhance or be the cause of pulmonary inflammation (see previous session).

CNT and graphene biodistribution profiles have been investigated by different groups exploiting diverse methods. The most used strategy is to radiolabel the materials with radioactive isotopes in order to follow their fate in the body. This method allows for both CNT quantification through gamma scintigraphy and CNT imaging *in vivo* by tomography techniques such as SPECT (single photon emission computed tomography) or PET (positron emission tomography). CNT signatures in tissues can be also identified by Raman spectroscopy techniques.

It is now clear that CNT biodistribution is dependent to several parameters as CNT surface modifications, surface density of functional groups, CNT aggregation and length (*Ali-Boucetta and Kostarelos 2013*). It has been found that non-covalently functionalized CNTs accumulate mainly in RES organs such as liver and spleen. Despite this, the type of CNT coating could influence in some extent their accumulation in such organs and enhance their blood circulation (*Ali-Boucetta and Kostarelos 2013*). To this regard, one of the first studies was carried out by Yang et al. who investigated pristine CNT biodistribution in mice using ^{13}C-enriched SWNTs coated with Tween 80 as dispersant. The materials could be followed in the body by mass spectrometry. CNTs were administered to the mice via a single tail vein injection. The materials were cleared from the blood stream quickly and distributed throughout most of the organs within 24 h where they accumulated mostly in the lungs, liver, and spleen. Noteworthy was the fact that the materials persisted in such organs over 28 days. Moreover, pristine CNTs could hardly be detected in urine and feces, suggesting other excretion ways, for example from the lung (*Yang et al. 2007*). In another study SWCNTs were coated with branched polyethylene glycol (PEG) and injected intravenously in mice. As detected by Raman spectroscopy, the materials could be retained in the blood circulation for longer time (up to 15 h). Moreover, CNT accumulation in the RES organs, especially the liver, was highly reduced and the materials could be cleared from the main organs in 2 months. It was suggested that the coating with the polymer, could avoid non-specific binding of blood proteins with the CNTs which could be, consequently, less recognized by the RES cells. Moreover, in this case, the excretion and clearance of SWCNTs from mice occurred via the bile and renal pathways (*Liu et al. 2008 A*). On the other hand, several evidences showed that covalently functionalized CNTs generally display a reduced uptake by RES organs and an increased excretion by the renal system. Despite this, as in the case of CNTs non-covalently coated, the type and degree of functionalization affect their *in vivo* fate (*Ali-Boucetta and Kostarelos 2013*). The first study toward this observation was performed by Wang et al. ^{125}I-labeled hydroxylated SWCNTs were intraperitoneally injected in mice. The materials were rapidly distributed in most organs having the highest affinity for the stomach, kidney and bone. Interestingly was the fact that the materials were almost completely excreted with the urines (*Wang et al. 2004*). Another example of covalently-functionalized CNT biodistribution, is given by the interesting work of Al-Jamal et al. MWCNTs were conjugated with DTPA (diethylene triamine pentaacetic acid), a molecule which allowed the complexation with radioisotopes. The resulting CNTs were radiolabeled with ^{111}I and followed throughout the body by SPECT/CT after injection into mice via the tail vein. All the complexes where rapidly cleared from the blood and distributed in the organs. Interestingly, the more the

CNTs were functionalized, the less their accumulation in the liver or spleen and the more urinary excretion were observed as highlighted in Figure 8 (*Al-Jamal et al. 2012*).

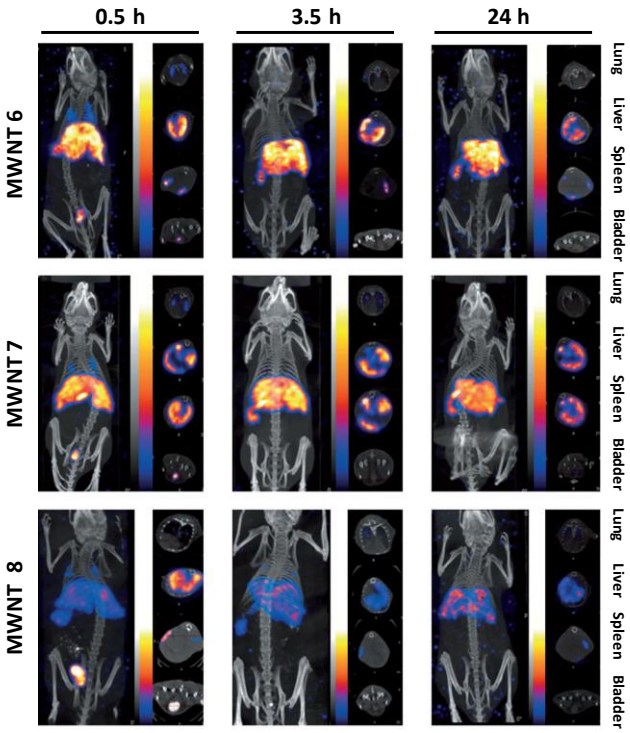

Figure 8. Nano-SPECT/CT fused images of the whole mouse. Images were taken at 0.5, 3.5 and 24 h post-injection for three types of MWNT having increasing degree of functionalization (from 6 to 8) (from *Al-Jamal et al. 2012*).

Several other works has been performed in order to enhance the circulation half life of CNTs, characteristic that is demanded for a molecule to efficiently reach its target tissues. For example, CNTs were covalently PEGylated. On the other hand, other parameters such as the size, diameter and dispersibility, could affect with some extent CNT biodistribution. These issues were investigated by several groups (*Al-Jamal et al. 2012; Wang et al. 2014*). Despite the abundant CNT pharmacokinetic studies published, a comparison between them is rather difficult for the large amount of parameters taken into account. However, the main findings toward CNT fate into the body can be evidenced in Figure 9. Generally, pristine/non-covalently functionalized CNTs are mainly retained in the RES organs, making their excretion difficult. Their biopersistence could then be associated with toxicity. On the other hand, covalently functionalized CNTs show a significant reduced accumulation in the RES organs and can be easily excreted trough the renal system, being more suitable for future biomedical applications (*Ali-Boucetta and Kostarelos 2013*).

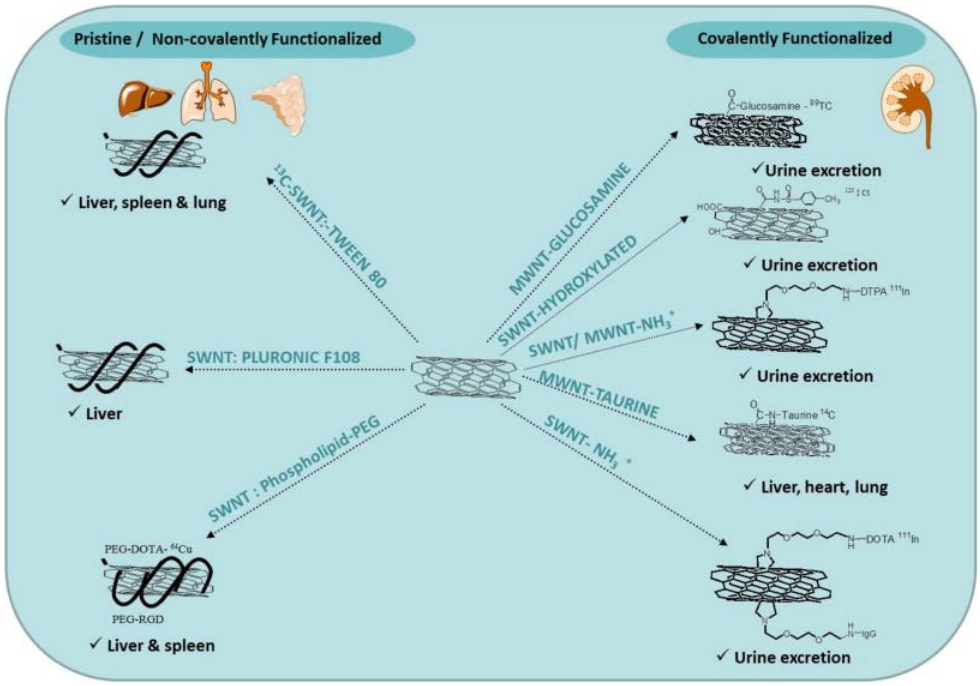

Figure 9. CNTs biodistribution based on the nature of functionalization (from *Ali-Boucetta and Kostarelos 2013*).

Similar studies have been recently published concerning the *in vivo* biodistribution of graphene. Such works were mostly performed with GO. One of the first works was carried out by Yang et al. where PEGylated nanographene sheets (NGS), derived from GO having a size range of about 10-30 nm, where intravenously injected in mice and followed inside the body after radiolabelling. The half life of the material in the blood circulation was about 7 hours. On the other hand, the material accumulated mainly in the RES organs (liver and spleen) over time. NGS complete clearance from these organs was achieved after about 2 months and they could be excreted via the biliary pathway into feces or via the renal system upon degradation as it will be described in the next session (*Yang et al. 2011*). More recently, the same group did a similar investigation using different PEG-GO derivatives and control GO. This time the routes of administration into mice were different since the materials were administered orally or were intraperitoneally injected. In the first case, the materials displayed a major accumulation in the stomach and intestine and no biodistribution in other organs, indicating their limited intestinal adsorption. In the other case, GO derivatives again accumulated mainly in the RES organs in which they were retained for up to 30 days. Interestingly, control GO could not be found in the liver or spleen, but it was observed agglomerated in the mouse abdominal cavity. They suggested that GO aggregated after injection to form big agglomerates that could not be taken up by the mouse organs (*Yang et al. 2013*).

I.3.4 Biodegradation

One important issue related to the pharmacokinetic studies concerns how therapeutic nanoparticles can be eventually decomposed in simple molecules allowing for their easier excretion from the body. Despite several progresses have been made toward the design of non-toxic carbon-based nanomaterials for biomedical applications, clinical use of such materials will be facilitated by the demonstration of their degradation *in vivo* (*Bianco et al. 2011, Li et al. 2014*). Nanomaterial special properties such as elasticity and rigidity make CNTs and graphene generally resistant to chemical treatments. For this reason, their biopersistence into organs and tissues was hypothesized with the fear of severe long-term side effects. Although further explorations in this context are certainly needed, there are already some encouraging evidences that both CNTs and graphene can be degraded by oxidative enzymes which are normally present in some cells of our body. Moreover, the ability of both materials to be degraded by the cells was also evidenced *in vitro* and *in vivo*.

Among all, peroxidases are one example of oxidative enzymes which are present in the phagocytic cell matrix. Physiologically, these enzymes are activated in order to oxidize molecules thus leading to the formation of compounds toxic for external pathogens. These types of enzymes require hydrogen peroxide for their functions that is generated during the respiratory burst. One example is given by the myeloperoxidase (MPO), produced mainly by neutrophil granulocytes but also by macrophages (*Hampton et al. 1998; Sugiyama et al. 2001*). The enzyme is stored in the lysosomes, and it contains a heme group as cofactor. MPO, when activated, produces hypohalous acids, mainly hypochlorous acid, from hydrogen peroxide and chloride anion. MPO can also oxidize tyrosines to tyrosyl radical. The resulting molecules are cytotoxic for bacteria and other pathogens allowing the cells to exert their immune function. Another important hemo-containing human peroxidase is the eosinophil peroxidase (EPO). This enzyme is mainly present in eosinophil granulocytes and, physiologically, it exerts anti-parasites functions. Being similar to MPO, EPO catalyzes the oxidation of molecules, specifically halides (such as bromide, chloride and iodide) and pseudohalides (such as thiocyanate) producing the corresponding hypohalous acids (*Hogan et al. 2008*). Moreover, this peroxidase is the major oxidating enzyme expressed in the human lung during inflammatory states (*Kinnula 2005*).

Starting for the observations described above, CNT and graphene degradation assays were performed, at the beginning, in cell-free environments; the materials were put in contact with horseradish peroxidase (HRP), a commonly used model of peroxidase derived from the horseradish plant (*Azevedo et al. 2003*). The enzyme was able to degrade oxidized SWCNTs in the presence of low concentrations of H_2O_2. Noteworthy was the fact that after ten days of HRP exposure, all the CNTs were degraded as it is shown in Figure 10A (*Allen et al. 2009*). More recently, the same

group carried out a study in which, in similar conditions, HRP catalyzed the oxidation of graphene oxide, which resulted in the formation of holes on its basal plane after ten days of exposure (Figure 10B). Moreover, in the same conditions, rGO structure was not affected by the enzyme (*Kotchey et al. 2011*). GO extracellular degradation was also shown by Li et al. who designed a non-toxic GO through its functionalization with biocompatible molecules PEG or BSA. However, PEG and BSA-coated GO were rather resistant to HRP degradation compared to free GO. Interestingly, they developed a method to conjugate the material with PEG or BSA *via* a cleavable bond obtaining a conjugated able to be degraded (*Li et al. 2014*). On the other hand, oxidized SWCNTs but not pristine, were also degraded by fluids which mimic the acidic phagolysosome environment such as the phagolysosomal simulating fluid (PSF) (*Liu et al. 2010*). Being formed by more concentric tubes, oxidized MWCNTs were more resistant to degradation but were also partially biodegraded by HRP or in PSF after two months of incubation (*Russier et al. 2011*).

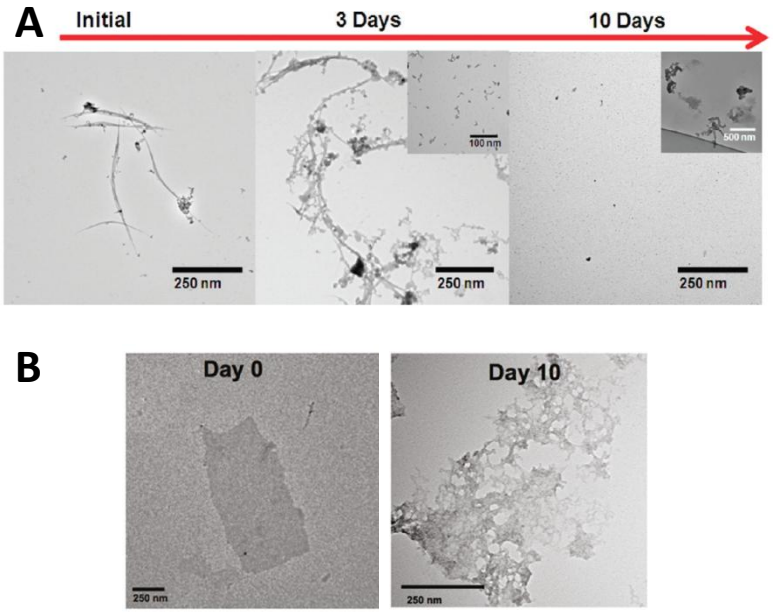

Figure 10. (A) TEM observations of carboxylated SWCNTs exposed for 10 days to HRP (adapted from *Allen et al. 2009*). (B) TEM observations of GO after 10 days of exposure to HRP (adapted from *Kotchey et al. 2011*).

More interestingly, CNT degradation was demonstrated in test tube studies in which they were put in contact with MPO and EPO, the two physiological peroxidases expressed mainly by neutrophils and eosinophils, respectively. Moreover, a strong role of the generated hypohalous acids HClO and HBrO was demonstrated (*Kagan et al. 2010; Vlasova et al. 2011*). Since these molecules are the product of physiological oxidation processes, these encouraging results allowed further *in vitro* exploration in cells. In fact, it has been evidenced that neutrophils, macrophages and eosinophils

were able to degrade oxidized SWCNTs *ex vivo* upon activation. In particular, primary human neutrophils were treated in order to trigger MPO production and then, were exposed to CNTs. In half a day, all the CNTs were degraded inside the cells as evidenced by Raman microscopy. Despite less evident, CNT degradation was observed also in macrophages, which produce MPO but to a minor extent. Moreover, the resulting products of CNT degradation did not elicit an inflammatory response when aspirated into the lung of mice (*Kagan et al. 2010*). Similarly, CNTs could be degraded by primary murine eosinophils. Contrarily to neutrophils, in this case the degradation occurred extracellularly since EPO is exocytosed upon cellular activation (*Andon et al. 2013*).

Finally, the last and most important evidence concerns CNT degradation *in vivo*. This phenomenon was suggested firstly by Elgrabli et al. Oxidized MWCNTs were intratracheally instilled into the rat lungs. As a consequence, alveolar macrophages where recruited in the organ in a dose-dependent manner, suggesting a proinflammatory response. Despite this, interestingly was the fact that, 15 days after instillation, MWCNTs underwent important modifications such as a decrease in their length. The authors proposed that macrophages, upon phagocytosis of the materials, were able to degrade the CNTs facilitating afterwards their elimination from the lung (*Elgrabli et al. 2008*). The *in vivo* degradation CNTs was later confirmed. In an interesting study, oxidized SWCNTs were instilled into the lung of both MPO knock-out and wild type mice. In the first case, phagocytized CNTs remained persistent in the neutrophils recruited in the organ thus inducing a strong fibrogenic response. On the contrary, the material was significantly decreased in the lung of wild type mice as evidenced through quantitative imaging. Moreover, 28 days after the instillation, CNT underwent degradation as their length was strongly reduced. This phenomenon was higher in wild type mice compared to MPO knock-out mice, reinforcing the evidence of MPO fundamental importance in the process. Since a certain rate of CNT degradation was also observed in MPO knock-out mice, other peroxidases such as EPO were probably involved in the process (*Shvedova et al. 2012*). CNT biodegradation was also demonstrated in the mouse brain. In this case, amino-functionalized MWCNTs were stereotactically injected into the motor cortex of the murine brain. CNTs were uptaken by diverse cellular types (see session I.4.1) including neurons and the phagocytic cells of the microglia. Noteworthy, already 2 days after administration, MWCNTs underwent structural deformation as observed by transmission electron microscopy (TEM) and further confirmed by Raman spectra (*Nunes et al. 2012*).

As it was described in this session, several studies concerning CNT biodegradation were carried out; but can graphene also be degraded *in vivo*? The answer came from Girish and co-workers who for first reported the phenomenon. After systemic administration, graphene oxide was localized in different organs of the mouse, such as lung, kidney and spleen. Structural defects in the graphene

structure were identified over a period of 3 months in the various organs. The biodegradation was predominant in graphene phagocytized by tissue-bound macrophages, result consistent with what obtained previously with CNTs. Macrophage-mediated graphene biodegradation was then confirmed *in vitro* in the same study (*Girish et al. 2013*).

Taken together, the results described in this session demonstrate the possibility of CNT and graphene oxide degradation upon administration in the body. Such evidences have important implications for the long-term toxicological profiles of these materials, particularly related to any potential clinical application. Further studies will be certainly needed to address the possible toxicity of CNT and graphene degradation products (*Bianco et al. 2011*).

I.4 CNT and graphene interaction with cells

I.4.1 Energy-dependent mechanisms of cellular internalization

Energy-dependent internalization processes, are normally used by the cells to engulf molecules that cannot pass through the hydrophobic cell membrane. On the other hand, in the case of immune phagocytic cells, these processes are involved, for example, in the digestion and immune responses toward pathogens or external materials. ATP-consuming internalization pathways are represented by four main processes that are the clathrin-mediated endocytosis, also called receptor-mediated endocytosis (RME), caveolae-mediated endocytosis (CME), macropinocytosis and phagocytosis, the latter being a feature of specific cells. In the first pathway external molecules bind to specific plasma membrane receptors. This event leads to membrane coating with clathrin protein and to the formation of a membrane invagination. As a consequence, the receptor and its ligand are internalized in clathrin-coated vesicles. Upon internalization of the complexes, the clathrin-coated vesicle uncoats and individual vesicles fuse to form the early endosomes. Two of the most known physiological functions of RME concern the internalization of low density lipoproteins (LDL) and transferrin (*McMahon and Boucrot 2011*). On the other hand, RME is also implicated in signal transduction from the cell periphery to the nucleus, as in the case of the epidermal growth factor (EGF) signaling pathway (*Vieira et al. 1996*). The second endocytic process is clathrin-independent and is mediated by small proteins named caveolins which are associated to the cell membrane lipid rafts. Caveolins oligomerize allowing the formation of caveolin-rich microdomains leading to plasma membrane invagination. This phenomenon is also helped by the increased levels of cholesterol at the invagination place. Caveolar vesicle can also fuse with the early endosomes. Physiologically, the uptake of albumin by endothelial cells and the internalization of the insulin receptor in primary adipocytes are mediated by this process (*Lajoie and Nabi 2010*).

Macropinocytosis is another clathrin-independ ATP-consuming internalization mechanism which consists in the invagination of the cell membrane to form a large vesicle and it is driven by actin filaments. This is a non-specific process where large volumes of extracellular fluid and molecules within it can be engulfed. The vesicle then travels into the cytosol and fuses with other vesicles such as endosomes and lysosomes. Macropinocytosis is important in several physiological processes. For example, it is highly used by macrophages and dendritic cells where it is a major pathway for the internalization of antigens but it is also relevant to cell migration and tumour metastasis (*Lim and Gleeson 2011*). Finally, phagocytosis occurs in specialized cells such as macrophages through an actin-based mechanism involving the interaction with various specialized cell surface receptors. This process is important in the internalization of solid agents such as bacteria and it is a major mechanisms used by immune system phagocytic cells to activate an immune response against external pathogens or to digest apoptotic cells. The latter are internalized upon the formation of large endocytic vesicles called phagosomes. The phagosome then fuses with the lysosomal compartment leading to the formation of phagolysosomes, where the foreign particles are enzymatically degraded (*Wynn 2013*).

Remarkable is the fact that the lysosome is often the last compartment of the different internalization pathways. The vesicle is characterized by an acidic lumen and by the presence of several hydrolytic enzymes. Extracellular materials such as microorganisms taken up by phagocytosis or macromolecules by endocytosis, reach this compartment in which they are digested and eventually recycled within the cells (*Grant and Donaldson 2011*).

I.4.2 Carbon nanotube and graphene internalization by cells

The interaction of CNTs and graphene with cells and their consequent ability to cross the plasma membrane is a critical issue which agrees with their possible use for drug delivery purposes. Cellular CNT internalization has been widely investigated in parallel to the development of CNT-based therapeutic strategies in the last decade. Few studies have been already carried-out showing also the graphene cell uptake. CNT and graphene internalization can be followed with diverse techniques. First, the conjugation with fluorescent probes allows for their detection by flow cytometry or their direct visualization within the cells by fluorescence microscopy. The materials can be followed inside the cells also by TEM or by other techniques such as Raman spectroscopy.

Despite some parameters and physicochemical properties can affect their cellular uptake pathways, it is now clear that CNTs are able to enter the cells by both passive diffusion and energy-dependent mechanisms. The passive CNT insertion and diffusion through the lipid bilayer of the plasma membrane have been suggested for the first time in 2004 by Pantarotto et al. The phenomenon was

visualized thanks to the CNT conjugation with a fluorescent peptide. The internalization was due to an energy-independent pathway since it was not affected by the temperature or by the presence of endocytosis inhibitors. Moreover, when the cells were exposed to the free peptide, the latter was not detected intracellularly. The result encouraged the CNT use to enhance the intracellular accumulation of therapeutic peptides (*Pantarotto et al. 2004* A). In the same year the same group published a study in which *f*-CNTs were conjugated with a plasmid DNA. By TEM observations they showed how single CNTs were able to pierce the plasma membrane of HeLa cells by the so called nanoneedle penetration mechanism (Figure 11A). Furthermore, the plasmid DNA was successfully expressed inside the cells encouraging CNT exploitation for gene delivery (*Pantarotto et al. 2004* B). More recently, models for CNT passive penetrations have been also elucidated by molecular dynamics methods which are based on the use of artificial membrane and informatics tools. Results obtained by these methods evidenced how the passive internalization process was often composed by three consecutive steps: landing and floating of the CNT on the membrane surface, penetration of the lipid headgroup area and finally sliding into the membrane core. Moreover, the study revealed that the degree of CNT functionalization influenced the two first steps and seems to specifically determine the CNT membrane penetration angle. Two representative models are shown in Figure 11B where the penetration features of low and highly functionalized CNT (model 1 and model 2, respectively) are evidenced (*Kraszewski et al. 2012*).

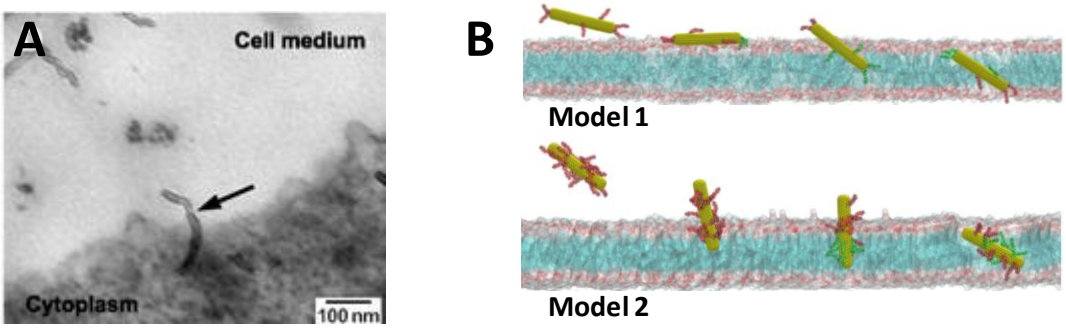

Figure 11. TEM image of a multi-walled carbon nanotube crossing the cell membrane of HeLa cells (A) (from *Pantarotto D et al. 2004*). Two proposed molecular dynamic models for CNT passive diffusion trough the plasma membrane (B) (adapted from *Kraszewski et al. 2012*).

On the other hand, several evidences showed how CNTs are also able to penetrate the cells by ATP-consuming cellular mechanisms as endocytosis or phagocytosis. First studies toward the hypothesis of an energy-dependent CNT internalization pathway were performed by Kam et al. In an early work, CNTs conjugated to fluorescent proteins were uptaken by the cells in which they localized

into endosomes, as assessed by confocal microscopy. Reinforcing this observation was the fact that protein-CNT complexes did not penetrate at 4 °C, condition in which the energy-dependent mechanisms are inhibited. Since the free protein did not penetrate inside the cells, this was another evidence of an enhanced accumulation of therapeutic molecules like proteins, inside the cells (*Kam et al. 2004*). The same group confirmed CNT ability to enter the cells trough endocytosis in another study. Moreover, CNT-protein conjugates were able to escape from the endosomes by endosomal rupture allowing the protein to express its biological functions as demonstrated by the induction of apoptosis (*Kam and Hongjie 2005*). Another early work demonstrated how CNTs were able to be actively ingested by phagocytic cells (*Cherukuri et al. 2004*). From these pioneering studies, CNT internalization by the two type of pathways were further confirmed by other groups and the mechanisms were further underlined (*Kostarelos et al. 2007; Raffa et al. 2010; Yaron et al. 2011; Al-Jamal et al. 2011*). On the other hand, specific endocytic pathways for CNT internalization were also investigated. Using specific inhibitors, it has been shown that clatrin-mediated endocytosis, caveolin-mediated endocytosis and macropinocytosis were all involved with some extent in CNT internalization by non-phagocytic epithelial cells (*Lacerda et al. 2012*).

Having a more recent history, graphene cellular uptake mechanisms are less investigated. Despite this, thanks to the strategies developed for CNTs, similar mechanisms were fast discovered. In fact, different groups have suggested both a passive diffusion and endocytic pathways for graphene internalization. It has been shown that protein-coated and fluorescent GO nanosheet internalization by murine myoblasts was mainly due to an energy-dependent process since it was inhibited of more than 80 % at 4 °C, as demonstrated by flow cytometry. Moreover, a size dependent GO internalization was demonstrated. In particular, smaller GO sheets displayed an increased internalization after 14 hours of cellular exposure compared to larger ones. Thanks to the use of specific inhibitors, it was also suggested that larger nanosheets entered the cells predominantly by phagocytosis, while smaller ones were internalized mostly by clathrin-mediated endocytosis. On the other hand, GO sheets were frequently observed adhering face to face onto the cell surface, but not bind perpendicularly, as shown by TEM (*Mu et al. 2012*). The involvement of a clathrin-mediated pathway of GO internalization was also confirmed by Huang et al., as investigated by surface-enhanced Raman spectroscopy upon conjugation of GO with gold NPs (*Huang et al. 2012).* In the study performed by Russier et al., TEM observations were carried out on primary macrophages exposed to GO samples having different sizes. First, smaller GO sheets were more internalized than largest ones, result consistent with the work of Mu et al. In addition, GO was found inside vesicles, suggesting again an endocytic/phagocytic internalization pathway, but also free in the cytoplasm. The latter observation could be correlated to a passive translocation of single sheets through the

plasma membrane. Single GO sheets were also found stacked parallel onto the cell membrane surface. The observed and so called "mask effect" could isolate cells from their environment and consequently be responsible for the GO impact on cellular parameters, but could also represent the first step in GO diffusion through the membrane (*Russier et al. 2013*). Finally, exploiting molecular dynamic membrane models, it has been suggested that microsized graphene can enter cells through passive diffusion through the cell membrane and that this process is initiated at GO corners or asperities. The proposed model is illustrated in Figure 12 (*Li et al. 2013*).

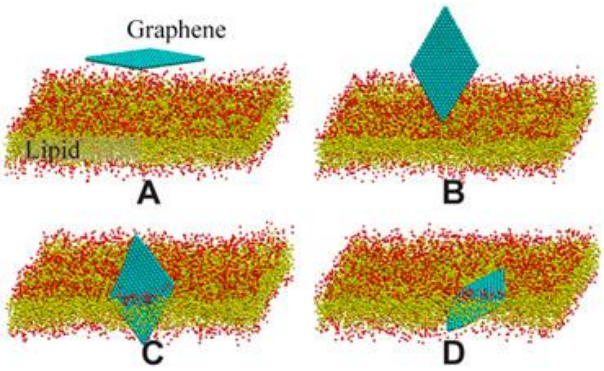

Figure 12. Molecular dynamic model of graphene passive diffusion trough the plasma membrane. The temporal steps of internalization are marked with letters from A to D (from *Ly et al. 2013*).

It has been proposed that, after internalization via one or more of the endocytic pathways, carbon nanomaterials are transported along the endolysosomal network inside vesicles with the help of motor proteins and cytoskeletal structures (Figure 13). Vesicles can transport their contents into sorting endosomes, or excrete/recycle them back to the cell surface by fusing with the plasma membrane. On the other hand endosomes can mature in lysosomes and this phenomenon is characterized by luminal acidification and recruitment of degradative enzymes, which target the vesicle contents for degradation (*Chou et al. 2011*). However, for drug delivery purposes, nanomaterials must be able to escape from the endolysosomal compartments in order to access cytoplasmic or nuclear targets. On the other hand, CNTs and graphene can be engineered in order to create a conjugate with a therapeutic molecule sensitive to pH. As an example, in a work performed by Sobhani et al, CNTs were functionalized on their surface with the chemotherapeutic drug Paclitaxel via a specific chemical bond which could be cleaved in acidic conditions, allowing a controlled release of the drug in the acidic tumoral environment or inside the lysosomes (*Sobhani et al. 2011*).

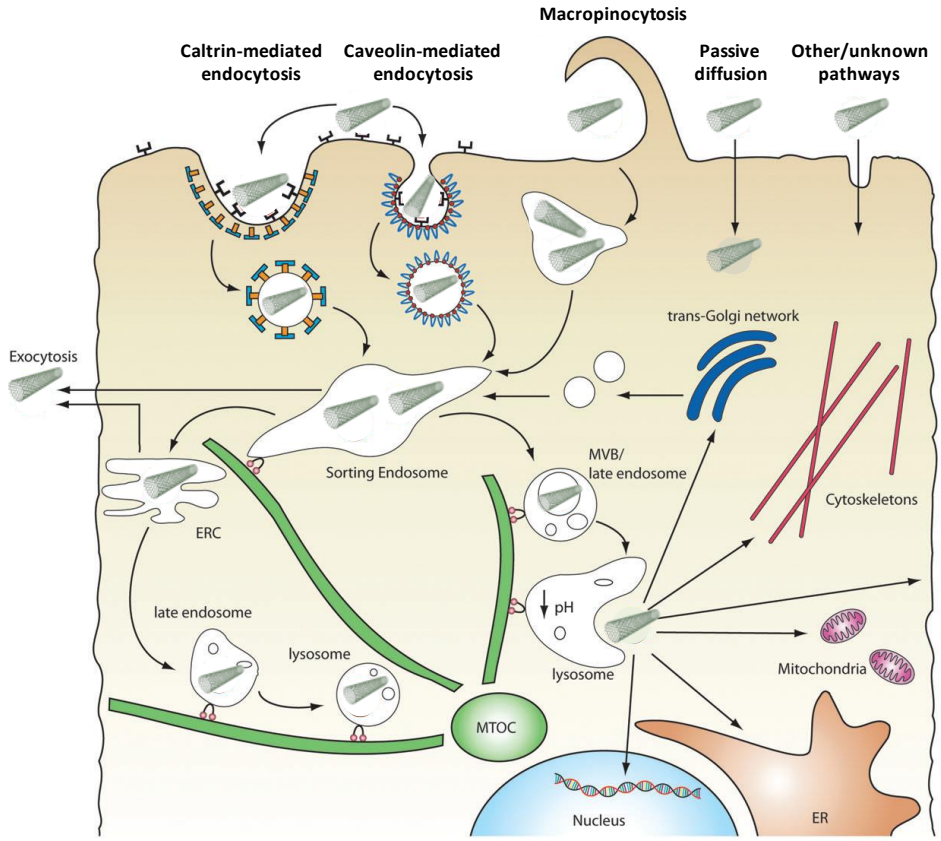

Figure 13. Endocytic uptake mechanisms of nanomaterials and their intracellular transport (adapted from *Chou et al. 2011*).

I.5 Carbon nanotubes and graphene for drug delivery: focus on anticancer therapy

I.5.1 Generalities

The administration of free drugs is often associated with several drawbacks. First, the poor solubility of the drug and its aggregation in biological fluids together with its possible premature inactivation and poor biodistribution could reduce the molecule bioavailability. On the other hand, the lack of selectivity of the drug for the diseased tissues may be the cause of severe side effects, associated with healthy tissue damage (*Bianco et al. 2004*). These are just some of the disadvantages of conventional therapies, particularly relevant in cancer, the latter being one of the main socially relevant disorder, together with autoimmune diseases. In fact, despite several progresses have been made toward the design of more powerful and specific anticancer therapies, the development of new strategies to achieve a better control of the disease is still demanded.

Drug delivery systems have been developed in order to improve the therapeutic profile of a drug. Among all, liposomes are one of the best known drug delivery systems. Such objects are made of a lipid bilayer and display a reduced cytotoxicity due to their similarity to the cell membrane. As their

inner cavity can be filled with one or more drug molecules, they have been developed, for instance, to replace conventional chemotherapy for the treatment of metastatic ovarian cancer (*Gabizon et al. 1994*). Despite this, liposomes are rather instable in solution for their amphiphilic nature. Another example of drug delivery systems under investigation is dendrimers, branched multi-shaped polymers having a diameter of few nanometers (*Gillies and Fréchet 2005*). Despite their favorable size and promising abilities to delivery molecules or nucleic acids, some dendrimers have shown significant cytotoxicity.

The special properties of CNTs and graphene, such as their high surface area, together with the development of chemical strategies to functionalize their external surface, opened the doors for their use as nano-platforms for the delivery of therapeutic molecules enhancing also the material biocompatibility (*Bianco et al. 2011*). In fact, as it was already described, any biological macromolecule can be conjugated to the surface of both materials or even encapsulated in the inner cavity of CNT. For example, CNTs and graphene can be conjugated with nucleic acids for plasmid DNA or siRNA delivery, having implications in gene therapy; with peptides, having implications on vaccine delivery; with proteins or antibodies, which can be useful for specific cellular targeting; with small therapeutic drugs, being promising tools for anticancer drug delivery (*Prato et al. 2008; Goenka et al. 2014*).

I.5.2 Eluding multi-drug resistance with nanomaterials

One of the major phenomena associated to the failure of conventional therapeutic strategies occurs at the cellular level. In fact, cancer cells can elude chemotherapy becoming resistant to a drug. Drug resistance affects patients with different types of cancer, from blood to solid tumors, including breast, ovarian, lung and gastro-intestinal cancers. This phenomenon could derive from a primary or intrinsic resistance or can be induced secondarily by a drug treatment. In both cases mutations in the genome of cancer cells and/or epigenetic changes are the factors responsible for the therapeutic failure (Figure 14), (*Rebucci and Michiels 2013*). For instance, gain of function mutations can occur in genes which are typically related to cell proliferation and survival (oncogenes). One example is the PI3K/Akt/mTOR signaling pathway which is activated upon the binding of a growth factor (such as epidermal growth factor, EGF) to its receptor. The pathway is critical in regulating the cell cycle entry but it is also involved in the regulation of apoptotic proteins. Several activating mutations of proteins which are part of this signaling pathway have been reported in human tumors (*Hafsi et al. 2011*). The Ras/Raf/MAPK or the NF-kB pro-survival signaling pathways are also impaired in tumors (*Dhillon et al. 2007, Dolcet et al. 2005*). On the other hand, loss of function genetic mutations were observed in tumor suppressor genes. One example is PTEN protein, which

is also involved in the PI3K signaling pathway, acting towards the mitotic signal derived from growth factors. The inactivation of the protein, by mutations in its gene or by methylation of the gene promoter, results in a strong pro-survival signal leading to cancer cell apoptotic-drug resistance (*Hollander et al. 2011*). Another example of tumor suppressor genes encodes for p53 protein which is one of the main relevant transcription factors, involved in the cell cycle arrest upon DNA damage. When the damage is so severe to not be repaired, cells undergo apoptosis and this response is mediated by p53. The gene is mutated in more than half human tumors. Due to its fundamental function in induce apoptosis, tumor cells harboring mutated p53 are more resistant to chemotherapeutic drugs as demonstrated in *in vitro* studies but also in patients (*Muller and Vousden 2014*). Several other mechanisms are then involved in drug resistance such as defective DNA damage response, which allow the cancer cells to survive despite the severe drug-induced DNA damage, or mutation in pro-apoptotic or anti-apoptotic proteins involved in the mitochondrial apoptosis pathway (*Rebucci and Michielis 2013*).

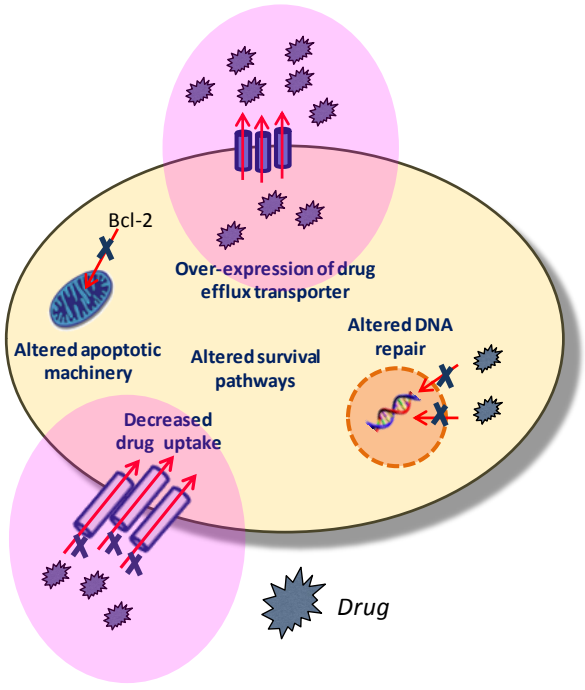

Figure 14. Overview of the cellular mechanisms involved in cancer cell resistance to common chemotherapeutic drugs. The mechanisms which could be eluded by the use of CNTs and graphene as drug carriers are highlighted in pink.

However, another interesting observation has been made in the past and consisted in the fact that cancer cells could be resistant to different related chemotherapeutic drugs, a phenomenon called multidrug resistance (MDR), (*Persidis 1999*). MDR is associated with a decrease in the cellular drug accumulation (Figure 14) by an ATP-consuming mechanism which is attributed to the

overexpression of particular members of the ATP-binding cassette (ABC) transporter proteins. ABC transporters are one of the largest and oldest families of transmembrane proteins which are highly conserved from prokaryotes to humans. Besides having a transmembrane domain, they are also composed of nucleotide binding domains necessary for ATP recognition and of a third domain named ABC signature motif, probably involved in the hydrolysis of ATP. In humans, 48 ABC genes that are organized into seven subfamilies (A–G) have been described. ABC proteins are responsible for the active transport of a large variety of molecules across the plasma-membrane, including phospholipids, ions, peptides, steroids, polysaccharides, amino acids, organic anions, bile acids, drugs, and other xenobiotics (*Leslie et al. 2005*). The first member of ABC proteins which was correlated to drug resistance is P-glycoprotein, encoded by the gene MDR1 (multidrug resistance 1) or ABCB1. Later, other members were discovered and found to be overexpressed in cancer cell lines which were resistant to chemotherapeutic drugs: the multidrug resistance protein 1 (MRP1, gene symbol ABCC1), MRP2 (gene symbol ABCC2), the breast cancer resistance protein (BCRP, gene symbol ABCG2) and others (*Persidis 1999; Leslie et al. 2005*). According to the particular overexpressed efflux transporter, cancer cells showed resistance to several chemotherapeutic molecules such as DNA crosslinking agents (e.g. platinum-based drugs), anti-microtubule drugs (e.g. taxols and vinca alkaloids) and topoisomerase inhibitors (e.g. doxorubicin and etoposide), all involved in blocking the cell replication. On the other hand, the drug accumulation inside cancer cells could be also reduced by a decrease in its active intracellular transport (Figure 14). For instance, cisplatin uptake has been correlated to the transporter Ctr1, physiologically involved in the intracellular uptake of copper. *In vitro* mutation or deletion of the Ctr1 gene results in increased cisplatin cell resistance and reduced intracellular accumulation of the drug (*Ishida et al. 2002*). Very recently, a study was performed in non-small cell lung cancer patients treated with platinum-based drugs. The study showed how patients having an undetectable Ctr1 expression in their tumors had reduced platinum concentration in the tissues and, consequently, a reduced tumor response compared to those with any level of Ctr1 expression (*Kim et al. 2014*).

As we have seen, the cellular mechanisms of drug resistance are various and can act also in a cumulative way resulting in therapeutic failure. Despite this, for some particular agents as platinum-based drugs, the reduction in the intracellular drug accumulation is the principal mechanism of resistance, accounting for 70–90% of total resistance (*Siddik 2003*). On the other hand, enhanced active transport of the drug outside the cell, but also the decrease in its uptake, requires the administration of higher doses. However, the non specific tissue accumulation of the therapeutic molecule upon administration could cause severe side effects limiting the amount of the drug that

can be dispensed. It is in this context that the use of CNTs and graphene as drug carriers could be very advantageous. In fact, as it was described previously in this thesis, CNTs and graphene have the ability to be efficiently internalized by endocytosis or passive diffusion by any cellular types and independently from the functional groups grafted on their surface (*Kostarelos et al. 2007*). As a consequence they could enhance the drug accumulation and retention inside the cells compared to the free drug, thus reducing the amount of compound administered. This behavior represents just one of multiple advantages which can be achieved using such materials as drug delivery platforms. In fact, they could also enhance the drug solubility and limiting aggregation phenomena. Moreover, in some cases, they could protect the molecule conjugated to their surface or inner cavity from premature inactivation, which could occur before the drug reach its target (*Siddik 2003*). In addition, the conjugation of the active molecule with both CNTs and graphene could be designed in order to achieve a controlled drug release. For instance, as mentioned, a drug could be linked to the materials through a pH sensitive cleavable bond. The molecule could be then released only once internalized by the cells in the acidic lysosomal lumen or in the acidic tumor environment, thus allowing a controlled release. Some successful works in which these and other strategies were exploited against cancer cells will be described in session I.5.5.

I.5.3 Passive tumor targeting by the enhanced permeability and retention effect

Another major problem related to the use of free drugs is the onset of severe secondary side effects due to the molecule accumulation in non-specific organs. In fact, chemotherapeutic agents generally act blocking at different levels the replication of fast-dividing cells, typical feature of cancer cells. However, they also affect cells that divide rapidly under normal circumstances such as cells in the bone marrow, digestive tract, and hair follicles thus inducing common side effect such as myelosuppression, inflammation of the digestive tract and hair loss. One example is given by cisplatin and its derivatives, which are used for the treatment of many types of cancer (including ovarian, cervical, head and neck, non-small cell lung, and lymphoma). This type of drugs are known to induce frequently nephrotoxicity and peripheral neurotoxicity, which derive from the non-specific drug uptake by the proximal tubule cells of the nephron and from its accumulation on the dorsal root ganglion, respectively (*Rabik et al. 2007*).

Besides helping in fighting drug resistance, another remarkable advantage in the use of CNTs and graphene as drug nanocarriers, is their ability to passively target tumor cells by the so called enhanced permeability and retention (EPR) effect (*Iyer et al. 2006*). The EPR effect is based on the observation made more than 30 years ago, that certain macromolecules accumulate preferentially to tumors (*Matsumura and Maeda 1986*). The phenomenon is based on the fact that most solid tumors

possess unique pathophysiological characteristics that are not present in normal tissues and organs. In fact, when a solid tumor reaches a size of 2-3 mm, cancer cells start to suffer of oxygen deficiency. Such stress induces the cells to secrete growth factors such as the vascular permeability growth factor (VEGF), which trigger angiogenesis from the adjacent capillaries. The process promotes the rapid development of irregular new blood vessels which differs widely from that of normal tissues. In fact, tumor blood vessels show an irregular shape and can be dilated and leaky, as endothelial cells are poorly aligned or disorganized. This results in large fenestrations in the capillaries that can reach sizes ranging from 200 to 2000 nm, depending on the tumor type, its environment and its localization. Moreover, the perivascular cells, the basal membrane and the smooth-muscle layer can be absent or defective. Such abnormalities promote an easy and enhanced extravasation of blood components to the tumor interstitium across the fenestrations of the discontinuous vascular bed. On the other hand, in normal tissues, the extracellular fluid is constantly drained to the lymphatic vessels allowing for the continuous renewal of interstitial fluid and the recycling of extravasated molecules back to the circulation. In tumors, the lymphatic system is impaired. Despite this, molecules having low molecular weight (e. g. free chemotherapeutic drugs) can diffuse back to the blood circulation being cleared through the renal system. However, bigger complexes like macromolecules and nanoparticles, are not cleared efficiently and accumulate in the tumor intersititium while the extravasation of such molecules to the tumor continues (Figure 15), (*Iyer et al. 2006*; *Bertrand et al. 2014*). For example, some studies in patients have shown the advantage of PEGylated liposomes conjugated with the chemotherapeutic agent doxorubicin (DOX) compared to the free drug. In these studies, the distribution of liposomes and their loaded agent in patient tumors was assessed. In particular, the drug concentration in malignant exudates and tumor biopsies was measured. The studies usually reported an increase tumor deposition of the liposomes compared to the free DOX. This behavior was correlated to the preferential accumulation of liposomes in the tumor *via* the EPR effect (*Bertrand et al. 2014)*.

According to these observations, the advantage in the conjugation of therapeutic molecules with CNTs or graphene compared to the fee drug can be also hypothesized. In fact, among all the other advantages described above, they have the correct size to exploit the EPR effect. Moreover, the ability of SWCNTs to accumulate in tumors *in vivo* has been already observed. In particular, in a work carried out by Liu et al., SWCNTs were subjected to different degree of PEGylation. The samples were intravenously injected in murine cancer bearing mice and the blood circulation and the biodistribution of the materials were assessed after two days. The materials accumulated preferentially into the tumors by the EPR effect, despite a certain rate of skin accumulation was also noticed. Interesting was the fact that the tumor accumulation increased in correlation with the

increase in the degree of PEGylation. This behavior was correlated with the fact that, increasing PEG chain densities and lengths, a significant prolonged SWCNT blood circulation was achieved (*Liu et al. 2011*).

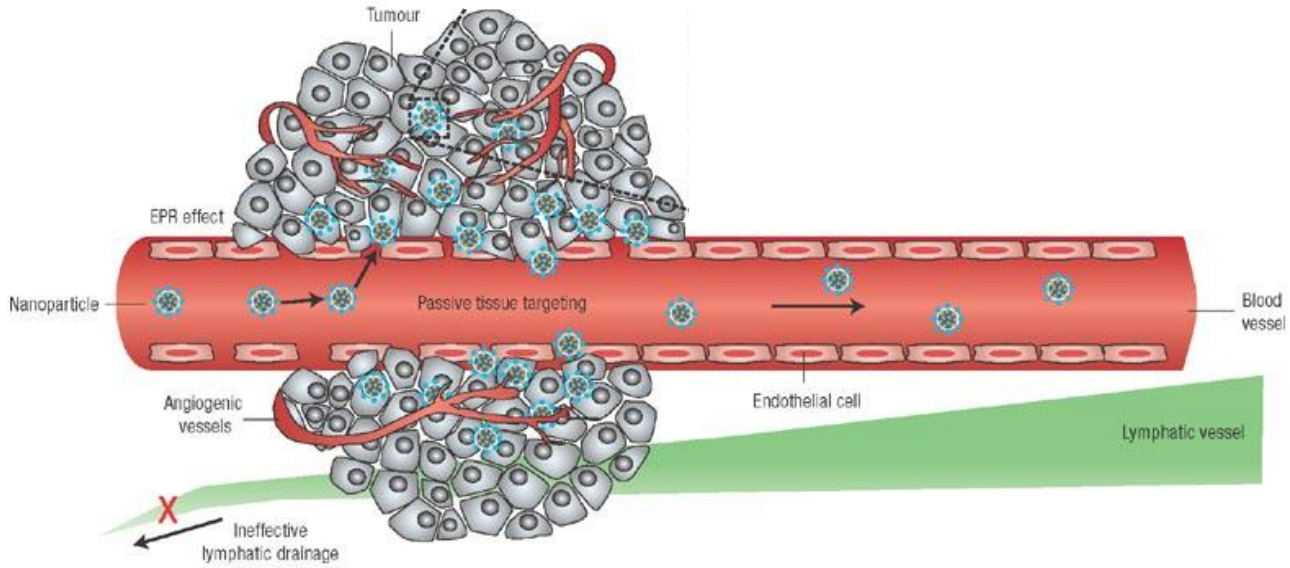

Figure 15. Schematic representation of the mechanism by which nanomaterials can deliver drugs to tumors by the EPR effect. Polymeric NPs are shown in this image as representative nanocarriers (adapted from *Peer et al. 2007*).

I.5.4 Carbon nanotubes and graphene for selective cell targeting

Although passive targeting approaches have demonstrated to be advantageous to enhance the drug accumulation in tumor tissues, such strategies suffer from some limitations. For example, certain tumors do not exhibit the EPR effect, and the permeability of vessels may not be the same throughout a single tumor. One way to overcome these limitations is to modify the nanocarriers in order to permit their active binding to specific cells after extravasation (*Peer et al. 2007)*. Before describing how CNTs and graphene can be good candidates to achieve this ambitious goal, a brief overview of targeted therapeutic strategies will be given.

Nowadays, the rational design of drugs able to target particular molecules which are specifically expressed or over-expressed by cancer cells but not by normal ones is the main focus of anticancer drug development and the basis of the so-called personalized medicine. The first step toward this objective is the identification of good biomarkers. These molecules have to be important for the cancer cell survival but less critical for normal tissues (*Bailey 2014*). Targeted therapies can be based on small molecules, typically developed for targeting intracellular biomarkers, or by monoclonal antibodies, commonly used for targets that are expressed on the cell surface. One good example of molecular target is represented by the ERBB receptor family (*Hynes and Lane 2005*).

ERBB are receptor tyrosine kinase (RTK) commonly known as epidermal growth factor receptors (EGFR). Other members of the family in humans are HER2, HER3 and HER4. Physiologically, ERBB receptors are expressed on the cell surface of various tissues such as epithelial, mesenchymal and neuronal. Upon activation by several ligands such as EGF, tumor necrosis factor α (TNF α), heparin-binding EGF and others, the homo- and hetero-dimerization of the receptor is induced. This leads to the phosphorylation on specifc tyrosine residues within the cytoplasmic tail of the receptor. The recruitment of a range of proteins on these phosphorylated residues leads to the activation of intracellular signaling pathways fundamentals for the cell proliferation and differentiation such as the PI3K/Akt/mTOR previously mentioned (see session I.5.2). ERBB receptors also show various types of alterations in human tumors. Among them, EGFR overexpression is often found in human cancers together with an enhanced production of EGF by the tumor cells themselves. These phenomena lead to a constitutive activation of the receptors promoting cancer cells survival, thus making ERBB receptors excellent candidates for selective anticancer therapies. In fact, several antibodies directed against the extracellular domain of such receptors or to their kinase domain are in clinical use. One example is Cetuximab, which is a potent inhibitor of cancer cells which display high EGFR activation. Cetuximab treatment was approved in 2003 for the treatment of advanced colorectal cancer. Another example is Trastuzumab, which is effective against HER2-overexpressing breast cancer cells. Despite the mechanisms of many targeting antibody have to be still clarified, generally, they are able to block the ERBB-induced intracellular signaling pathways thus leading to cancer cell depletion. Together with ERBB receptors several other tumor biomarkers and related targeted therapies have been approved by the FDA (*Bailey et al. 2014*).

On the other hand, targeted therapies showed advantages not only in cancer treatment, but also in autoimmune diseases (*Townsend et al. 2010*). Most of the approaches in this context are directed toward a specific cell population that is represented by B lymphocytes. In fact, B cells have a role in several autoimmune diseases such as Systemic Lupus Erythematosus (SLE) or Rheumatoid Arthritis (RA) in which autoreactive B lymphocytes, the direct precursors of autoantibody-secreting cells, are involved in the exacerbation of the disease (*Yanaba et al. 2008*). To give an example, important progresses have been made with the use of the chimeric antibody Rituximab, which specifically targets the CD20 molecule (*Gürcan et al. 2009*). CD20 is mainly expressed at the surface of B lymphocytes, and its function is to enable an optimal B cell immune response. B cells can be depleted upon recognition by anti-CD20 antibodies (*Anolik et al. 2004*).

Although significant progresses have been made in the field of targeted therapies they are not free from disadvantages. In fact, not all patients respond in the same way to the targeted anticancer treatments; secondary side effects and acquired resistance to targeted therapies were also evidenced

(*Hynes and Lane 2005; Widakowich et al. 2007*). On the other hand, despite Rituximab therapy has been reported to be successful for systemic autoimmune diseases such as RA (*Keystone et al. 2008*), trials with the same antibody gave variable results in other autoimmune diseases such as SLE (*Albert et al. 2008*). Secondary side effects upon Rituximab administration were observed also in this context (*Carson et al. 2009*). The latter observations evidence the fact that other strategies are demanded for a better specific depletion of cells involved in the disease pathogenesis.

We have seen how chemical reactions have been developed for CNT and graphene multiple functionalization (*Prato et al. 2007; Spinato et al. 2014*) allowing them to carry several molecules at once. The latter characteristic makes the materials advantageous, compared to other nanocarriers, in the treatment of cancer, but also of other diseases in which the specific depletion of a cell population is demanded. In fact, both materials can be conjugated with the targeting antibodies described above but also with a large variety of other groups, able to recognize molecules specifically expressed on the surface of a particular cell population. This, together with the ability to carry a suitable therapeutic molecule, which can also be encapsulated in the inner cavity of CNTs makes the materials powerful tools for a combined and more effective therapeutic strategy (Figure 16).

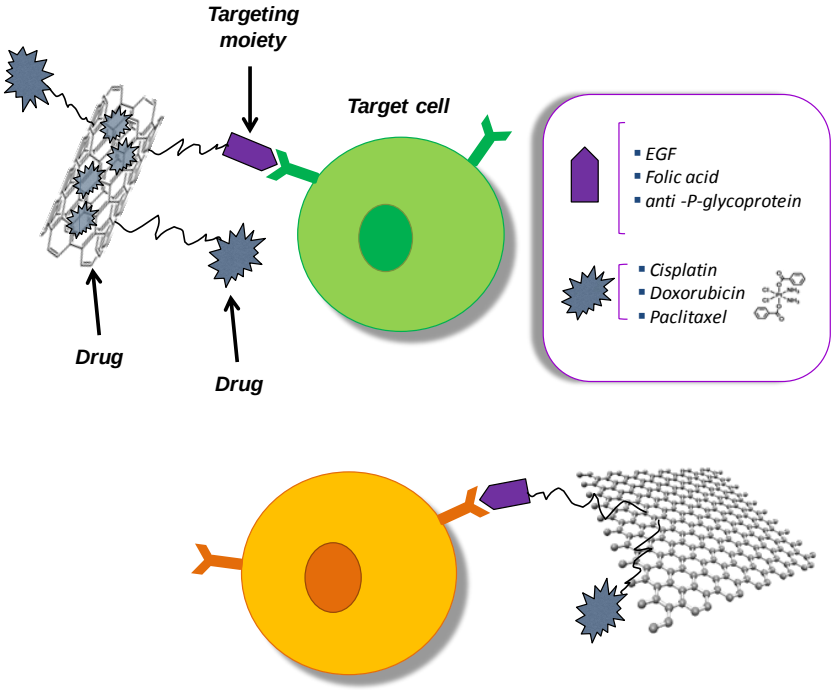

Figure 16. Targeted drug delivery using CNTs and graphene. Some examples of targeting and therapeutic moieties which can be conjugated with the materials are also shown.

In order to better understand the potentiality of CNTs and graphene towards anticancer therapy, all the advantages can be summarized with an example. CNTs could be filled with a chemotherapeutic

drug, which could be also designed in order to achieve a controlled drug release (e. g. only after cellular internalization), while their external surface could be functionalized with a specific targeting molecule such as the monoclonal antibodies Cetuximab or Transtuzumab. Once injected into patients, having cancer overexpressing EGFR or HER2, the conjugates could specifically target the tumor tissues by both the EPR effect and active targeting. Moreover, in this case, the antibodies could exert both a targeting function but also therapeutic as they are able to block ERBB-induced intracellular survival signaling pathways leading to cancer cells depletion. CNTs could be also internalized by the cancer cells (e. g. by receptor-mediated endocytosis) allowing the cytotoxic drug, encapsulated within their inner cavity, to be release and exert its cytotoxic effect. Such example show how, by the use of CNTs as multiple drug delivery platform, we could specifically reach cancer tissues combining two different mechanisms of tumor targeting, avoiding the unwanted drug accumulation in non-specific tissues and consequently the onset of secondary size effects. In addition, cancer cells could be killed *via* a powerful strategy which combines two different mechanisms: the first derived by the targeting antibody and the second exploiting the cytotoxicity of the encapsulated drug.

I.5.5 Delivery of anti-tumor agents using carbon nanotubes and graphene

In this session, some examples of successful *in vitro* and *in vivo* studies in which the mechanisms described above were exploited using CNTs and graphene as anti-cancer drug carriers will be described.

In a work carried out by Liu et al. in 2007, the chemotherapeutic drug DOX was non-covalently conjugated to the surface of PEGylated SWCNTs. The complexation between DOX and the materials was pH dependent, allowing the drug to be released in acidic conditions (as in tumor environment or inside the cells in the lysosome lumen). The DOX-SWCNTs were then tested for their anticancer activity on human glioblastoma cancer cells. In this case, the complexes showed the same cytotoxicity as the free drug in the *in vitro* test. However, in the same study, DOX-SWCNT complexes were further conjugated with the RGD peptide (arginylglycylaspartic acid). The latter acts recognizing the integrin $\alpha_v\beta_3$ which is a receptor over-expressed in a wide range of solid tumors where it is implicated in tumor angiogenesis. The conjugate was tested towards the glioblastoma cancer cell line which was $\alpha_v\beta_3$-positive and showed enhanced drug delivery ability compared to the CNTs without RGD. Moreover, the IC_{50} value (half maximal inhibitory concentration), was smaller compared to both the free drug and the derivative without the targeting peptide, thus making RGD-DOX-SWCNTs more cytotoxic then DOX-SWCNTs (*Liu et al. 2007*). In another study, the same drug was non-covalently conjugated on the surface of SWCNTs which were also functionalized with an antibody directed towards P-glycoprotein (P-gp) the latter being one of the major player in

the phenomenon of MDR (see session I.5.2). The construct was then used to treat human leukemia cells, over-expressing P-gp and consequently resistant to DOX. Upon near-infrared cell irradiation, the drug could be released from the carrier. After 24 hours, DOX was localized inside the cells in much higher quantities compared to cells exposed to the drug alone or together with the anti P-gp antibodies but without CNTs. Moreover, the free drug could only partially inhibit cell growth, while the construct was more efficient in killing the DOX-resistant cancer cells and in a time-dependent manner (*Li et al. 2010*). Several other drug types have been conjugated with carbon nanotubes. An example is the anti-microtubules agent Paclitaxel (PTX) which has been attached on the surface of PEGylated SWCNTs through an ester bond, allowing a controlled drug release in acidic conditions or upon enzymatic hydrolysis of the ester. The construct was then tested both *in vitro* in a murine breast cancer cell model (4T1) and then *in vivo* in 4T1 murine breast cancer mice model. While in the *in vitro* experiment the conjugate displayed the same toxicity as the free drug, the *in vivo* experiment gave promising results as the SWCNT-PTX complex was able to inhibit the tumor growth two times more compared to the free drug Taxol®. Despite a higher PTX amount was found in the RES organs, biodistribution studies showed that PTX levels in the tumors were 10 times higher for the SWCNT-PTX derivative compared to the free drug 2 hours post-injection. The accumulation in normal organs was also reduced, thus evidencing a better selectivity of the CNT-delivered drug for the tumor due to the EPR effect (*Liu et al. 2008 B*). The last example in the use of CNTs for tumor targeted drug delivery involves the platinum-based chemotherapeutic drug cisplatin. In the study performed by Bhirde et al, SWCNTs were covalently conjugated with cisplatin. At the same time the materials carried EGF as targeting moiety, in order to selectively act on EGFR over-expressing cancer cells. The conjugate was first tested for its *in vitro* ability to specifically target human head and neck squamous cancer cells (HNSCC), using also the non targeting control SWCNT-cisplatin without EGF. The bioconjugates were rapidly uptaken by the cancer cells. Limited uptake occurred for control cells without EGF, and uptake was blocked by siRNA knockdown of EGFR in cancer cells, revealing the importance of EGF-EGFR binding. Moreover, when the conjugates were injected into mice bearing HNSCC tumor, the EGF-CNTs showed a much higher accumulation in the tumor compared to the control CNTs without the targeting group. In addition, the tumor growth in the case of the targeting complex was inhibited in a larger extent compared to the control CNT-cisplatin alone, demonstrating the efficient and selective deliver of the drug towards EGFR over-expressing tumors (*Bhirde et al. 2009*).

Inspired by the encouraging studies towards the use of CNTs in drug delivery, promising results have been obtained also with graphene, in particular in the form of graphene oxide. Liu et al. investigated for first the possibility to deliver water insoluble anticancer drugs into cells using GO

as nanocarrier. After GO covalent PEGylation, an analogue of the chemotherapeutic drug camptothecin (CPT) was non-covalently conjugated with GO and tested on a cell line of human colorectal carcinoma (HCT-166). Interestingly, PEGylated CPT-GO was 1000 times more cytotoxic compared to the drug alone, thus evidencing the potential of graphene in drug delivery (*Liu et al. 2008 C*). The same group demonstrated the possibility to use graphene also for cell targeting conjugating PEG-GO with the antibody Rituximab directed towards the molecule CD20, expressed on the surface of B lymphocytes. GO was also non-covalently conjugated with DOX whose binding was pH dependent thus allowing a controlled release of the drug. The complex efficiently targeted a B cell lymphoma cell line CD20 positive, but not a control cell line not expressing the target molecule. Moreover, *in vitro* cytotoxicity experiments showed a significant increased efficacy toward Raji cells of the GO-PEG-Ab/DOX conjugate compared to both free DOX and the GO conjugate without the targeting antibody (*Sun et al. 2008*). Finally, the ability of GO to target tumor neovasculature was demonstrated *in vivo* in a proof of concept study. For this purpose, GO was covalently conjugated with an antibody (TRC105) directed against CD105, an endoglin almost exclusively expressed on proliferating endothelial cells, thus being an ideal marker for tumor angiogenesis. After observing the specific targeting ability toward CD105 positive cells *in vitro*, the complexes were injected in mice bearing 4T1 breast tumors (which express high levels of CD105 on their vasculature). The biodistribution of the conjugates could be then followed by PET because GO was radiolabeled. Results showed a significantly higher uptake in the tumors in the case of TRC105-GO compared to the non targeted GO (*Hong et al. 2012*).

I.5.6 Delivery of other therapeutic molecules

Besides the small anti-cancer drugs described in the previous session, other molecules of biological interest/therapeutic can be conjugated with both CNTs and graphene exploiting diverse chemical strategies. For instance, the materials can be conjugated with nucleic acids having important implication in gene therapy, the latter being another promising research area which has the purpose to treat genetic disorders and cancer by replacing/silencing the diseased gene responsible for the impaired phenotype. Successful gene therapy requires efficient and safe gene vectors that protect DNA or RNA from nuclease degradation as well as facilitate their uptake with high transfection efficiency. CNTs and graphene have been explored for their ability to efficiently protect and deliver plasmid DNA to diverse cellular models enhancing the transfection efficiency in comparison to other standard transfection systems. Similarly, the materials successfully delivered small interfering RNA (siRNA) to cells showing silencing activity towards specific genes (*Vashist et al. 2011; Goenka et al. 2014*). The majority of such studies were performed *in vitro* thus requiring further

exploration to validate the *in vivo* use of this methodology. However, in a recent work, a siRNA specific for the proto-oncogene Braf, was delivered topically to a mouse melanoma model resulting in the successful attenuation of tumor growth (*Siu et al. 2014*).

Another class of CNT-based therapeutic candidates consists in complexes between the material and synthetic peptide for immune system activation (*Pantarotto et al. 2003*). A B cell epitope from a coat protein of foot and mouth-disease virus (FMDV) was conjugated to CNTs. The antigenic and immunogenic properties of the materials were then measured in mice. The conjugates were able to elicit a higher antibody response in comparison to the non-conjugated peptide. Furthermore, the generated antibodies neutralized the virus, thus demonstrating the potential of carbon nanotubes as components for synthetic vaccine development.

Finally, CNTs could be useful for the delivery of radioactivity to tumors as the materials can be filled in their inner cavity with particular radioisotopes and then sealed to avoid non-specific leakage of the carried agent (*Zhang et al. 2010*). In fact, once again, the CNT-isotope conjugate could passively target solid tumors by the EPR effect or actively, after conjugation with targeting groups thus allowing for a targeted anti-cancer radiotherapy.

I.6 Other biomedical applications of carbon nanotubes and graphene

I.6.1 Hyperthermia therapy

In the medical field, hyperthermia consists in a rise in temperature of body tissues, globally or locally. Concerning cancer therapy, this elevation in temperature can be modulated intentionally to induce cancer cell death. If very high temperatures are used, cancer cells can die immediately, largely through necrosis. This is often called local hyperthermia or thermal ablation. On the other hand, the temperature of a part of the body (or even the whole body) can be raised a few degrees higher than normal helping other cancer treatments such as radiation, immunotherapy, or chemotherapy to work better. This is called regional hyperthermia or whole-body hyperthermia (www.cancer.org). Carbon nanotubes and graphene offer a great combination of characteristics for the development of a new generation of the so-called photothermal agents. In fact, following exposure to near infrared radiation (NIR), CNTs and graphene enter an excited state and release vibrational energy that is transformed into heat (*Singh and Torti 2013*). Several *in vitro* and *in vivo* preclinical studies were performed in cancer models exploiting carbon nanotubes as hyperthermia agents (*Singh and Torti 2013*). For instance, a study carried out by Burke and co-authors evidenced how CNTs can be superior to other heat delivery modalities in ablating cancer stem cells. Triple-negative breast cancer stem cells (BCSCs) were markedly resistant to traditional hyperthermia and become enriched in the surviving cell population following treatment. However, BCSCs were found

to be sensitive to the nanotube-mediated thermal therapy and lost their long-term proliferative capacity after the treatment. Moreover, the use of this strategy *in vivo* promoted complete tumor regression and long-term survival of mice bearing cancer stem cell-driven breast tumors (*Burke et al. 2012*). The thermal ablation of tumors has been performed also with graphene. A study showed how PEGylated nano-graphene sheets were able to accumulate into tumors in mice, in different xenograft tumor models. Highly efficient tumor destruction was then achieved by intravenous NGS injection followed by low power NIR laser irradiation (*Yank et al. 2010*).

I.6.2 Tissue regeneration

CNTs and graphene are protagonists of another fundamental biomedical field that is tissue engineering, being particularly relevant in the context of neurodegenerative diseases or traumatic injuries. In fact the damage to the central nervous system (CNS) is particular devastating because of its limited regenerative capacity. The strategies to repair the CNS address the regrowth of injured axons, the plastic remodeling of neuronal circuitry and the generation of new neurons or other CNS cell types by stem-cell transplantation. These objectives require governing several processes. For instance, axon regrowth necessitates of proper axonal spatial organization, target recognition and the reconstruction of functional synapses. On the other hand, stem cell transplantation requires cell survival and appropriate differentiation toward the specific cells of interest. To reach these goals, the design of new neuroregeneration-supporting scaffolds is demanded. Such scaffolds must be biocompatible and should promote the cellular reorganization toward a functional neuronal assembly. Proof-of-concept studies showed how CNTs could be promising candidates to develop synthetic material-based implants (*Fabbro et al. 2013*). In fact, CNTs, but also graphene, possess the ability to highly improve neural cell adhesion and growth, improve cell viability and mimic the extracellular matrix environment due to their nanoscale organization and rugosity. For instance, CNT scaffolds showed to promote neuronal cell growth and neurite elongation, but also to increase the spontaneous synaptic activity of nerve cells. Moreover, it has been suggested that the same material could promote neural stem cell (NSC) differentiation toward the neuronal lineage (*Fabbro et al. 2013*). Concerning graphene, an interesting paper evidenced how graphene-polycaprolactone hybrid scaffolds could promote NCS differentiation into olygodendrocytes, simply mimicking their *in vivo* microenvironment (Figure 17). Such observation is promising has the differentiation of NSCs into this cell type is particularly challenging and could have great implications in demyelinating diseases such as multiple sclerosis (*Shah et al. 2014*).

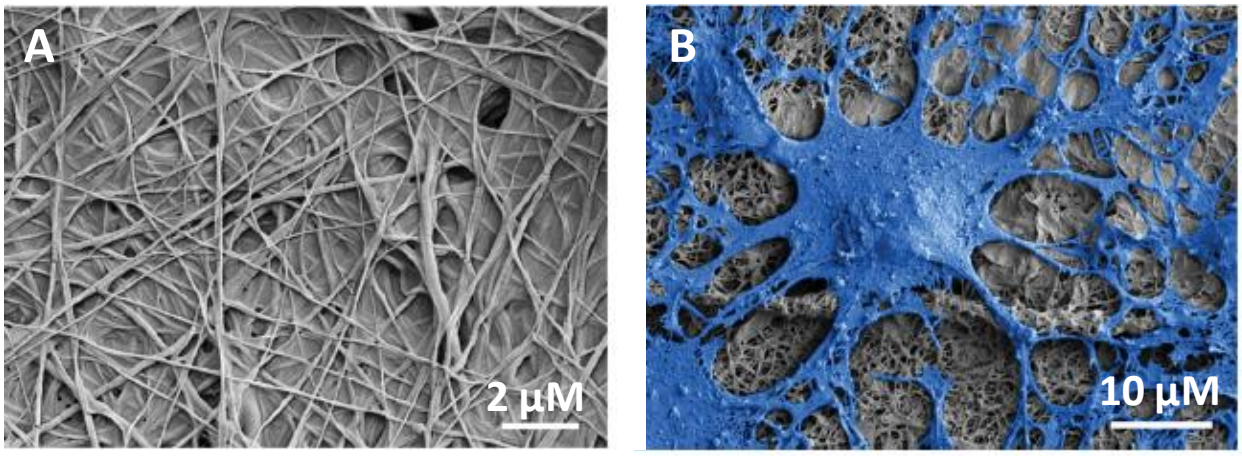

Figure 17. Field emission-scanning electron microscope **(**FE-SEM) images of PCL nanofibers coated with GO (a). FE-SEM of differentiated NSCs cultured on graphene-nanofiber hybrid scaffolds after six days of culture (b). The cells are pseudo-colored blue for contrast and display the typical morphological characteristics of oligodendrocytes (adapted from *Shah et al. 2014*).

I.6.3 Biosensing

A biosensor is a device able to detect a certain biologically relevant molecule quantity and transduce it into a signal. The development of new material-based biosensors is of fundamental importance in healthcare, where new diagnostic tools, are needed to improve clinical treatment. Carbon nanotubes and graphene have shown great promises also in this field as they can be used as building blocks for the fabrication of highly sensitive and selective biosensors. In fact, their nanoscale size allows improving the sensor performance as the sensing elements have the same dimensions (*i.e.* nm) of the biological entities that have to be detected. To do this, they have to be composed of a recognition unit that provides a selective interaction with the analyte and of a transduction unit that converts the recognition event into an observable signal. Concerning the first unit, CNTs and graphene can be conjugated with any biological entity of interest, as a molecule complementary to the one which has to be detected (e.g. single stranded-DNA). Upon analyte recognition, the signal can be transduced in several ways according also to the type of material. For example, the binding with the molecule of interest can change the charge of the carrier or can change its fluorescent spectrum (in the case of auto-fluorescent semi-conducting CNTs) (*Kruss et al. 2013*). Complementary molecules can be also conjugated with a fluorophore and the binding with the analyte is detected exploiting the phenomenon of fluorescence resonance energy transfer (FRET). The use of graphene for FRET-based biosensors is of particular interest (*Wang et al. 2011*). Examples of biological entities that were successfully detected by these types of biosensors are shown in Figure 18. For instance, the ability to detect changes in DNA sequence and structure may be useful for applications in personalized medicine, while the detection of proteins and

biomarkers, either circulating in body fluids, or displayed in the cell surface, is indicative of relevant diseased states such as cancer. Other interesting molecules involved in important cellular processes were detected by CNT-based biosensors: ATP, reactive oxygen/nitrogen species (ROS), H_2O_2, nitric oxide (NO) and glucose (*Kruss et al. 2013*).

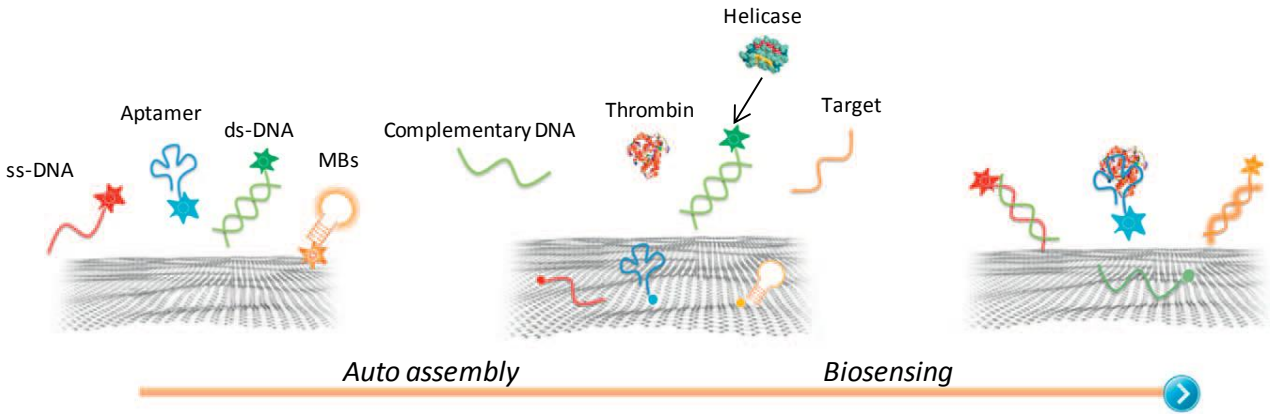

Figure 18. Principles of graphene-based FRET biosensors. ssDNA, aptamers and MBs (molecular beacons can be adsorbed onto the surfaces of graphene. Fluorophore labels on the ends of probes are quenched rapidly when adsorbed onto the graphene surface. When analytes (e.g. complementary DNA, thrombin and a designed complementary ssDNA are introduced into the systems and bind their probes (ssDNA, aptamer and MB, respectively), the probe fluorescence is recovered, thus allowing detection. Conversely, double stranded DNA remains fluorescent before an enzyme (e.g. helicase) is introduced; ssDNA is then released, and fluorophore on the ssDNA is quenched by graphene-based nanomaterials (from *Wang et al. 2011*).

Aims of the thesis

The work presented in this thesis has been carried out both at Sapienza Università di Roma under the supervision of Dr. Gianfranco Scarsella and Dr. Gianfranco Risuleo and at the Institut de Biologie Moléulaire et Cellulaire in Strasbourg. In the latter, I could develop my research in the team of Dr. Alberto Bianco as a guest for fourteen months of my PhD. During the three years of my PhD internship, I was involved in three different projects, all based on the investigation of the effects of carbon nanomaterials in a biological environment. Furthermore, I investigated the possibility to use these materials for biomedical applications.

In detail, the project started by our group in Roma as a new project that involved the use of carbon nanotubes. This was possible thanks to the experience obtained by precedent works on the application of other types of nanomaterials such as cat-anionic vesicle systems as transfection vectors. The project was carried out in collaboration with the chemistry and physics department at the same university. As mentioned in the first chapter, a careful assessment of carbon nanomaterial toxicity is still an issue under intense investigation; the aim is the further exploitation of such materials in nanomedicine. For this reason, the project started with the assessment of the cytotoxicity of pristine single-walled carbon nanotubes using different cell lines and exploiting various techniques. In particular, the idea was to disperse CNTs using biocompatible molecules that, after adsorption on their surface, could increase their solubility in aqueous media and could protect the materials from their intrinsic toxicity. To this end, CNTs were dispersed with Bovine Serum Albumin (BSA) and several cell vital parameters such as cell viability, cell activation and cellular interaction mechanisms, were investigated.

Hereafter, my research has focused more on the bio-applications of carbon nanomaterials. Therefore, the second project, in which I was involved in the group of Alberto Bianco, concerned the use of carbon nanotubes for drug delivery, aimed particularly to anticancer therapy. For this purpose, a hydrophobic Pt(IV) prodrug of cisplatin was encapsulated within the internal cavity of two types of functionalized multi-walled carbon nanotubes with different diameter in order to allow a controlled release inside the cell. Subsequently, the anticancer efficacy, the possible induction of a pro-inflammatory response and the cellular uptake were investigated on different cell types. The intracellular platinum accumulation after exposure to the different complexes was also explored. In addition, the effect of the diameter of multi-walled carbon nantubes on the release and activity of the Pt(IV) prodrug was examined for the first time.

Finally, following the experience gained with carbon nanotubes, the theme of my research moved on graphene. Like carbon nanotubes, the first important step in view of a possible biological application of graphene is the investigation of its toxicity. For this reason, initially, different types

of graphene were tested for their cytotoxicity, cell activation and internalization mechanisms on different cell lines and primary macrophages. Afterwards, the final part of my research was focused on one of the most interesting bioapplication of carbon nanomaterials: the specific cell targeting. For this purpose, graphene oxide was conjugated by non-covalent interaction with Hen Egg Lysozyme (HEL). The complexes were then tested for their ability to target a model of B cells genetically modified to overexpress a B cell receptor specific for lysozyme.

The results obtained during the development of the projects are presented in three different chapters. Moreover, each chapter is designed to have its own concise and appropriate introduction as well as conclusions and its own experimental section.

CHAPTER II

BSA-dispersed single-walled carbon nanotubes for an enhanced biocompatibility

II.1 Introduction

Thanks to their unique size-related properties, having a diameter included between 0.7 and 3 nm, single-walled carbon nanotubes are a promising type of CNTs to be exploited in the field of nanomedicine (*Liang and Chen 2010*). However, development of SWCNT-based cellular technologies necessitates several advances over multiple aspects. First, as already described, the generation of biocompatible SWCNTs that are not toxic and/or elicit immune responses is demanded. In addition, it is important to remember that one severe problem arises when CNTs are used in biology and is related to their poor dispersibility in aqueous media. In fact, strong van der Waals attractions among the tubes lead to their aggregation in large bundles (*Haddon 2002*). At the beginning, bundled, non-purified and long SWCNTs have been associated with toxicity and negative cellular effects (*Kolosnjaj et al. 2007; Holt et al. 2010*). However, CNT dispersibility in aqueous media can be improved using several dispersant molecules such as DNA (*Zheng et al. 2003; Tardani and Sennato 2014*), proteins (*Matsuura et al. 2006; Nepal and Geckeler 2006*), polymers (*Rice et al. 2006*) and others. Among them, protein dispersions are of particular interest in the context of SWCNT bioapplications. In fact, it has been shown that the interaction of some proteins with CNTs can enhance their biocompatibility with respect to pristine CNTs (*Shim et al. 2002; Ge et al. 2011*). On the other hand, as extensively described in the first chapter, the surface of CNTs can also be externally functionalized improving the CNT solubility in aqueous media and also biocompatibility (*Bianco et al. 2011*). Despite this, there are a few studies in literature aiming at improving SWCNT biocompatibility, in terms of both solubility and toxicity, after functionalization with proteins.

For a better understanding of the behavior of protein-stabilized SWCNTs in biological environments, in this proof-of-concept study, pure and pristine SWCNTs were dispersed with BSA protein. BSA-stabilized SWCNTs were then tested for their cytotoxicity and induction of a proinflammatory response toward murine fibroblast 3T6, human embryonic kidney cells HEK 293 and murine RAW 264.7 macrophages. The poorly investigated long-term effects of SWCNTs were also analyzed, in terms of cellular proliferation, after cells were let recover from the materials. The internalization/interaction mechanisms of protein-stabilized CNTs with cells and their membranes are poorly investigated as well (*Holt et al. 2012*). For this reason, the cellular uptake of BSA-

SWCNTs was explored by Transmission Electron Microscopy. Furthermore, the CNT effect on specific dielectric parameters of the plasma membrane was investigated by a biophysical technique named electrorotation.

II.2 Experimental section

Materials

Pure high-pressure carbon monoxide (HiPco) single-wall carbon nanotubes were purchased from Unidym. Main characteristics are shown in Figure 1. SWCNTs were dispersed in 0.5 % BSA in deionized water. Stock solutions of 1 mg/ml were prepared sonicating the samples for 2 h in an ice/water bath. CNTs were diluted to the appropriate concentrations in complete medium prior to cellular exposure.

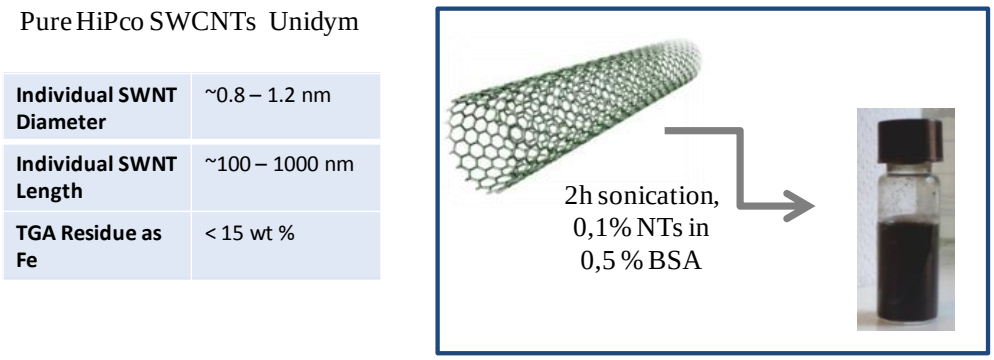

Figure 1. Commercial Unidym pure HiPco SWCNT characteristics and preparation.

The dispersions thus obtained were characterized by Atomic Force Microscopy (AFM) and Dynamic Light Scattering (DLS) techniques in collaboration with the Chemistry and Physics Department at Sapienza University in Rome. Briefly, for AFM observations, a representative CNT sample was deposited on freshly cleaved mica, incubated for 10 min, then rinsed with Milli-Q water, gently dried and observed with a Dimension Icon (Bruker AXS) AFM instrument. DLS measurements were performed with a Malvern Zetasizer ZS unit equipped with a He−Ne laser operating at a wavelength of 633 nm. The stability of one representative BSA-SWCNT dispersion was analyzed following the absorbance changes at 600 nm over time, using a Varian Cary 50 UV-Vis Spectrophotometer. Prior to the analysis, the 1 mg/ml SWCNT solution was diluted 1:10 either

in water or in complete cell culture medium (the latter being useful to avoid an effect of the medium components on the complex stability).

Cell cultures

Human embryonic kidney cells HEK 293, murine fibroblast 3T6 and murine macrophages RAW 264.7 were used in this study. All the cell lines were purchased from ATCC (VA, USA). HEK 293 and 3T6 cells where maintained in DMEM medium supplemented with 10 % FBS and penicillin/streptomicyn (100 U/ml and 100 µg/ml, respectively). Media and solutions were purchased from Euroclone. RAW 264.7 cells were cultured in RPMI 1640 medium supplemented with 10 % heat inactivated FBS and 100 U/ml gentamycin with the addition of 50 µM β-mercaptoethanol and 20 mM HEPES. Media and solutions were purchased from Lonza. All the cells were incubated at 37 ºC in humidified air containing 5% CO_2. When confluency reached 70-80 %, HEK 293, 3T6 or RAW 264.7 cells were washed with phosphate buffered saline (PBS), detached with trypsin or with SE buffer in the case of RAW 264.7 cells (PBS containing 2 mM EDTA and 2 % FBS), and subcultured every 2-3 days. Prior to CNT exposure, cells were detached, counted and reseeded in proper well size and density (see each particular experiment for details) and allowed to adhere overnight.

Mosmann colorimetric assay (MTT)

The cytotoxicity of BSA-SWCNTs towards HEK 293 and 3T6 cell lines was first evaluated by the MTT assay. NAD(P)H-dependent cellular oxidoreductase enzymes are capable of reducing the tetrazolium dye MTT 3-(4,5-dimethylthiazol-2-yl)-2,5-diphenyltetrazolium bromide to its insoluble formazan, which has a purple color. The color intensity can be directly correlated to the number of viable cells.

HEK 293 or 3T6 cells were seeded into 24-well culture plates at a density of 10^5 or $5 \cdot 10^4$ cells per well, respectively, and allowed to adhere overnight. The cells were then exposed to different concentrations of the CNT samples (from 10 to 100 µg/ml during 24, 48 or 72 h). Dimethyl sulfoxide (DMSO-20 %) was used as cellular death positive control. MTT powder (sigma M5655) was dissolved in distilled water according to manufacturer's instruction. Prior to use, MTT was diluted 1:5 in serum/antibiotics free medium. At the end of the CNT exposures, cells were washed with PBS and 420 µl of the diluted MTT were added to each well. Cells were then incubated for about 4 h at 37 ºC (5% CO_2). At the end of the incubation, formazan crystals were dissolved adding 700 µl of acid isopropanol (0.08 M HCl) and the absorbance at 570 nm was read using a Varian Cary 50 ultraviolet–visible (UV-Vis) Spectrophotometer.

Cell counts

Cell counts after exposure to BSA-SWCNTs were performed in order to investigate the long-term effect of our CNT samples on cellular proliferation. Briefly, HEK 293 or 3T6 cells were seeded into 24-well culture plates at a density of 10^5 or $5 \cdot 10^4$ cells per well, respectively, and allowed to adhere overnight. The cells were then exposed to 100 µg/ml of BSA-SWCNTs during 24, 48 or 72 h. At the end of the incubation, cells were harvested and subcultured in same number for another 24, 48 or 72 h. After these times, cells were again detached and counted using a Neubauer chamber.

Flow cytometry analysis

Cell viability

Cell viability of HEK 293 and 3T6 cells after exposure to our CNT samples was further investigated by flow cytometry.

Cells were seeded into 96-well plates at a density of $2 \cdot 10^4$ cells per well concerning HEK 293 and 3T6 and at a density of $1 \cdot 10^5$ cells/well in the case of RAW 264.7 and allowed to adhere overnigh. The cells were then exposed to the same concentrations used for the MTT assay of pristine SWCNTs or BSA-SWCNTs during 24, 48 or 72 h. DMSO (20 %) was used as cellular death positive control. After incubation, RAW 264.7 supernatants were collected and kept at -20 ºC for further investigations and cells were harvested with trypsin (HEK 293 and 3T6) or SE buffer (RAW 264.7) and stained with both FITC-Annexin V (AnnV; BD Pharmingen 556419) and propidium iodide (PI, 0.2 µg/ml; Sigma-Aldrich) in a calcium containing buffer. Cells that are considered viable are negative for both AnnV and PI stainings, while cells that are in early apoptosis are AnnV positive but PI negative, and cells that are in late apoptosis or necrotic are positive for both stainings. The percentage of live (AnnV-/PI-), early apoptotic (AnnV+/PI-) and late apoptotic/necrotic (AnnV+/PI+ and AnnV-/PI+) cells was determined by acquiring at least 30000 events using a Gallios flow cytometer (Beckman Coulter, Villepinte-France) and analysing the data with FlowJo software.

Cell activation

RAW 264.7 activation was explored through CD86 expression levels. Briefly, cells were seeded as previously described for the cell viability experiments. After incubation with CNTs cells were detached with SE buffer and stained with PE-Rat anti-Mouse CD86 antibodies (Clone GL1, BD Pharmingen 553692), prior to flow cytometry acquisition. Lipopolysaccharide (LPS, 1 µg/ml) was used as cell activation positive control. The CD86 associated fluorescence intensity was determined by acquiring at least 30000 events using a Gallios flow cytometer (Beckman Coulter, Villepinte-France) and analysing the data on live cell gated population (AnnV-/PI-) with FlowJo software.

TUNEL assay

The apoptosis induction by BSA-dispersed SWCNTs towards HEK 293 and 3T6 cell lines was specifically evaluated by TUNEL (Terminal deoxynucleotidyl transferase dUTP nick end labeling) assay (DeadEnd^{TM} Fluorometric TUNEL System, Promega). The TUNEL system measures the fragmented DNA of apoptotic cells by catalytically incorporating fluorescein-12dUTP at 3´-OH DNA ends using the Terminal Deoxynucleotidyl Transferase, Recombinant, enzyme (rTdT). The damaged DNA can then be visualized directly by fluorescence microscopy.

HEK 293 or 3T6 cells were seeded into 6-well plates on glass coverslips at a density of $3 \cdot 10^5$ cells per well and allowed to adhere overnight prior to exposure to 30 or 100 µg/ml of BSA-SWCNTs during 24 h. The assay was then performed according to the manufacturer protocol. Briefly, cells were fixed in 4% paraformaldehyde for 25´ at 4 ºC. Cells were then washed with PBS and permeabilized with 0.2 % triton X-100 solution for 5´. Cells were extensively washed with PBS. A positive control was prepared incubating control cells with DNase I. The samples were then equilibrated and incubated with a mixture of equilibration buffer, nucleotide mix and rTdT enzyme for 1 h in a humidified chamber. After a subsequent 15´ incubation with saline-sodium citrate (SSC) buffer, cells were washed and the nuclei were stained with Hoechst 33342 (2 µg/ml in PBS) for 10´. The coverslips were then washed with deionised water, mounted on slides and analysed by fluorescence microscopy. For each sample, 300 nuclei were counted, in order to calculate the percentage of TUNEL-positive cells.

Cytokine determination

RAW 264.7 macrophages supernatants were collected after treatment for cell viability experiment and the levels of murine pro-inflammatory cytokines tumor necrosis factor alpha (TNF α), and interleukin 6 (IL6), were detected by a double sandwich ELISA (enzyme-linked immunosorbent assay). Lipopolysaccharide (LPS, 1 µg/ml) was used as pro-inflammatory cytochine production positive control. Polyvinyl microtiter plates (Falcon) were coated overnight at 4 °C with 50 µl/well of purified Hamster Anti-Mouse/Rat TNF α (BD Pharmingen 557516) or purified Rat Anti-Mouse IL6 (BD Pharmingen 554400) diluted in 0.05 M carbonate buffer, pH 9.6. After washings with PBS containing 0.05 % Tween (PBS-T), a saturation step was performed by adding 100 µl/well of PBS containing 10% FBS for 1 h at 37 °C. After washings with PBS-T, 50 µl/well of culture supernatants or Recombinant Mouse TNF (BD Pharmingen 554589) or Recombinant Mouse IL6 (BD Pharmingen 554582), diluted in PBS-10% FBS, were added for 2 h at 37 °C. Plates were then washed with PBS-T and 50 µl/well of secondary Biotin Rabbit Anti-Rat/Mouse TNF (BD Pharmingen 557432) or Biotin Rat Anti-Mouse TNF (BD Pharmingen 554402), diluted in PBS-

10% FBS, were incubated for 1 h at 37 °C. Plates were washed with PBS-T, and 50 µl of streptavidin conjugated to horseradish peroxidase diluted in PBS-10% FBS were added per well. After 30 min incubation at 37 °C, plates were washed extensively and the enzymatic reaction, revealing the presence of cytokines in the tested supernatants, was visualized by adding 75 µl/well of 3,3',5,5'-tetramethylbenzidine diluted in 0.1 M citrate buffer, pH 5, in the presence of H_2O_2. The resulting absorbance was measured at 450 nm after the reaction was stopped with 25 µl/well of HCl 1 N.

Transmission Electron Microscopy

For TEM observation, HEK 293 or 3T6 cells were seeded into 24-well plates on glass coverslips at a density of $5 \cdot 10^5$ cells per well and allowed to adhere overnight prior to exposure to 50 µg/ml of BSA-SWCNTs during 24 h. Cells where then washed with PBS and fixed overnight with 2.5% glutaraldehyde diluted in PB buffer (0.1 M phosphate buffer pH 7.2). The day after, cells were washed with distilled water and post-fixed with 0.5 % aqueous osmium tetraoxide for 1h at room temperature. Cells were rinsed extensively with distilled water and a series of dehydratation baths was performed: twice with 50 % ethanol (10 min), once with 70 % ethanol (20 min), once with ethanol 95 % (10 min), twice with absolute ethanol (10 min) and finally twice with propylene oxide (for 10 min each). Samples were then embedded in epoxy resin Epon (LX 112 Embedding Kit, LADD). Mixtures of propylene oxide and Epon resin in 2:1 (1 h) and 1:2 (1 h) ratio and finally with pure resin (1 h) were added to the samples. On the last day, resin was replaced with fresh one and further incubated during three hours. Polymerized block with embedded cells were then prepared filling gelatine capsules with fresh resin and placing them upon the glass coverslips on which cells were grown. The capsules were then polymerized at 60 °C for 48 h, afterwards glass coverslips were removed from the polimerized block surface and ultrathin sections (70 nm thick) were obtained using an ultramicrotome (Leica) with a diamond knife (DiATOME). The ultrathin sections were then collected on butvar-coated single-slot copper grids and examined by TEM (Hitachi H600 or Hitachi H7500).

Determination of cell membrane parameters by electrorotation

Electrorotation was introduced by Zimmerman (*Arnold and Zimmermann 1988*) and allows to measure cellular properties like the capacitance and conductance of cellular membranes. The technique is based on the fact that cells in a low ionic strength electrolyte solution subjected to a rotating electric field start to rotate. The rotation time depends on the conductivity (σ) of the solution and the frequency of the applied field.

3T6 cells were seeded in 6-well culture plate at a density of $3 \cdot 10^5$ cells/well and allowed to adhere overnight prior to exposure to 100 µg/ml of BSA-SWCNTs during 24 h. Cells were then harvested with trypsin, washed two times with PBS and resuspended in 1 ml of different sucrose 0.3 M solutions differing in conductivity (0.3 M sucrose or 0.3 M sucrose + 0.5, 1 or 1.5 mM NaCl). The samples were kept on ice during all the measuring time. An amount of 10 µl of the cellular suspension was added to a cell connected to a generator of a rotating electric field. The signal frequency can be varied from 240 Hz to 500 KHz in 12 values while the amplitude of the signal is fixed at 12V. The rotating cell images can be recorded. The rotation times of at least 25 cells for each frequency were determined manually and the acquisitions were repeated for each 4 sucrose solutions. The average time of rotation (T_m) was put in graph as a function of the frequency of the applied field:

$$T_m(f) = T_{min} \frac{1+(f/f_{c1})^2}{2(f/f_{c1})}$$

The frequency corresponding to the dielectric relaxation (f_{c1}) was determined for each sample calculating the minimum value of the curve. Finally, the 4 relaxation frequencies obtained were put in graph as a function of the conductivity of the specific sucrose solution. A linear relation is obtained and can be written by the formula $f_{c1}=a\sigma+b$. Calculating the angular coefficient and the intercept, these parameters can be replaced in the formulas $a=1/\pi rC$ and $b = G/2\pi C$ where C and G represent the capacitance and the conductance of the cell membrane, respectively.

Statistical analysis

The experiments shown (where it is not otherwise specified) are a summary of the data from at least three separate experiments run in triplicate for each cell line. Data are presented ± SEM. Statistical analyses were performed using a two-way ANOVA test followed by Bonferroni's post-test. All p values < 0.05 were considered significant.

II.3 Results and discussion

II.3.1 BSA-SWCNT characterization

Pure commercial SWCNTs (1 mg/ml) were dispersed in solutions of BSA at various concentrations (from 0.1 to 1 % w/v). The quality of the dispersions was preliminary evaluated by optical microscopy and 0.5 % BSA was finally chosen as the best concentration capable of giving a good CNT dispersion without many visible aggregates. The BSA-SWCNT dispersion was also relatively

stable, as demonstrated following the 600 nm absorbance over time after a 1:10 dilution in both BSA solution and complete culture medium (Table 1). In fact, no changes in absorbance were detected after 2 weeks from CNT preparation and only a slight sedimentation was noticed after 3-4 weeks. Taken together these first observations are in agreement with the possibility to use these materials for biomedical applications, since CNT biocompatibility is highly dependent on their solubility and dispersion in biological, aqueous-based environments (*Bianco et al. 2011*).

Table 1. Absorbance measurements of BSA-SWCNT dispersion diluted 10 times in 0.5 % BSA solution or complete culture medium over time.

Weeks	A_{600} in BSA solution (100 µg/ml)	A_{600} in complete medium (100 µg/ml)
1	$2{,}1992 \pm 0{,}01$	$2{,}3488 \pm 0{,}01$
2	$2{,}0818 \pm 0{,}01$	$2{,}2972 \pm 0{,}01$
3	$1{,}8473 \pm 0{,}01$	$2{,}0973 \pm 0{,}01$
4	$1{,}8473 \pm 0{,}01$	$2{,}0973 \pm 0{,}01$

BSA-SWCNTs were characterized by AFM. Height distribution analysis showed the presence of two CNT populations, having an average diameter of about 5 to 9 nm (Figure 2A).

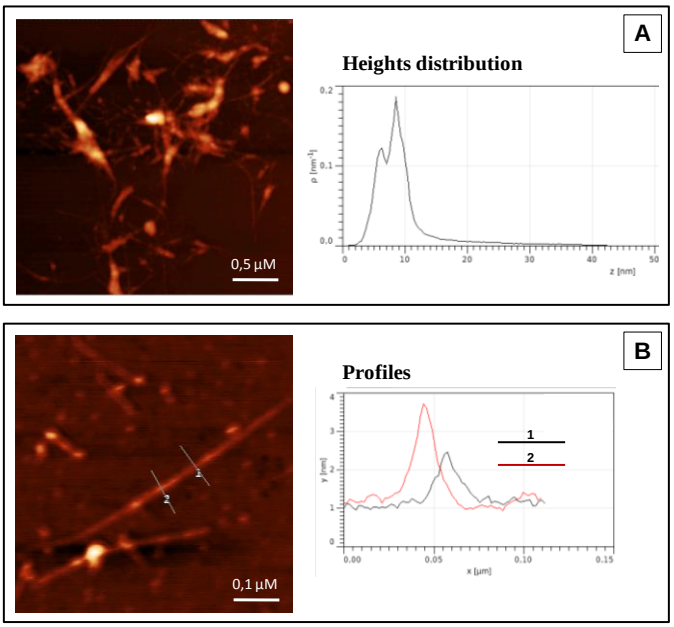

Figure 2. AFM observation of SWCNTs dispersed in 0.5 % BSA. The SWCNT height distribution is shown in panel A while two profiles of a single SWCNT can be observed in panel B.

In the first case, the increase in CNT diameter compared to the original size (about 1-2 nm) can be ascribed to the protein layer surrounding the nanotube while a 10 nm average diameter can be

attributed to CNT aggregation. In Figure 2B the diameter of two section of a single nanotube are reported. In particular, the different size of the two sections (about 3.8 nm and 2.5 nm) can be ascribed to the uneven distribution of BSA on the surface of CNTs. Results are consistent with BSA-SWCNT characterizations described by the work of Ge et al. were a single protein molecule on the SWCNT surface was about 2.5 nm in height (*Ge et al. 2011*). Moreover, increasing amount of BSA molecules was added to the complex, SWCNT surface was saturated by the protein. Therefore, additional binding of BSA could only occur onto the earlier layer accumulating on the CNT surface. The latter observation is consistent with the increase in SWCNTs profile 1 observed in Figure 2B.

II.3.2 investigation of BSA-SWCNT cytotoxicity

To investigate the biocompatibility of BSA-SWCNTs, cytotoxicity, cellular proliferation and apoptosis were examined by different methods after cellular exposure to the nanomaterials in question. Different cell lines were chosen to verify the effect of the CNT samples on cells having different characteristics and origin. In particular, cells capable of different internalization mechanisms were compared. The materials were tested on murine fibroblast 3T6, known to be phagocytic cells (*Lee et al. 1996*) and human embryonic kidney cells HEK 293 (non-phagocytic). The complexes were further tested on murine RAW 264.7 macrophages, also to assess the induction of a possible proinflammatory effect induced by the BSA-SWCNTs.

II.3.2.1 Analysis of the cell viability, proliferation and apoptosis

MTT assay

As a preliminary step in our study, cell viability and proliferation after exposure to BSA-SWCNTs were evaluated both on 3T6 and HEK 293 cells by MTT test. For this purpose, cells were exposed to different concentration of CNTs, ranging from 10 to100 µg/ml, for 24, 48 and 72 hours. During these first experiments, a typical optical microscopy image of 3T6 cells was taken, after exposure to 100 µg/ml of CNTs for 24 hours (Figure 3). The picture shows how CNTs could highly interact with the cells in which they seem internalized or stacked on their surface.

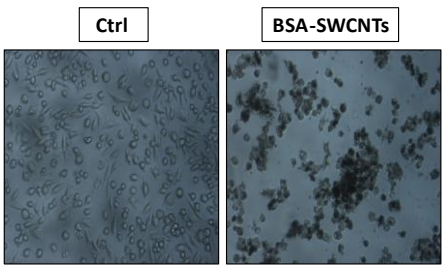

Figure 3. Optical microscopy images of 3T6 control cells or incubated with 100 µg/ml of BSA-SWCNTs.

A different response to the CNT samples was observed in the two cell lines. In fact, in the case of 3T6 (Figure 4A), despite a slightly significant difference was noticed also at a CNT concentration of 30 µg/ml, an important reduction (about 30 %) in the cell viability as compared to the control (***p<0.001) was observed only in the case of the highest CNT concentration (100 µg/ml) after 48 or 72 hours. On the other hand, HEK 293 cells showed a general higher sensitivity to the samples in comparison to 3T6 cells (Figure 4B). In fact, a significant reduction in cell survival (of about 20 %) was observed already after exposure to 10-30 µg/ml of CNTs during 48 or 72 hours. The higher cytotoxic effect compared to 3T6 cells was more evident at 50-100 µg/ml CNT concentrations where a decrease of about 40 % in cell viability was detected after 48 or 72 hours. Neither cell types showed a reduction in cell viability after a 24 hour CNT exposure demonstrating that long-term experiments can be necessary to probe a CNT biological effect. Surprisingly, the non-phagocytic cell line, and thus perhaps able to internalize less materials, resulted more sensible to BSA-SWCNTs.

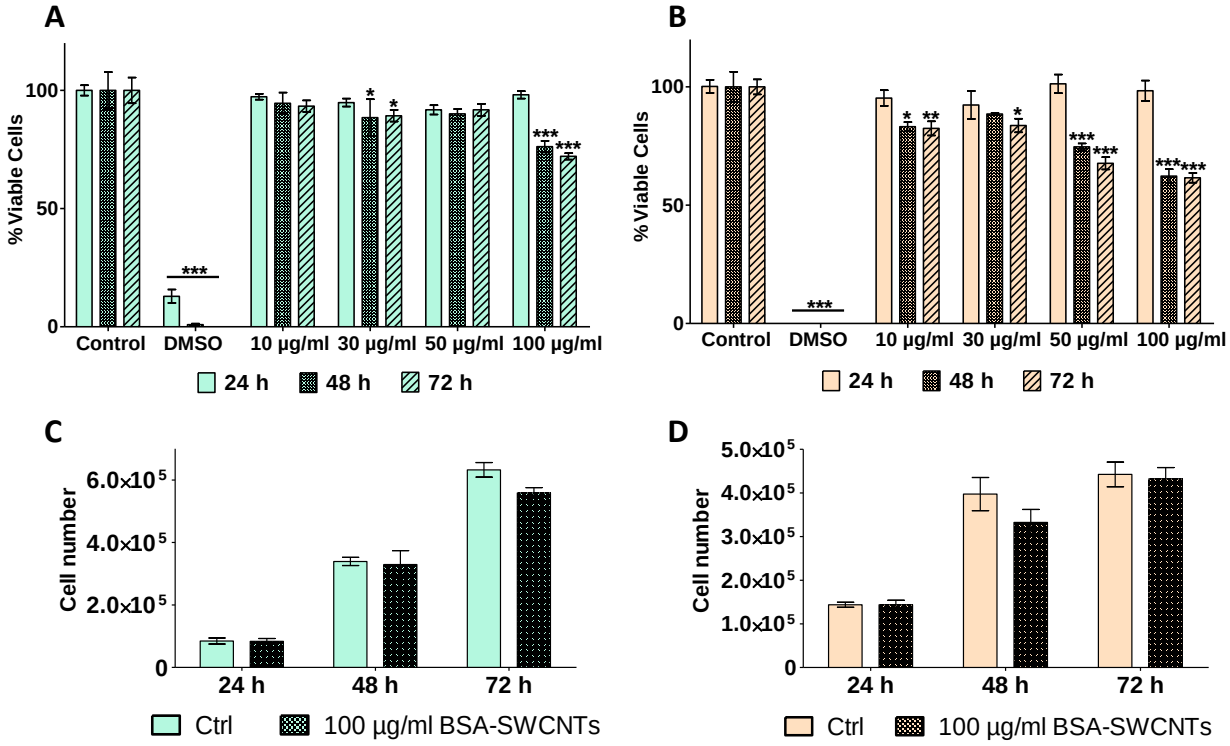

Figure 4. MTT analysis of cell viability in 3T6 cells (A) and HEK 293 cells (B) exposed to different concentrations of BSA-SWCNTs for 24, 48 or 72 h. Two-ways ANOVA followed by Bonferroni's post-test was performed to determine the statistical differences *versus* control cells (*p<0.05; **p<0.01; ***p<0.001). The total cell number after exposure to 100 µg/ml of BSA-SWCNTs during 24, 48 or 72 h is shown in panels C (3T6) and D (HEK 293).

As the MTT test measures the cellular ability to convert the dye into its reduced form, results obtained by the test could derive both from a reduction in the metabolic activity of the cells and from a decrease in their proliferation. To try to discriminate between the two events, the cell proliferation was determined counting the total cell number after 24, 48 or 72 hours of exposure to 100 µg/ml of BSA-SWCNTs, concentration able to induce the major cytotoxic effect in both cell lines. Concerning both 3T6 and HEK 293, no significant change in the total cell number was observed (Figure 4 C and D). This suggests that the reduction in the absorbance obtained by the MTT test could be due to a reduction in the cellular metabolic activity rather than cellular proliferation

TUNEL assay

For a better understanding of the mechanisms responsible for the cytotoxicity both on murine and human cells in response to BSA-SWCNTs, we checked the apoptotic cell death since this is one of the principal pathways for a cell to die. For this purpose, 3T6 and HEK 293 were exposed to 50 or 100 µg/ml of BSA-SWCNTs during 48 hours. Time and concentrations were chosen according to the results obtained by the previous test, as they were able to induce a significant reduction in cell viability (Figure 4). Typical fluorescence images obtained in the case of 3T6 or HEK 293 cells are shown in Figure 5 where the green fluorescence is associated to the damaged DNA of apoptotic cells. Positive nuclei were then counted. A significant induction of apoptosis was not observed in any case. In fact, the percentage of apoptotic 3T6 cells was only 2-3 % after exposure to 50 µg/ml of the material and about 4 % in the case of 100 µg/ml concentration (Figure 5A, bottom panel). Regarding HEK 293 cells, despite slightly increased, the same situation was monitored as the percentage of apoptotic cells was about 4 and 5 % after cellular exposure to 50 or 100 µg/ml of BSA-SWCNTs, respectively.

The slight level of apoptosis observed by TUNEL assay could not account for the BSA-SWCNT cytotoxicity obtained by MTT test suggesting alternative cell death mechanisms. For example, the strong CNT interaction with the cell membrane could directly promote its damage eventually leading to necrotic cell death. Moreover, it has been shown that CNTs could interfere with the MTT assay (*Belyanskaya et al. 2007*). Taking together these considerations, the cytotoxicity induced by BSA-SWCNTs was further explored.

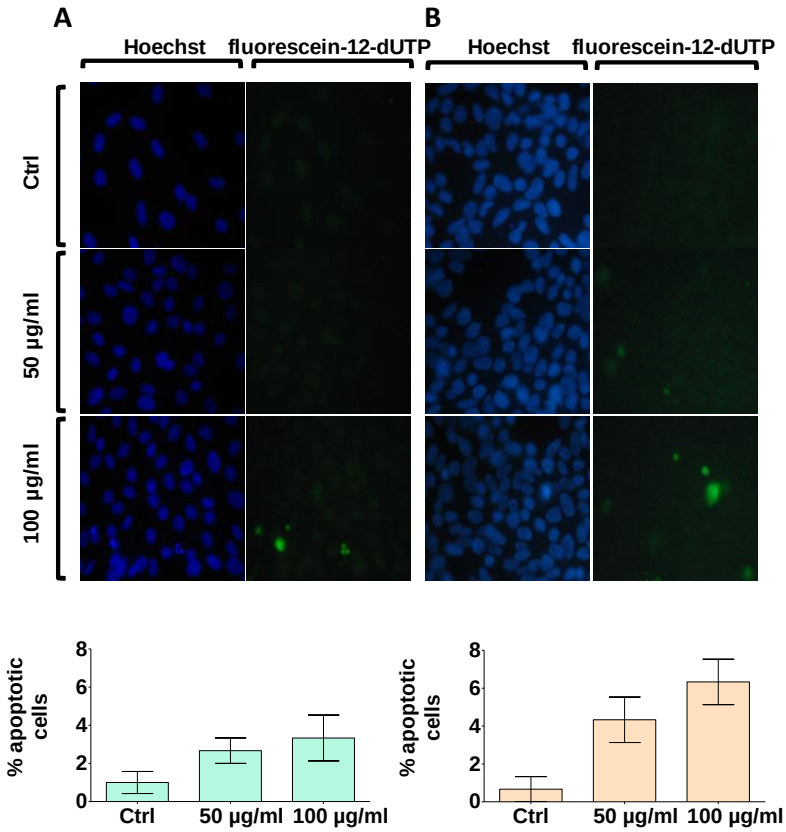

Figure 5. Analysis of apoptosis by fluorescence microscopy using TUNEL assay in 3T6 (A) or HEK 293 cells (B) exposed to 50 or 100 µg/ml of BSA-SWCNTs during 48 h. In the corresponding bottom graphs, the percentages of TUNEL-positive cells are shown.

Flow cytometry analysis

The cell viability of HEK 293 and 3T6 cells after exposure to our CNT samples was then further investigated by flow cytometry after AnnV/IP staining. The analysis was also performed on RAW 264.7 macrophages since these immune cells can be considered the primary sentinels of our body to infectious organisms but also to external materials (*Wynn et al. 2013*). For this purpose, cells were incubated in the same conditions used for the MTT assay of BSA-dispersed but also with pristine SWCNTs as controls. At the end of the incubation, cells were harvested and analyzed by flow cytometry. According to the analysis, no changes in cell viability were observed in the case of both 3T6 (Figure 6A) and HEK 293 (Figure 6B) cells at all treatment times, both in the case of pristine and BSA-dispersed SWCNTs. On the contrary, the viability of both cell lines was affected by DMSO, used as positive (toxic) control. Therefore, the discrepancy between MTT test and flow cytometry data confirms the fact that MTT is not a good method to investigate carbon nanotube cytotoxicity. On the other hand, the results of flow cytometry measurements on 3T6 and HEK 293 cells are consistent with the poor apoptosis observed by TUNEL assay. Nevertheless, the possible reduction in the metabolic activity of AnnV/PI negative cells cannot be excluded and could explain

the MTT results.

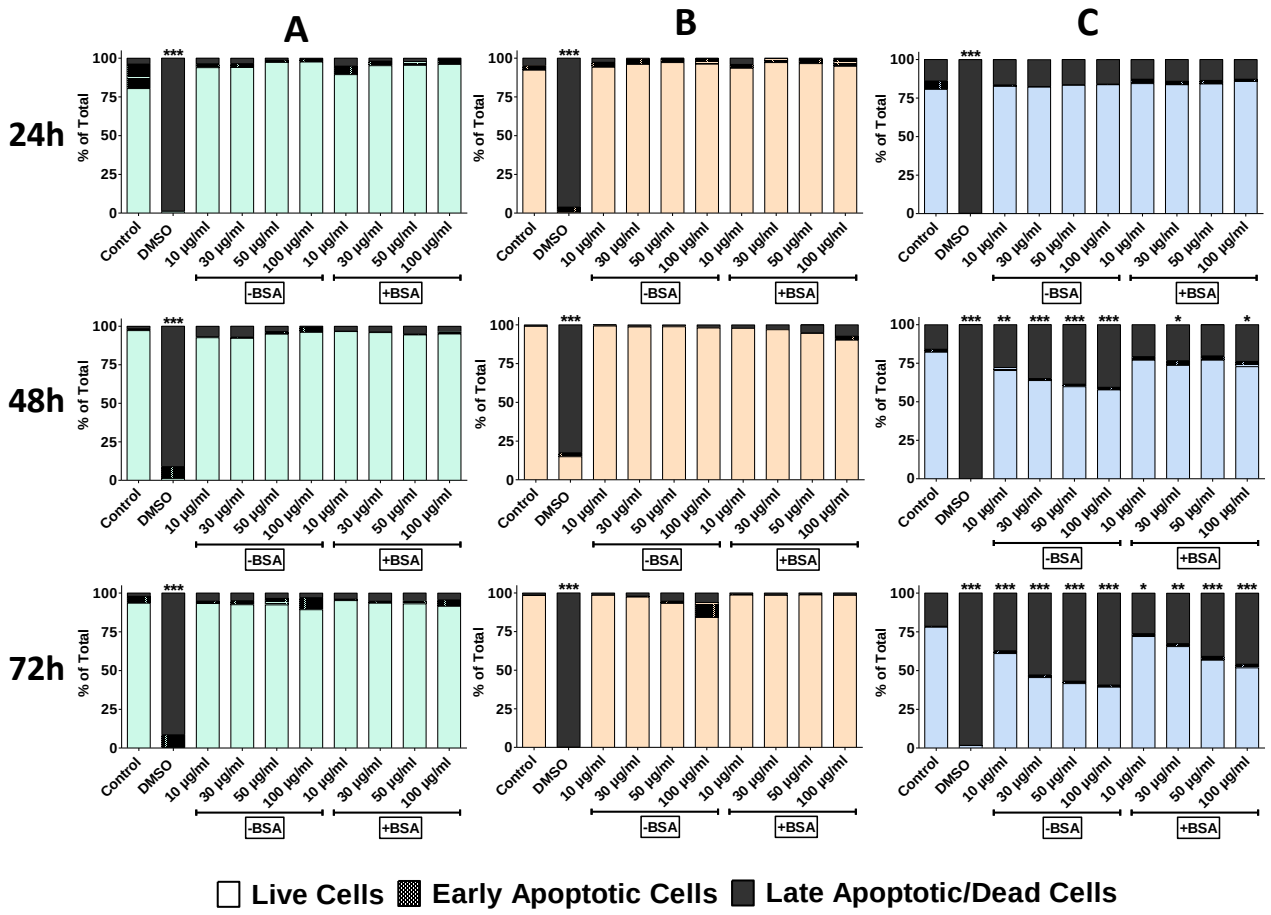

Figure 6. Flow cytometry analysis of cell viability in 3T6 (A), HEK 293 (B) and RAW 264.7 cells (C) exposed to different concentrations of SWCNTs (BSA-dispersed or not) during 24 h, 48 h, 72 h. Two-ways ANOVA followed by Bonferroni's post-test was performed to determine the statistical differences *versus* control cells (*p<0.05; **p<0.01; ***p<0.001).

On the contrary, RAW 264.7 showed a different sensitivity to the materials as compared to 3T6 or HEK 293 cells (Figure 6C). In fact, despite any effect was observed after an exposure of 24 hours, both pristine and BSA-dispersed SWCNTs were able to induce a significant reduction in cell viability after 48 hours or 72 hours. In more details, after an exposure of 48 hours to pristine CNTs, RAW 264.7 evidenced a concentration-dependent reduction in the percentage of viable cells, ranging from about 10 % to 20 % of control (concerning the smallest and highest CNT concentrations, respectively). Even though this decrease was not dramatic, it is interesting to note that, in the case of BSA-dispersed CNTs, the same concentration-dependent behavior was not observed after 48 hours. In fact, the cell viability was only slightly reduced, compared to the control cells (5-7 %), in all concentration ranges. This difference between the effects of pristine or BSA-coated CNTs was further confirmed after a cellular exposure of 72 hours. In this context, a concentration-dependent cytotoxicity was detected with both SWCNT samples (coated or

uncoated). Nevertheless, cells displayed a significantly higher mortality after contact with pristine SWCNTs as compared to BSA-coated ones. In fact, the residual cell viability ranged from 60 to 39 % or from 70 to 50 % for pristine or BSA-dispersed SWCNTs, respectively.

BSA-SWCNT long-term impact on cell proliferation

To our knowledge, the CNT long-term impact on cell viability was in general poorly investigated. Since no effect on both 3T6 and HEK 293 cells was observed by flow cytometry even after 72 hours of cellular contact with the highest concentration of both pristine and BSA-coated CNTs, we wondered if an effect could be observed some time after the end of exposure. In order to verify this issue, cells were exposed to 100 µg/ml BSA-SWCNTs during 24, 48 or 72 hours; thereafter cells were harvested, counted and subcultured, in the same number, in fresh medium (CNT free). Proliferation was chosen, in this case, as readout of cellular behavior. Therefore, both 3T6 and HEK 293 cells were counted after they were allowed to grow for further 24, 48 or 72 hours. Regarding 3T6 cells, no changes in their ability to proliferate, compared to the control, was observed in any case (Figure 7A) demonstrating how fibroblast could highly tolerate BSA-SWCNTs. On the other hand, in the case of the human cellular model (Figure 7B), a slight reduction in cell number, compared to control cells, was noticed 72 hours after the cells were treated with CNTs for 24 hours (upper panel). This decrease was more evident in the case of a 48 hours exposure to the materials (middle panel). Indeed, in this context, HEK 293 cells showed a reduction in cell number of about 20 %, with respect to controls, after cells were allowed to grow for further 48 and 72 hours. Despite same behavior was not observed 48 hours after an exposure to CNTs of 72 hours (bottom panel), 72 hours later, HEK 293 cell number was reduced of about 30 % in comparison to control cells.

The latter result on HEK 293 cells demonstrates that CNT-induced cytotoxic effect can arise even some times after the end of the exposure.

Taken together, all our results on cytotoxicity shed more light on the SWCNT impact on living cells. In fact, conflicting results exist in literature about the toxicity of this specific type of CNTs and must be better investigated also in view of their possible future applications in biomedicine. The discrepancy between the various literature results can be explained by the fact that several factors act synergistically in determining single-walled nanotube impact on cells: these factors include CNT size, metal catalyst contaminants, dispersant types and surface modifications (*Lanone et al. 2013; Ong et al. 2014*). Furthermore, SWCNT-induced cytotoxic effect can also vary depending on the particular cell type analyzed.

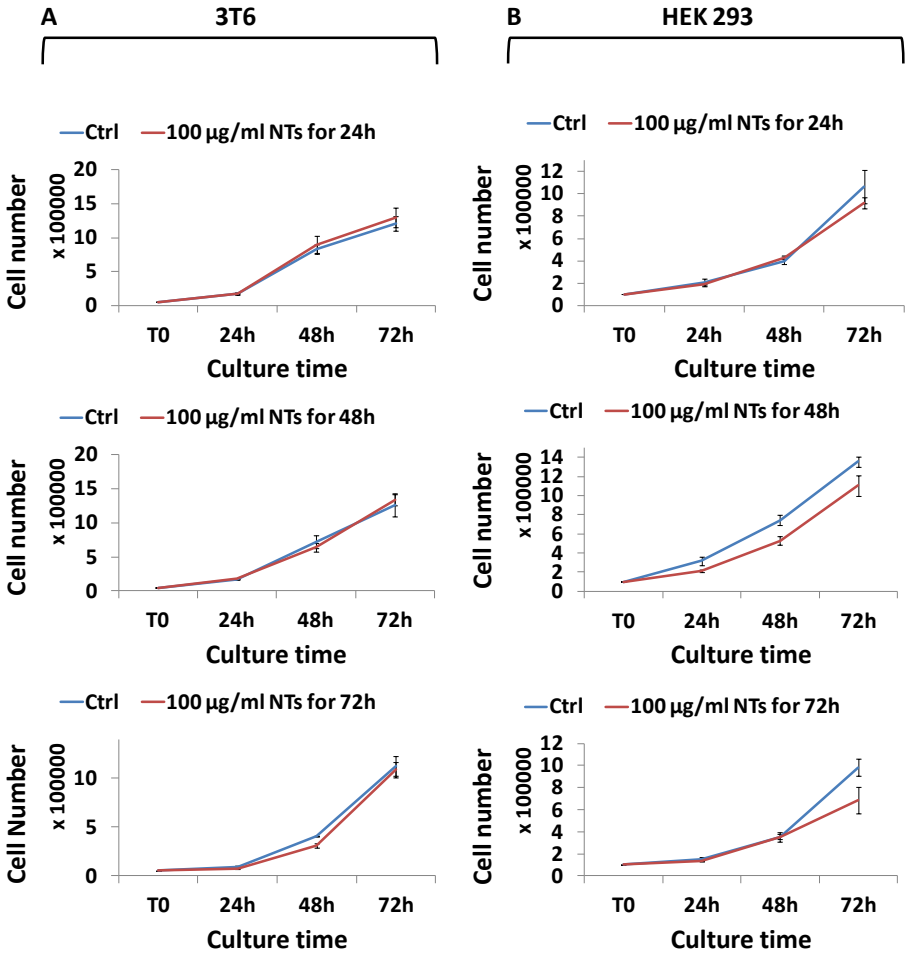

Figure 7. Determination of the total cell number in 3T6 cells (A) or HEK 293 cells (B) exposed to 100 µg/ml of BSA-SWCNTs for 24 h (upper panel), 48 h (middle panel) or 72 h (bottom panel) and subcultured for further 24, 48 or 72 h after the treatment.

In our study, the nanomaterials were dispersed with BSA in order to assess if a "protection effect" could be noticed after coating the CNT surface with this biocompatible molecule. In a work by Ge et al. different SWCNTs were dispersed with several blood proteins. They demonstrated how the diverse protein-nanomaterial conjugates displayed different outcome towards acute monocytic leukemia cells (THP-1) or human umbilical vein endothelial cells (HUVEC). First, both cell types presented a high sensitivity to pristine SWCNTs (*Ge et al. 2011*), situation that was not found in our study concerning both 3T6 and HEK 293 cells, thus confirming the variability between different cellular types. This behavior was reversed when the materials were coated with different types of blood proteins among which BSA, observation consistent with our results on murine macrophages. SWCNT cellular impact was described also by Holt et al. in different studies. In an earlier work, they found that dispersed and purified SWCNTs are relatively benign with regard to cytotoxicity as it was investigated in a human cervix cancer cell line. However, despite an acute cytotoxicity was

not observed, cell proliferation was greatly reduced with an increase in actin-related division defects (*Holt et al. 2010*). This behavior was not found in all our cell models but only in the case of HEK 293 cells which were allowed to recover from the materials during 48 or 72 hours (Figure 7). This confirms the variability between different cell models and the idea that several factors interplay in SWCNT-induced cytotoxicity. Other two works from the same group showed how BSA-stabilized SWCNTs could be promptly uptaken by human mesenchymal stem cells, HeLa or murine fibroblast (3T3) without apparent acute deleterious cellular effects, encouraging the efficacy of BSA as a biocompatible dispersant and a mediator of bioactivity (*Holt et al. 2011; Holt et al. 2012*). On the other hand, the literature on SWCNT cytotoxicity toward macrophages is consistent with our results. These immune cells can be considered the first barrier of our body since they are able to engulf infectious organisms but also external materials (*Wynn et al. 2013*). Due to their ability to internalize a high quantity of exogenous molecules, an increased sensitivity to CNTs can be easily hypothesized. In a previous study, the cytotoxic effects of either single or multi-walled CNTs toward RAW 264.7 macrophages were compared to carbon black (a material produced by the incomplete combustion of heavy petroleum products and known to be carcinogenic). The murine cell line displayed both a cyto and genotoxicity in response to all the tested materials which were able to induce necrosis, chromosomal aberrations, ultrastructural damage and apoptosis (*Di Giorgio et al. 2011*). In another recent study, pristine SWCNTs were able to induce a dose-dependent reduction of cell viability in the same cell line. The observed toxicity was related to the induction of autophagy accompanied by apoptosis and endoplasmic reticulum stress (*Park et al. 2014*). In our context, BSA protein grafted on SWCNT surface could rather protect RAW 264.7 from their cytotoxicity (Figure 5C), making BSA a good dispersant agent for the development of SWCNT-based biotechnologies.

II.3.2.2 Evaluation of a possible proinflammatory effect

The induction of a proinflammatory response by CNTs was reported previously, as described in the first chapter; therefore, we wanted to explore the cell activation and cytokine production in RAW 264.7 macrophages after exposure to our CNT samples. On the other hand, it was interesting to see if BSA protein grafted around the nanotubes could modify the macrophage immunological response to the materials as it was observed during flow cytometry analysis (Figure 5C).

For the first purpose, CD86 was chosen as readout since this molecule is expressed by macrophages upon activation (*Nolan et al. 2008*). At the end of the incubation with CNTs for 24, 48 or 72 hours, CD86 levels were evaluated by flow cytometry. Results are shown in Figure 7. In our case, no increase in CD86 expression in comparison to control cells was observed at all concentrations and

treatment times, in the case of both pristine and BSA-coated CNTs, instead they responded well to LPS, used as positive control. Surprisingly, a similar situation was found when the levels of two proinflammatory cytokines were examined by ELISA immunoassay in RAW 264.7 cellular supernatants. In particular, neither IL6 (Figure 8A), nor TNFα (Figure 8B) were found in the supernatants.

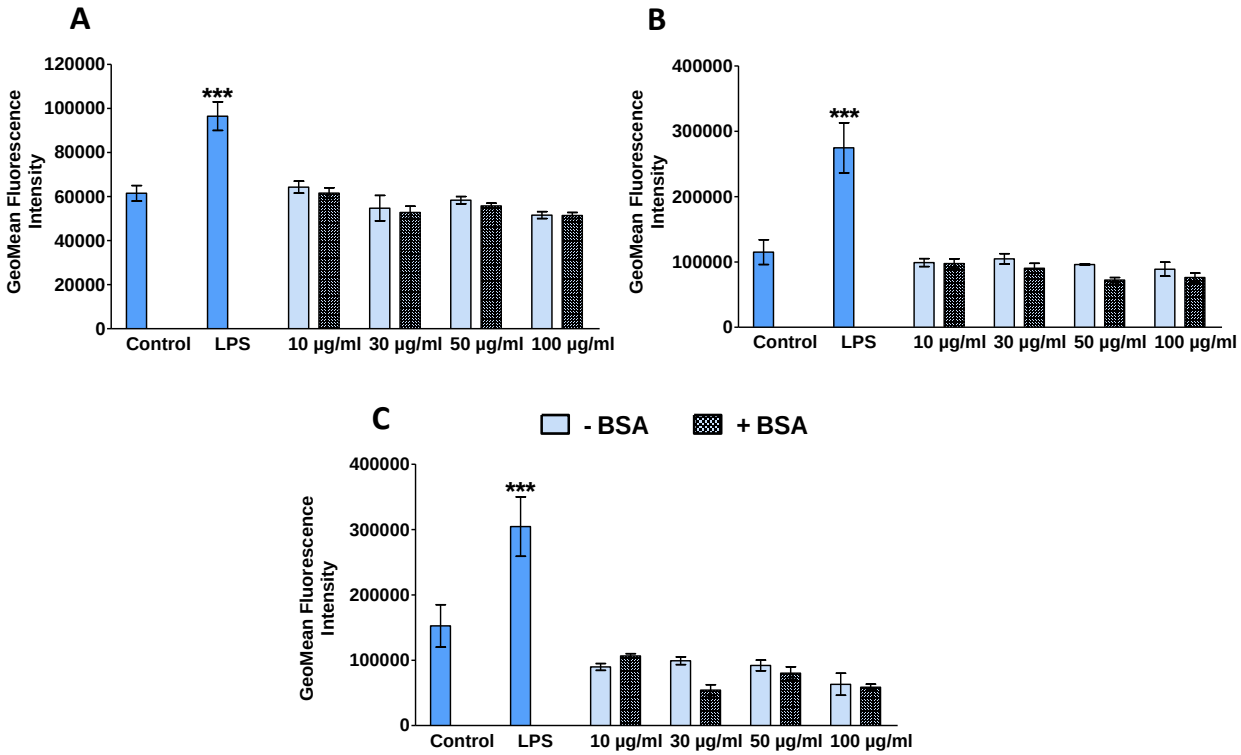

Figure 7. Flow cytometry analysis of CD86 expression in RAW 264.7 exposed to different concentrations of SWCNTs (BSA-dispersed or not) during 24 h (A), 48 h (B) or 72 h (C). Two-ways ANOVA followed by Bonferroni's post-test was performed to determine the statistical differences versus control cells and to compare the two CNT samples to each other (*p<0.05; **p<0.01; ***p<0.001).

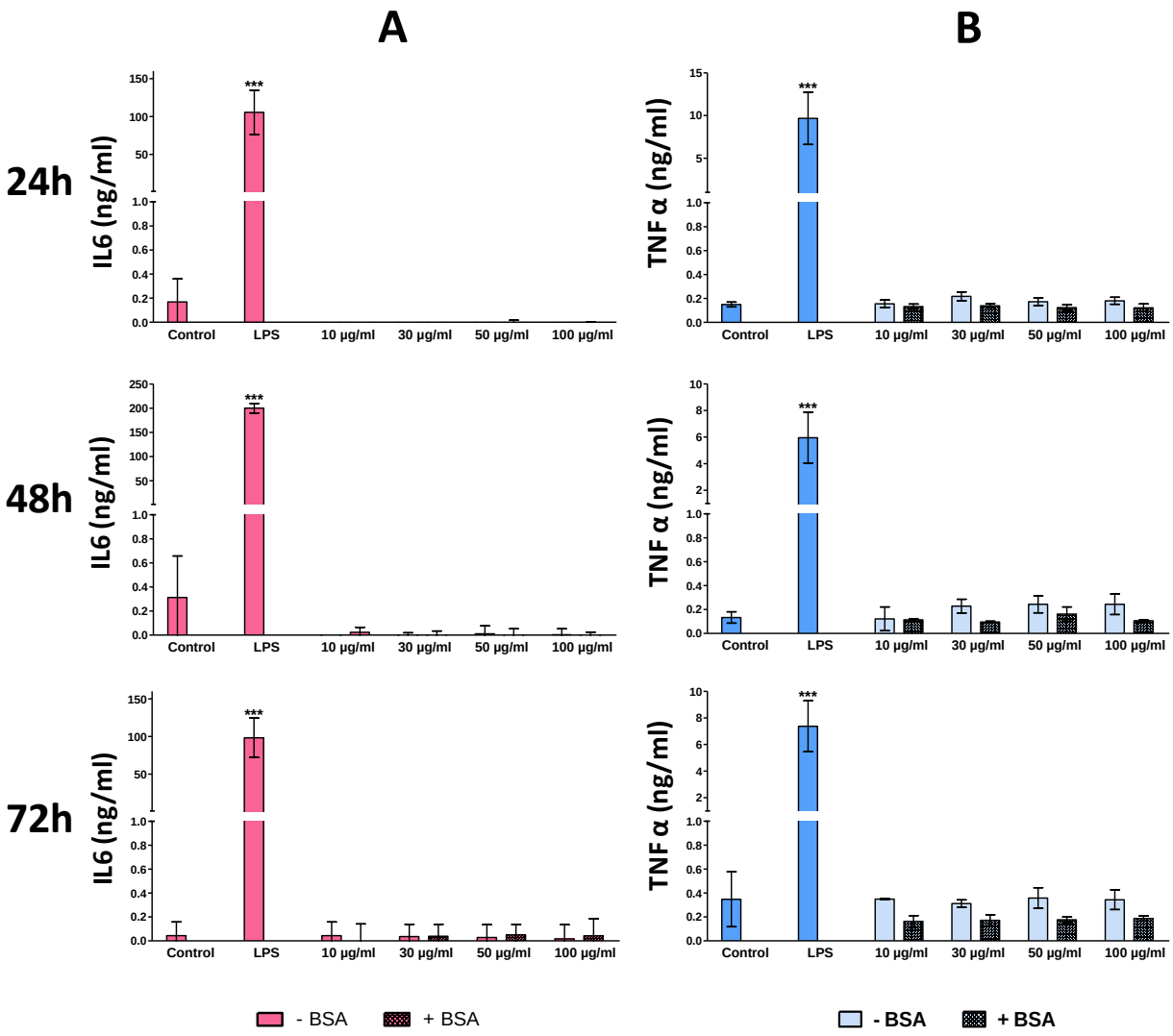

Figure 8. Cytokine production by RAW 264.7. IL6 (A) and TNF α (B) levels were determined after incubation with different concentrations of SWCNTs (BSA-dispersed or not) during 24 h (upper panel), 48 h (middle panel) or 72 h (bottom panel). Two-ways ANOVA followed by Bonferroni's post-test was performed to determine the statistical differences versus control cells and to compare the two CNT samples to each other (*p<0.05; **p<0.01; ***p<0.001).

In the work performed by Di Giorgio et al., despite SWCNTs were able to reduce RAW 264.7 cell viability, no inflammatory response was observed, result consistent with our observations (*Di Giorgio et al. 2006*). On the other hand, several *in vivo* studies showed that SWCNTs caused an acute inflammatory response in the lungs of mice as a result of the high levels of IL6 released in the organ, after exposure to pristine SWCNTs (*Park et al. 2014*). Previously, Murphy et al. revealed the mechanisms of pleural inflammation by long carbon nanotubes. Long fiber-like CNTs were able to interact with macrophages stimulating them to amplify proinflammatory response in mesothelial cells (*Murphy et al. 2012*). In fact it has been shown that *in vivo* toxicity is highly dependent upon various factors (*Dumortier 2013*) such as CNT size since shorter nanotubes could be engulfed by

macrophages and consequently cleared trough the lymphatic system unlike long CNTs (*Kostarelos 2008*). Since no effect on both RAW 264.7 activation and cytokine production was noticed in our study, it was not possible to elucidate the role of BSA protein in the protection of SWCNTs in terms of a proinflammatory response. Despite this, the use of relatively short SWCNTs together with the improvement of their solubility and stability in aqueous media are encouraging characteristics to stimulate a further exploration of BSA-SWCNT proinflammatory effect *in vivo*.

II.3.3 BSA-SWCNT cellular interaction

II.3.3.1 Observation by transmission electron microscopy

It has been demonstrated that carbon nanotubes are able to enter any cell type (*Kam et al. 2006; Kostarelos et al. 2007*). Furthermore, it has been described that functionalization of their external surface can enhance carbon nanotube water-solubility leading to an augmented cellular uptake (*Kostarelos et al. 2007; Bianco et al. 2011*). This is obvious, since a reduced rate of CNT aggregation leads to an easier penetration of isolated nanotubes trough the plasma membrane, mainly by passive diffusion. Despite these considerations, we showed that BSA is able to improve to a large extent the solubility of pristine SWCNTs in aqueous media. The observation suggested that our BSA-SWCNT complexes could be efficiently internalized even by non-phagocytic cells.

In order to verify the latter hypothesis and to investigate BSA-dispersed SWCNT internalization mechanisms, 3T6 and HEK 293 cells were exposed to 30 µg/ml CNTs for 24 hours. Samples were then processed for TEM observations. In Figure 9, it is possible to observe that BSA-coated SWCNTs were found inside both cell types. In particular, the materials were mostly packaged inside vesicles, suggesting that energy-dependent pathways were involved in the internalization (*Lacerda et al. 2012*). In addition, it appeared that the tubes could be better internalized by murine fibroblasts (A) with respect to human epithelial cells (B). The result was not surprising as fibroblasts are known to be phagocytic cells, as it was also evidenced by the presence of large vesicles in the cytoplasm. Furthermore, small bundles of CNTs were found also free in the cytoplasm (black arrow in Figure 9B). This latter observation could be the result of a passive translocation of CNTs through the plasma membrane, or escape from endosome via disruption of the organelles. Moreover, it was possible to identify some nanotubes (red arrows in Figure 9) which seem to pierce the cellular membrane perpendicularly suggesting a nanoneedle penetration mechanism (*Pantarotto et al. 2004*).

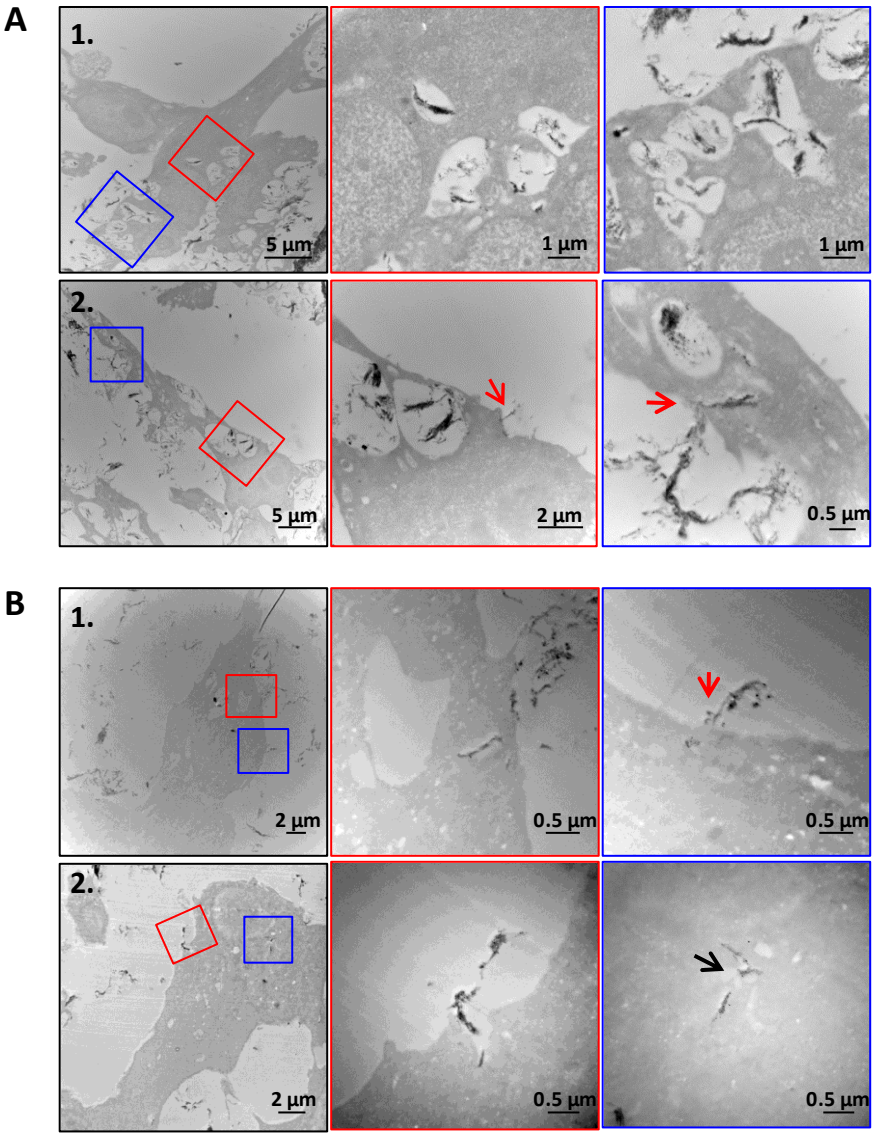

Figure 9. TEM images of 3T6 (A) and HEK 293 cells (B) incubated with BSA-SWCNTs (30 µg/ml) during 24 h. The doted areas in the left images are enlarged in the respective right pictures.

The two latter observations are in contrast with what was reported by Yaron et al. In fact they have clearly shown how pluronic-stabilized SWCNTs could penetrate HeLa cells by energy-dependent pathways but not trough passive diffusion. Furthermore, according to their model, SWCNTs were associated with vesicles but not able to disrupt them (*Yaron et al. 2011*). On the contrary, TEM analysis allowed us to observe free CNTs in the cytoplasm. Therefore the possibility of a SWCNT energy-independent internalization or endosome disruption cannot be ruled out. Further investigations involving the use of specific internalization inhibitors should be performed to better identify BSA-SWCNT specific cell internalization pathways. Finally, no CNTs were found inside the nuclei of both 3T6 and HEK 293 cells. Furthermore, the cytoplasmic and nuclear structures of both cell types were well preserved suggesting that BSA-SWCNTs did not induce cell damages. This result is consistent with what obtained by the cell viability experiments. The ability of our

BSA-stabilized materials to efficiently penetrate different cell types, without inducing cytotoxicity, makes the complexes suitable for drug delivery purposes.

II.3.3.2 Effect on the plasma membrane: electrorotational study

Although neither necrosis nor apoptosis were observed in our cellular models after exposure to the nanomaterials, we decided to investigate BSA-SWCNT impact on the cellular membrane by an unexplored technique called electrorotation. This technique was already adopted by our team, to investigate cellular toxicity mechanisms and the derived membrane damage in a number of biological models, induced by different bioactive molecules (for recent works see *Milardi et al. 2014; Stefanutti et al. 2014*). In our case, the technique was exploited for a different purpose. In fact, the ability of CNTs to interact with cell membrane and to be internalized by our cellular models, both by endocytosis or passive diffusion was observed. Therefore, CNTs bound on the cell surface or penetrating the cell, could disturb the lipid bilayer creating deformations which lead to changes in the dielectric properties of the plasma membrane.

The 3T6 cell line was chosen for this purpose, as this cellular type could interact with CNTs to a larger extent in comparison to HEK 293 cells, as observed by TEM. Thereafter, murine fibroblast were incubated or not with 100 µg/ml BSA-SWCNTs. After 24 h of exposure, cells were processed for electrorotational studies (*Arnold and Zimmermann 1988*). The technique allowed us to measure two characteristic cellular membrane parameters known as capacitance and conductance. Despite a little reduction in the cell membrane capacitance was obtained in comparison to the control (Table 2), this decrease was not significant and it was consistent in both cases with previous studies (*Milardi et al. 2014*). Furthermore conductance values were again comparable to control cells. Capacitance (C) is correlated to the plasma membrane ability to behave like a condenser, since the lipid bilayer, impermeable to ions, isolates the negatively charged internal compartment from the positively charged external layer. On the other hand, conductance (G) is associated with the plasma membrane permeability to ions. Given our results, we can conclude that BSA-SWCNT cellular interaction has little, if any, effect on plasma membrane characteristics. This is an innovative result since the impact of nanotubes on the plasma membrane dielectric characteristics and ion flux has been very poorly investigated up to date.

Table 2. Cellular membrane parameters capacitance (C) and conductance (G) determined in control 3T6 cells or in 3T6 exposed to 100 µg/ml of BSA-SWCNTs during 24 h.

	C (µF/cm^2)	SD	G (S/m^2)	SD
Ctrl	0.95	0.32	2567	416.3
BSA-SWCNTs	0.85	0.12	2550	217.9

II.4 Conclusions

In this Chapter, pure commercial SWCNTs were dispersed with BSA protein to improve their biocompatibility. The best w/w ratio able to give a good SWCNT dispersion, without relevant aggregates, was 1:5 for SWCNT and BSA. Moreover, the dispersion was stable in time as demonstrated by UV-VIS spectroscopy. The materials were tested on different cell lines, murine fibroblasts, human embryonic kidney cells or murine macophages. Cytotoxicity results obtained by several methods, showed a different responsiveness to our materials based on the specific cellular type. In particular, no changes in the cell viability profiles were monitored in the case of both 3T6 and HEK 293 cells after exposure to different concentrations of pristine or BSA-SWCNTs. On the other hand a cytotoxic effect was observed in the case of murine macrophages treated with both pristine and BSA-stabilized CNTs. Interestingly, this effect was minor when CNTs were coated with the BSA suggesting an increased biocompatibility. A possible long-term effect on 3T6 or HEK 293 cells was explored after treatment with BSA-SWCNTs and subsequent subculturing. Cellular proliferation was then determined counting the total cell number. In the case of fibroblasts, no changes in cellular proliferation compared to the control were observed, while HEK 293 cell number was reduced of about 20 % or 30 % of the control after 48 or 72 hours of subculturing in a CNT-free medium, respectively. The latter result on HEK 293 cells suggests the possibility that a cytotoxic effect could arise, in some cases, even times after the end of the exposure to the nanomaterials. Both pristine and BSA-stabilized CNTs were not able to induce an *in vitro* proinflammatory response in macrophages as investigated by cell activation and cytokine production. For this reason it was not possible to evidence a role of BSA protein in this context, suggesting that further *in vivo* studies are needed. Thanks to the good dispersion quality, BSA-SWCNTs were well internalized by both phagocytic and non-phagocytic cell types. Moreover, TEM observations suggest that the materials could penetrate the cells by a passive and energy-dependent mechanism such as endocytosis. Finally, no changes in the dielectric parameters typical of 3T6 cell membrane were detected after exposure to BSA-SWCNTs, despite their strict interaction with the plasma membrane.

Taken together, these findings suggest how the surface modification of SWCNTs with bio-compatible molecules could be advantageous and should be considered during the design and preparation of CNTs for safe biomedical application purposes.

CHAPTER III

(Adapted from the article *Muzi et al., Nanoscale* submitted)

Carbon nanotube diameter-dependent release of a cisplatin pro-drug encapsulated in their inner cavity

III.1 Introduction

Chemotherapy, either alone or in combination with surgery and radiation therapy, is widely used to treat different types of cancer. However, limited drug solubility, rapid elimination and lack of appropriate selectivity for tumor tissues causing severe side effects, are some of the drawbacks faced by current chemotherapeutics. Moreover, various cancers display both an intrinsic and acquired multidrug-resistance. As mentioned above, this phenomenon can be ascribed to the P-glycoprotein, an efflux pump able to recognize and transport the drug out from the cell once internalized, thus attenuating the drug-induced cytotoxic effect (*Thiebaut et al. 1987*).

Among all, Pt(II) cisplatin analogues, together with carboplatin or oxaliplatin, have a central role in cancer chemotherapy, including pathological targets such as testis, cervix, head and neck, ovarian and non-small-cell lung cancer (*Wang and Lippard 2005*). Pt(IV) complexes have been also synthesized as inactive cisplatin prodrugs, which can be converted to their active Pt(II) form upon cleavage of the axial ligands (*Shi et al. 2012*). On the other hand, the poor specificity of these drugs induces numerous side effects, such as nephrotoxicity, emetogenesis, ototoxicity and neurotoxicity, which limit their applications (*Rabik and Dolan 2007*). Cisplatin mechanism of action involves the formation of DNA interstrand cross-links. A so severe cellular DNA damage disrupts the normal replication and transcription processes activating cell cycle checkpoints leading to apoptosis To make this possible, once internalized, cisplatin undergoes a series of aquation reactions. The active mono-aquated form of cisplatin is a highly reactive species which can be recognized by several endogenous nucleophiles, thus making the drug potentially vulnerable and leading to a premature cytoplasmic inactivation (*Siddik 2003*). Moreover, in some cancer cells, reduction of drug accumulation is the main mechanism of cisplatin resistance. In addition to an increased expression of efflux pumps, the mechanism is also associated with the down-regulation of the plasma membrane copper transporter Ctr1 involved in cisplatin uptake. An increased DNA damage tolerance and the loss of its propagation signals to the apoptotic machinery are other downstream cellular resistance mechanisms to cisplatin (*Siddik 2003; Ishida et al. 2002; Rebucci and Michiels 2013*).

As described in the first chapter, nanomaterials can help to overcome the limitations described

above, offering great advantages to the delivery of therapeutic molecules to the tumors. They can help the delivery of drugs with poor solubility and stability, reduce their non-specific accumulation and toxicity, improve the pharmacokinetics and bioavailability and increase local drug concentrations. As a whole effect, they can enhance both drug permeability and retention at the target tissue. Several nano-carriers have been used for the delivery of platinum-based anticancer drugs including liposomes, micelles, dendrimers, polymeric nanoparticles and carbon nanotubes (*Patel et al. 2013; Oberoi et al. 2013; Wang and Guo 2013*). Among them, as already described in the first chapter, *f*-CNTs have shown to be very promising tools for biomedical applications.

In this study, a hydrophobic Pt(IV) prodrug of cisplatin was entrapped within the inner cavity of two different diameters fluorescently-labeled multi-walled CNTs and the complexes were tested for their activity on two different cellular models. A number of studies on the efficacy of cisplatin-filled carbon-based nanomaterials, in particular single-walled CNTs have been published (*Ajima et al. 2005; Feazell et al. 2007; Dhar et al. 2008; Ajima et al. 2008; Bhirde et al. 2009; Guven et al. 2012*). However, the small diameter of SWCNTs allows encapsulating lower amount of drug molecules compared to MWCNTs. Furthermore, another advantage of our complexes derives from the use of a prodrug, designed to achieve an intracellular controlled release of the cytotoxic Pt(II) species. In fact, upon chemical reduction by endogenous reducing agents such as glutathione, the prodrug can be released from the CNT cavity being converted into its active hydrophilic Pt(II) form which is able to react with DNA (Figure 1). This avoids a fast and premature drug release (unlike what happens with cisplatin), preventing also its possible inactivation (*Li et al. 2012*).

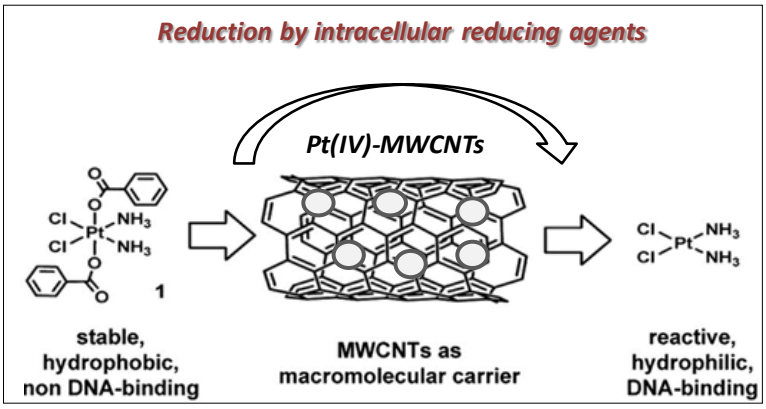

Figure 1. The design concept based on hydrophobic entrapment of a platinum(IV) prodrug within MWCNTs. (Adapted from *Li et al. 2012*).

The group of Alberto Bianco and collaborators, previously demonstrated that Pt(IV)@CNTs can significantly enhance the drug accumulation in some tissues after being intravenously injected in mice without inducing any abnormal inflammation. Moreover, both kidney and liver accumulation

were reduced thus decreasing eventual nephrotoxicity, a typical side effect of cisplatin (Li et al. 2014). For a better understanding of Pt(IV)@CNT complexes activity, in the current study, the cytotoxicity, the possible induction of a pro-inflammatory response and the cellular uptake were investigated on human cancer cells HeLa and murine macrophages RAW 264.7. The intracellular platinum accumulation after exposures to the different complexes was also explored. In addition, the effect of MWCNT diameter on the release and activity of the Pt(IV) prodrug was examined.

III.2 Experimental section

Materials

Two types of multi-walled carbon nanotubes with different diameter and length distributions were used in this study. Small diameter MWCNTs (named hereafter S-CNTs) were provided by Nanocyl (Thin MWCNT 95+ % C purity, Nanocyl 3100, batch no. 071119) and they had an average external diameter and length of 10 nm and 1.5 µm, respectively. Large diameter MWCNTs (L-CNTs) were synthesized by Prof. Ramaprabhu (Indian Institute of Technology, Chennai, India) with a purity > 95%. L-CNTs had a bigger external diameter (38 nm in average) and length ranging from 200 nm to several microns. The average inner diameter of S- and L-CNTs was 4 nm and 10 nm, respectively. To reduce their length, both types of CNTs were treated in acid conditions. After oxidation the average length of shortened S- and L-CNTs was 274 nm and 855 nm, respectively. Therefore, both types of CNTs have similar aspect ratio in the range of 19-21. To monitor the trafficking of CNTs upon interaction with cells, the nanotubes were labeled with Cy5 after an amidation step (Figure 2). Cy5 loading on the nanotube surfaces was characterized by Kaiser test and it was 235 µmol per gram of S-CNTs and 565 µmol per gram of L-CNTs. Both derivatives were filled with platinum(IV) prodrug (Figure 1) by nano-extraction procedure and the platinum content was determined by inductively coupled plasma optical emission spectrometry (ICP-OES). High Pt(IV) levels were measured inside both types of CNTs: 37.3 % and 35.6 % w/w of Pt(IV) for S-CNTs and L-CNTs, respectively. Finally Pt(IV) localization within both CNT types was evaluated by high resolution TEM (HR-TEM). S- or L-CNTs were dispersed in sterile de-ionized water (200 µg/ml) by sonicating the samples for 30´. Fresh solutions were prepared prior to cellular treatment at appropriate dilutions in complete cell culture medium.

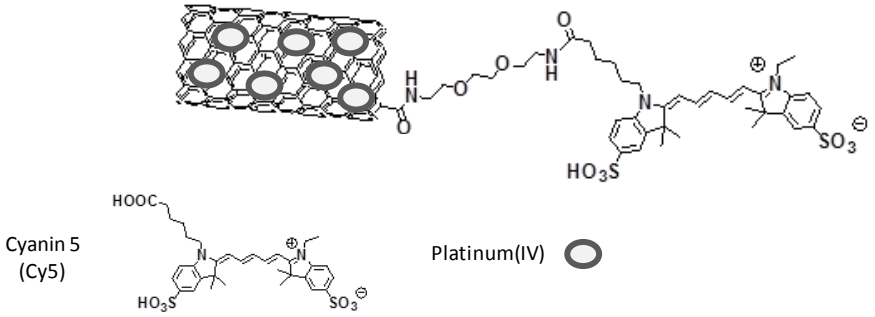

Figure 2. S- and L- CNTs derivatives after the various functionalization steps.

Cell cultures

Non-phagocytic human cervix cancer cells HeLa, were selected as a common neoplastic model to study the anticancer efficacy of the Pt(IV)@CNT samples. Phagocytitc murine macrophages RAW 264.7 were chosen to compare the behavior in two different cell systems of the conjugates and to evaluate their proinflammatory effect.

Both cell lines were purchased from ATCC (VA, USA) and were maintained in RPMI 1640 medium supplemented with 10 % heat inactivated FBS and 100 U/ml gentamycin with the addition of 50 μM β-mercaptoethanol and 20 mM HEPES for RAW 264.7 macrophages and incubated at 37 ºC in humid 5% CO_2 atmosphere. Media and solutions were purchased from Lonza. When confluency reached 70-80 %, HeLa or RAW 264.7 cells were washed with PBS, detached with trypsin or with SE buffer (PBS containing 2 mM EDTA and 2 % FBS), respectively, and subcultured every 2-3 days. Prior to CNT exposure, cells were detached, counted and reseeded in a proper well size and density (see each particular experiment for details) and allowed to adhere overnight.

Flow cytometry analysis

Cell viability

The cytotoxicity of the Pt(IV)@CNTs towards human and murine cell lines was evaluated by flow cytometry. For the first series of experiments, cells were seeded into 96-well culture plates at a density of 10^5 cells per well and allowed to adhere overnight. The cells were then exposed to our different CNT samples at drug concentrations ranging from 0.5 μM to 10 μM during 24 h. For the second series of experiments, cells were seeded into 96-well plates at a density of $2 \cdot 10^4$ cells per well and allowed to adhere overnigh. The cells were then exposed to the conjugates at Pt(IV) concentration ranging from 0.1 μM to 2 μM during 6 h before the medium was renewed with fresh

medium and cells were allowed to grow during further 72 h. In both experiments, the free drug and the empty CNTs were used as control and the corresponding CNT concentrations were back-calculated from Pt(IV) loading inside CNTs while DMSO (20 %) was used as cellular death positive control. After incubation, RAW 264.7 supernatants were collected and kept at -20 ºC for further investigations and cells were harvested with SE buffer (RAW 264.7) or tripsinized (HeLa) and stained with both FITC-Annexin V and propidium iodide as previously described in chapter II. The percentage of live, early apoptotic and late apoptotic/necrotic cells was determined by acquiring at least 15.000 events using a Gallios flow cytometer (Beckman Coulter, Villepinte-France) and analysing the data with FlowJo software.

Cell activation

RAW 264.7 cell activation was explored through CD86 expression level. Briefly, cells were seeded as previously described for both cell viability experiments. After incubation with CNTs cells were detached with SE buffer and stained with PE-Rat anti-Mouse CD86 antibodies (Clone GL1, BD Pharmingen 553692), prior to flow cytometry acquisition. Lipopolysaccharide (LPS, 1 μg/ml) in combination with interferon γ (IFN γ, 1 ng/ml) was used as cell activation positive control. The CD86 associated fluorescence intensity was determined by acquiring at least 15.000 events using a Gallios flow cytometer (Beckman Coulter, Villepinte-France) and analysing the data on live cell gated population (AnnV-/PI-) with FlowJo software.

Cellular uptake

HeLa and RAW 264.7 cells were seeded into 24-well plates at a density of $2 \cdot 10^5$ cells/well and allowed to adhere overnight prior to exposure to Pt(IV)@CNTs at drug concentration ranging from 1 μM to 7.5 μM during 6 or 24h. After incubation, cells were washed twice with PBS, detached with trypsin (HeLa) or with SE buffer (RAW 264.7) and analyzed by flow cytometry. The mean fluorescence intensity of at least 25.000 events was measured using a Gallios flow cytometer (Beckman Coulter-Villepinte, France) and the data on live cell gated population were analyzed with FlowJo software.

Cytokines determination

RAW 264.7 macrophages supernatants were collected after treatment for flow cytometric analysis of cell viability and the levels of murine pro-inflammatory cytokines tumor necrosis factor alpha (TNF α), and interleukine-6 (IL6), were detected by a double sandwich ELISA. Lipopolysaccharide (LPS, 1 μg/ml) in combination with interferon γ (IFN γ, 1 ng/ml) was used as pro-inflammatory cytochine production positive control. The detailed procedure was described previously in chapter II.

Transmission electron microscopy

For TEM observation, cells were seeded into 24-well plates on glass coverslips at a density of $5 \cdot 10^5$ cells per well and allowed to adhere overnight prior to exposure to 10 µg/ml of empty or Pt(IV)@CNTs during 6 or 24 h. (See chapter II for the detailed preparation protocol).

Inductively coupled plasma atomic emission spectroscopy (ICP/AES)

For the analysis of the intracellular platinum content, HeLa or RAW 264.7 were seeded in quadruplicate into 6-well plates at a density of $6 \cdot 10^5$ cells per well and allowed to adhere overnight prior to exposure to the free drug or to Pt(IV)@CNTs at a platinum concentration of 1 µM during 6 h. Cells were then detached as previously described and the cells in the 4 wells were collected together in a glass vial. Samples were then subjected to ICP/AES analysis on an Agilent 7500ce apparatus.

Statistical analysis

The experiments shown are a summary of the data from at least three separate experiments run in triplicate for each cell line (HeLa, RAW 264.7). Data are presented ± SEM. Statistical analyses were performed using a two-way ANOVA test followed by Bonferroni's post-test. All p values < 0.05 were considered significant.

III.3 Results and discussion

III.3.1 Cell viability after exposure to P(IV)@CNTs

As a first step in our investigation, the cytotoxicity of the two different Pt(IV)@CNTs compared to the free drug was evaluated in cells with different characteristic and origin. For this purpose, human cervix cancer cells HeLa (non-phagocytic) and murine macrophages RAW 264.7 (phagocytic) were chosen. As previously described, nanotubes, defined as S- and L-CNTs, differ only in their diameter and length, whereas they have similar aspect ratio and drug loading. In an initial experiment, cells were incubated with the free drug or with Pt(IV)@CNT complexes at Pt(IV) concentrations ranging from 1 to 15 µM (HeLa) or from 0.5 to 10 µM (RAW 264.7) during 24 h. The corresponding amount of CNTs used was back-calculated from the loading of the prodrug inside the tubes (Table 1). As Pt(IV) loading inside S- and L-CNTs was rather similar (37.3% and 35.6%, respectively), almost equal concentrations of the two CNT types were used. At the end of the incubation, cell viability was determined by flow cytometry.

Table 1. Concentrations of Pt(IV), Small Pt(IV)-CNTs and Large Pt(IV)-CNTs used for the cell treatment. The corresponding MWCNTs concentrations were back-calculated from Pt(IV) loading inside MWCNTs.

Pt(IV) molar concentration (μM)	Pt(IV) (μg/ml)	Small Pt(IV)-MWCNTs (μg/ml)	Large Pt(IV)-MWCNTs (μg/ml)
0.1	0.05	0.15	0.15
0.2	0.11	0.29	0.30
0.5	0.27	0.72	0.76
1	0.54	1.45	1.52
2	1.08	2.90	3.00
3.5	1.89	5.07	5.31
5	2.70	7.24	7.58
7.5	4.05	10.86	11.38
10	5.40	14.48	15.17
15	8.10	21.75	22.80

Results are shown in Figure 3. In the case of HeLa cells (Figure 3A), a concentration-dependent cytotoxicity was observed with both CNT samples and also the free drug. Furthermore, there was no significant difference comparing the free drug to Pt(IV)@L-CNTs in the whole concentration range. On the contrary, both the free drug and the larger CNTs were more cytotoxic compared to the smaller ones.

This first experiment allowed us to demonstrate the role of MWCNT diameter in the release of the embedded drug. As previously described, hydrophobic Pt(IV) prodrug is selectively released by chemical reduction and hydrophobicity reversal from the inner cavity of CNTs by reducing agents, being converted in its active Pt(II) species (*Li et al. 2012*). In view of this, a plausible hypothesis to explain the different efficacy of the two CNT samples could be represented by a limited accessibility to the intracellular reducing agents, such as glutathione, in the case of MWCNTs with smaller diameter compared to the larger tubes. Consequently, the active form of the drug could be released more slowly by S-CNTs compared to L-CNTs, thus explaining their lower cytotoxicity after 24 hours.

On the other hand, RAW 264.7 cells displayed a general higher sensitivity to the samples compared to HeLa cells. In fact, same dose-dependent cytotoxicity but at lower concentrations was observed in RAW 264.7 cells (Figure 3B). Moreover, the free drug was significantly more effective compared to both Pt(IV)@L-CNTs and Pt(IV)@S-CNTs. This is consistent with the results obtained after exposure to 20% DMSO used as positive control. In fact, the residual cell viability was about 50 % in the case of HeLa and 0 % in RAW 264.7, suggesting an overall higher sensitivity of the murine macrophages with respect to the other cell line. Despite this, as observed in HeLa cells, Pt(IV)@S-CNTs were again less cytotoxic compared to Pt(IV)@L-CNTs, result consistent with the previous hypothesis.

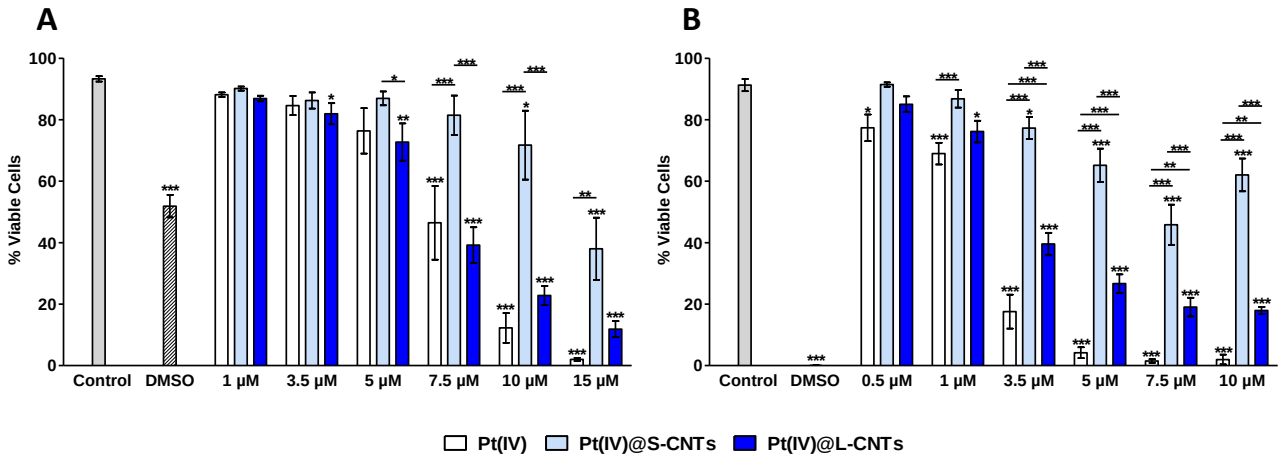

Figure 3. Flow cytometry analysis of cell viability in HeLa cells (A) and RAW 264.7 cells (B) exposed to different concentrations of Pt(IV)@CNTs for 24 h. AnnV-/PI- live cells are shown in this graph. Two-ways ANOVA followed by Bonferroni's post-test was performed to determine the statistical differences *versus* control cells and to compare the two CNT samples to each other and to Pt(IV) (*p<0.05; **p<0.01; ***p<0.001).

As a slower release of the encapsulated drug was hypothesized in the case of S-CNTs compared to L-CNTs, long-term cell viability experiments were performed. For this purpose, both HeLa and RAW 264.7 cells were incubated with the free drug or CNTs at concentrations ranging from 0.1 to 2 µM Pt(IV) for 6 hours before the medium was renewed with fresh medium and cells were allowed to grow during further 72 h. In this experiment, HeLa cells began to show a significant mortality compared to the control already at 0.2 µM Pt(IV) concentration for both CNT samples (Figure 4A). In this case, Pt(IV)@S-CNT cytotoxicity was comparable to the free drug although they were poorly effective after 24 hours even at higher concentrations. The gain of function of Pt(IV)@S-CNTs after a relatively long period of time is fully consistent with our hypothesis. In fact, the intracellular reducing agents had more time to induce the release of the drug from the small diameter CNTs, resulting in a higher cytotoxicity. On the other hand, the larger CNTs induced higher cellular mortality in comparison to both the free drug (from 0.5 to 1 µM) and the smaller ones (from 0.5 to 2 µM) even though they showed same cytotoxicity as the free drug in the previous experiment. This again supports our explanation. In contrast to the first experiment, the two CNT samples but also the free drug displayed a negligible cytotoxicity on RAW 264.7 cells (Figure 4B) in comparison to HeLa response. In fact, the residual viability after the treatment with all the conjugates was not less than 75% up to a drug concentration of 1 µM for both the free drug and the CNTs. In the examined concentration ranges, the free drug was more cytotoxic compared to the Pt(IV)@CNTs and there was no difference on the effect between the two CNT types. This result can be rationalized by a "recovering" of the murine macrophages after a relatively short exposure to

low concentrations of the conjugates, contrarily to HeLa cells, while a continuous exposure to high doses of the complexes during 24 h induced a severe cytotoxicity.

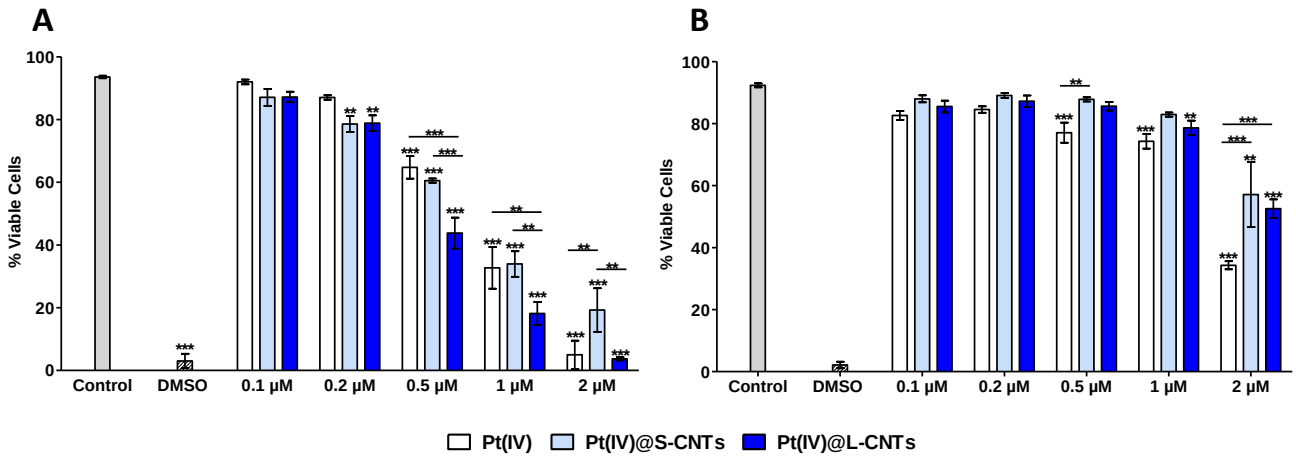

Figure 4. Flow cytometry analysis of cell viability in HeLa cells (A) and RAW 264.7 cells (B) exposed to different concentrations of Pt(IV)@CNTs for 6 h and allowed to grow for further 72 h. AnnV-/PI- live cells are shown in this graph. Two-ways ANOVA followed by Bonferroni's post-test was performed to determine the statistical differences *versus* control cells and to compare the two CNT samples to each other and to Pt(IV) (*p<0.05; **p<0.01; ***p<0.001).

It has to be noticed that the observed toxicity on the two cell types was only due to Pt(IV)@CNT hybrids. In fact, no reduction in cell viability was detected after exposure to same concentrations of the empty nanotubes during 24 hours (Figure 5A and B for HeLa and RAW 264.7, respectively) or during 6 hours, followed by a cellular growth of another 72 hours (Figure 5C and D for HeLa and RAW 264.7, respectively).

The results obtained on the cell viability experiments demonstrate the efficacy of both Pt(IV)@CNT complexes and suggest their possible use as nanovectors for anticancer drugs. Moreover, as already mentioned, one of the advantages of our complexes is the use of a platinum(IV) prodrug that can be reduced to release the cytotoxic compound cisplatin upon entry into the cells. The advantages of Pt(IV)@CNT complexes compared to Pt(II)@CNT, leveraging on the greater aqueous stability of Pt(IV) prodrugs, has already been demonstrated by the Lippard and collaborators (*Feazell et al. 2007; Dhar et al. 2008*). In their previous reports, the Pt(IV) prodrug was non-covalently linked on the external surface of CNT, while in our work, the drug was entrapped within the inner cavity of CNTs. This strategy of hydrophobic entrapment shields the prodrug from premature inactivation (*Siddik 2003*) and enables controlled drug release by reduction, contrary to Pt(II) complexes, that are rapidly extruded from the cavity (*Li et al. 2012*). In this report, we demonstrated that the diameter of CNT plays an important role in determining the rate of drug

release and directly affects the efficacy of the Pt(IV)@CNT construct. Therefore, CNT diameter should be taken into account when in the design and fine-tuning of these delivery vectors.

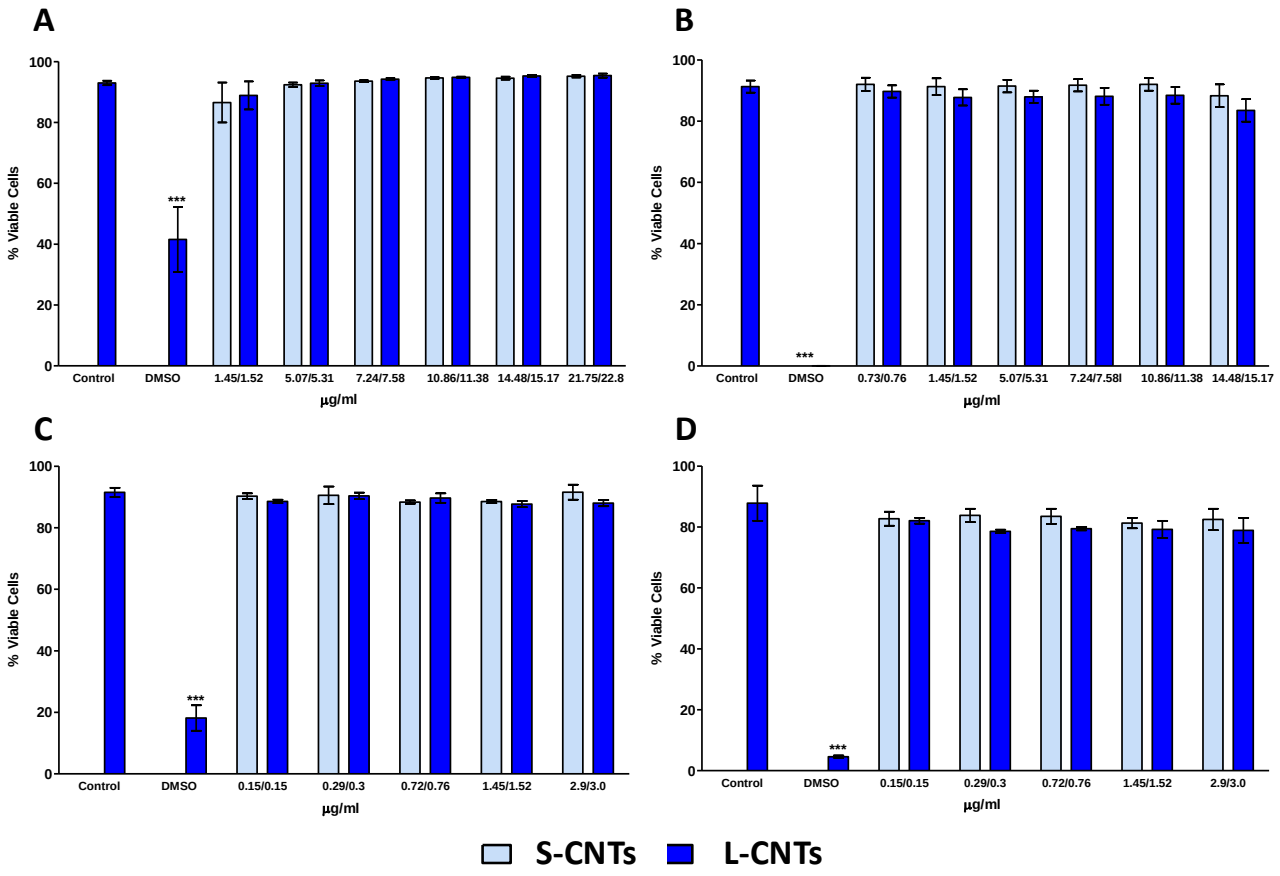

Figure 5. Flow cytometry analysis of cell viability in HeLa or RAW 264.7 cells exposed to different concentrations of empty-CNTs during 24 h (panels A and B for HeLa and RAW 264.7, respectively) or 6 h followed by a cellular growth of another 72 h (panels C and D for HeLa and RAW 264.7, respectively). AnnV-/PI- live cells are shown in this graph. Two-ways ANOVA followed by Bonferroni's post-test was performed to determine the statistical differences *versus* control cells and to compare the two CNT samples to each other (*p<0.05; **p<0.01; ***p<0.001).

III.3.2 PT(IV)@CNT effect on macrophage activation

Avoiding inflammation is of primary importance, especially in cancer therapy, where its insurgency can also play decisive roles at different stages of tumor and affects responses to the therapy (*Coussens and Werb 2002; Grivennikov et al. 2010*). As mentioned previously, the induction of a pro-inflammatory response is an important issue of investigation in the case of CNTs (*Qu et al. 2012; Wang et al. 2013*). Therefore, cell activation and cytokine production by RAW 264.7 macrophages were explored after exposure to all CNT samples. Once again, macrophages were chosen since they can be considered the primary sentinels of our body to infectious organisms but also to exogenous materials (*Wynn et al. 2013*). For the first purpose, CD86 expression was again

chosen as appropriate readout of macrophage activation. Thereforee, RAW 264.7 cells were treated with different concentrations of CNTs as previously described in the case of the cell viability experiments (from 0.5 to 10 µM for 24 h or from 0.1 to 2 µM for 6 h followed by a further 72 h cell growth). CD86 expression on live cell gated population was then measured by flow cytometry. After 24 hours (Figure 6A), a significant increase in CD86 expression compared to the control and the free drug was observed for the two types of CNTs, starting from a Pt(IV) concentration of 3.5 µM. Moreover, at this concentration, a major activation in the case of Pt(IV)@L-CNTs was observed in comparison to Pt(IV)@S-CNTs. This behavior was not measured at higher concentrations. In fact, while in the case of S-CNTs CD86 expression followed a concentration-dependent trend, its levels decreased as the concentration of the L-CNTs increased. This can be explained by the fact that L-CNTs promoted a higher cell mortality at a drug concentration higher than 3.5 µM compared to the smaller tubes (Figure 3B). Therefore, the observed reduction of CD86 expression could be due to the death of highly activated cells that were consequently not detected. On the other hand, while the cytotoxicity experiments showed an increased responsiveness of HeLa cells to low Pt(IV)@CNTs concentrations 72 h after a 6 h exposure (Figure 4A), only a slight RAW 264.7 activation ($^{*}p<0.05$) at the highest Pt(IV)@CNT doses was observed (Figure 6B). Furthermore, there was no difference between the two CNT types.

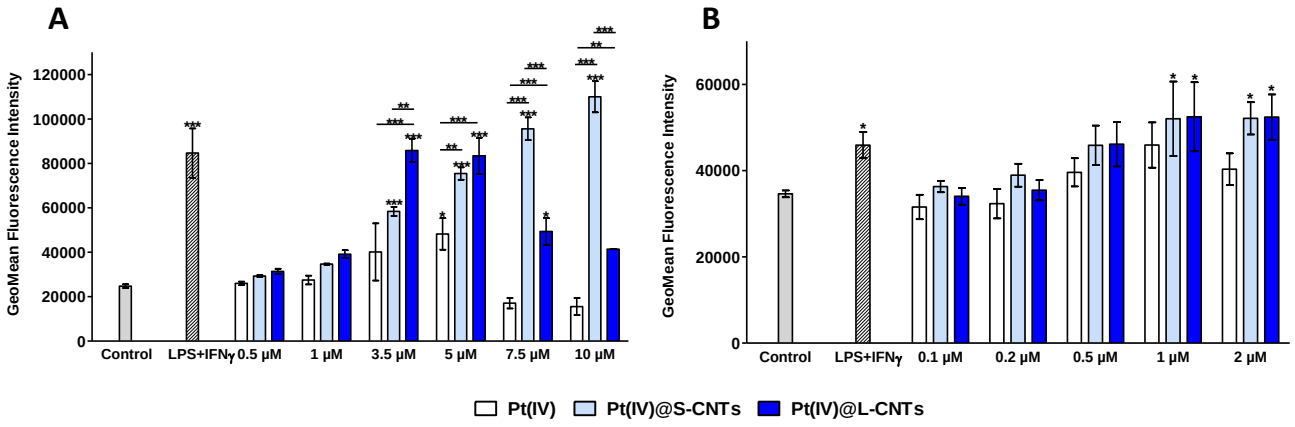

Figure 6. Flow cytometry analysis of CD86 expression in RAW 264.7 exposed to different concentrations of Pt(IV)@CNTs for 24 h (A) or 6 h and allowed to grow for further 72 h (B). Two-ways ANOVA followed by Bonferroni's post-test was performed to determine the statistical differences versus control cells and to compare the two Pt(IV)@CNT samples to each other and to Pt(IV) (*p<0.05; **p<0.01; ***p<0.001).

To investigate further the macrophage activation profile in response to the conjugates, the cell culture supernatants were collected from the previous experiments on RAW 264.7 macrophages and the levels of two pro-inflammatory cytokines (IL6 and TNF α) were determined by ELISA. After a

24 hour treatment, no IL6 production was detected in the supernatants (Figure 7A).

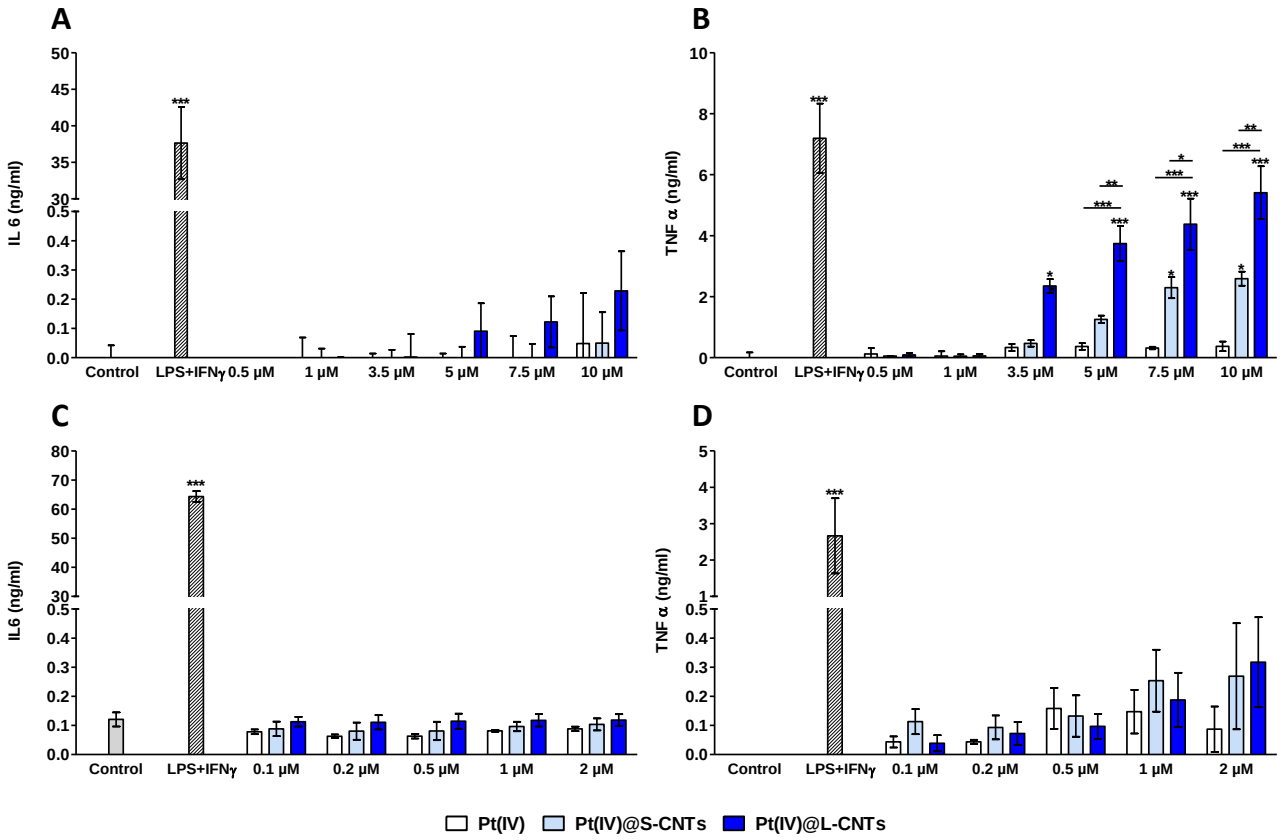

Figure 7. Cytokine production by RAW 264.7. IL6 (A) and TNF α (B) levels were determined after incubation with different concentrations Pt(IV)@CNTs for 24 h or after the cells were grown for further 72 h after a 6 h treatment (C and D for IL6 and TNF α, respectively). Two-ways ANOVA followed by Bonferroni's post-test was performed to determine the statistical differences versus control cells and to compare the two Pt(IV)@CNT samples to each other and to Pt(IV) (*p<0.05; **p<0.01; ***p<0.001).

On the contrary, the TNF α secretion started to rise significantly, as compared to the control, from a 3.5 µM Pt(IV) concentration in the case of L-CNTs (Figure 7B). A minor effect on TNF α production was detected after treatment with Pt(IV)@S-CNTs. In fact a significant difference between the two types of nanotubes, starting from 5 µM Pt(IV), could be observed. This is consistent with the previous result obtained for RAW 264.7 cell activation. Before the cells started to display a high mortality rate, we could observe a more important increase in CD86 levels concerning the largest CNTs in comparison to the smaller tubes (Figure 6A). On the other hand, neither IL6 nor TNF α production were detected 72 hours after the 6 hour cellular exposure to the different complexes at concentrations ranging from 0.1 to 2 µM Pt(IV) (Figure 7C and D, respectively). This experimental observation is again consistent with the data obtained previously (Figure 6B), where only a slight macrophage activation was observed. We can also exclude an intrinsic MWCNT pro-inflammatory action (*Pescatori at al. 2013*) because no effect on cell

activation or cytokine production was observed after exposure to the two empty CNT species (Figure 8).

Taken together the results on cell activation and cytokines production encourage further *in vivo* investigations in view of their possible use as nanovectors for cancer therapy. Obviously, as is the case of most drugs, safety is dependent on Pt(IV)@CNTs concentrations.

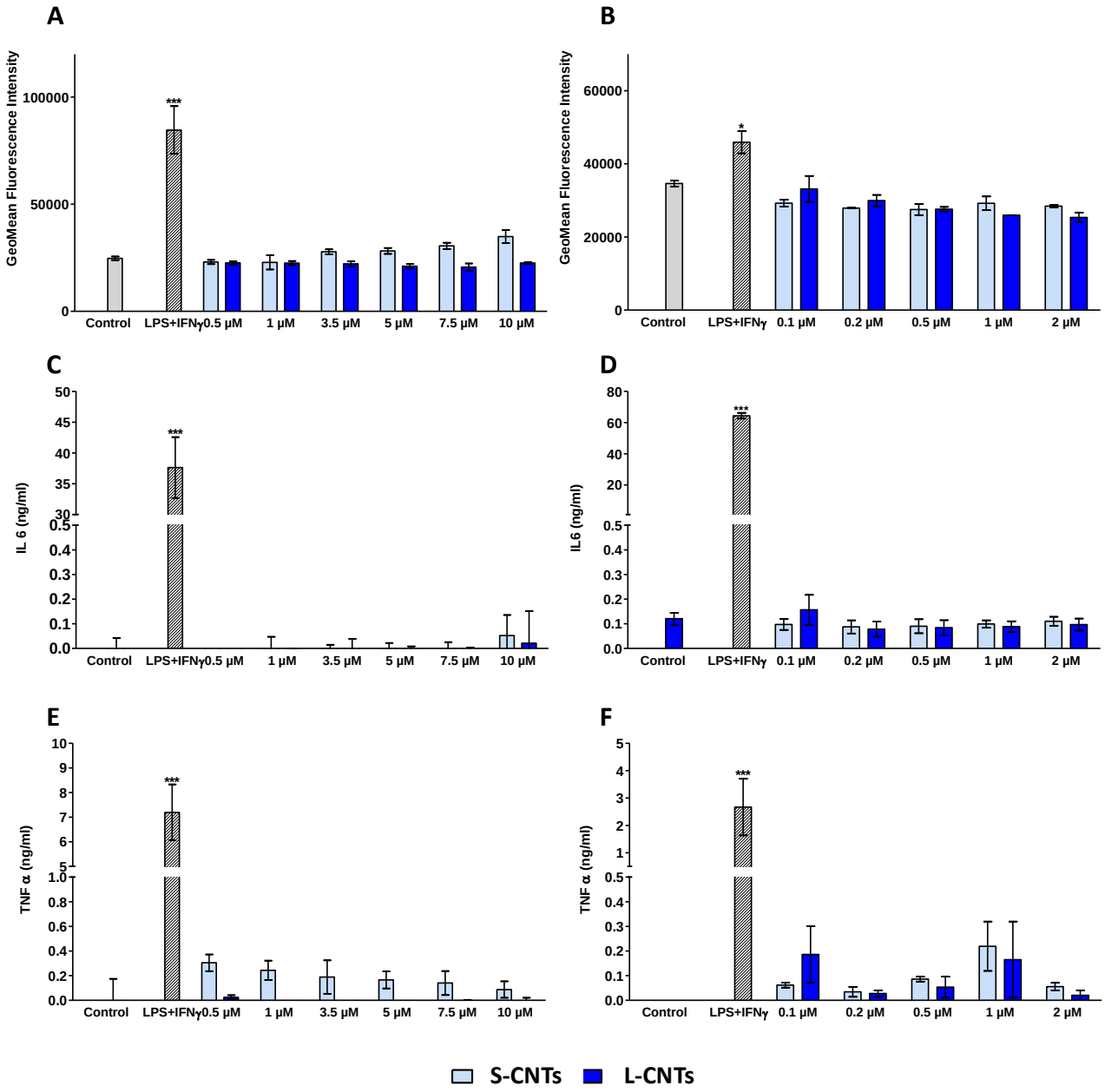

Figure 8. Flow cytometry analysis of CD86 expression in RAW 264.7 exposed to different concentrations of empty MWCNTs for 24 h (A) or 6 h and allowed to grow for further 72 h (B). IL6 and TNF α production by RAW 264.7 cells after exposure to empty MWCNTs for 24 h (C and E) or after cells were allowed to grow for 72 h after a 6 h exposure to CNTs (D and F). Two-ways ANOVA followed by Bonferroni's post-test was performed to determine the statistical differences versus control cells and to compare the two Pt(IV)@CNT samples to each other and to Pt(IV) (*$p<0.05$; **$p<0.01$; ***$p<0.001$).

III.3.3 PT(IV)@CNT cellular uptake

The results obtained with the cell viability experiments evidenced that the Pt(IV)@CNTs can preserve the cytotoxic activity of the encapsulated Pt(IV) prodrug. In fact, upon cellular exposure to the complexes, a reduction in cancer cell viability was observed and it was comparable to the free drug, or even increased in the case of Pt(IV)@L-CNTs (Fig. 6A). These results suggested an efficient drug transport inside the cells and thus the cellular internalization of both CNT complexes. To confirm and visualize the CNT cellular uptake and possibly identify its mechanisms, HeLa or RAW 264.7 cells were exposed to 10 µg/ml of S- or L-CNTs during 6 h and the samples were processed for TEM observations. Both CNT types were found inside the human and murine cells, thus confirming their cellular uptake (Figure 9). In more details, aggregation of CNTs inside vesicles can be observed in all cases. This suggests an endocytic (HeLa) or phagocytic (RAW 264.7) internalization pathway (*Kostarelos et al. 2007; Lacerda et al. 2012*). It was also possible to identify some CNTs free into the cytoplasm. The latter observation is consistent with the previously reported ability of CNTs to penetrate the cells by passive diffusion as nanoneedles (*Kostarelos et al. 2007*). In fact, upon inhibition of energy-dependent internalization pathways, CNTs can be still internalized by different types of cells, as it has been reported in a previous work performed in our laboratories (*Lacerda et al. 2012*). On the other hand, the free CNTs could be the result of endosome rupture. In Figure 9, a single CNT outside the endosome is evidenced by a red arrow. Such behavior is particularly relevant, as nanomaterial ability to escape from the endolysosomal network could facilitate the drug access to its target (*Chou et al. 2011*). No CNTs were found into the nucleus of the two cell types. Despite this, the drug was able to reach the nucleus and exert its function blocking DNA replication (*Cepeda et al. 2007*) as evidenced by the cellular viability experiments. Besides the nuclear DNA, the free drug could have triggered apoptosis also by affecting the mitochondrial DNA or by other mechanisms, such as damage of cytoplasmic proteins or of the cytoskeleton (*Gonzalez et al. 2001*). A model for Pt(IV)@CNT activity mechanism could first consist on their internalization by both passive diffusion or endocytosis/phagocytosis. The internalized CNTs could be then transported throughout the endolysosomal pathway, subsequently escaping from these compartments and slowly release the Pt(II) active form of the drug within the cytoplasm (*Li et al. 2012*). Finally, the free drug translocates into the nucleus or to the mitochondrion exerting its cytotoxic function. Finally, the same TEM observations were carried out after an incubation of 24 hours with Pt(IV)@CNTs. In this case, a strong impairment of the general cellular structure due to the transported drug effect could be observed. Some examples are reported in Figure 9C (HeLa) and D (RAW 264.7), in which the cytoplasm of both cell lines shows a wide presence of vacuoles and lysis residues.

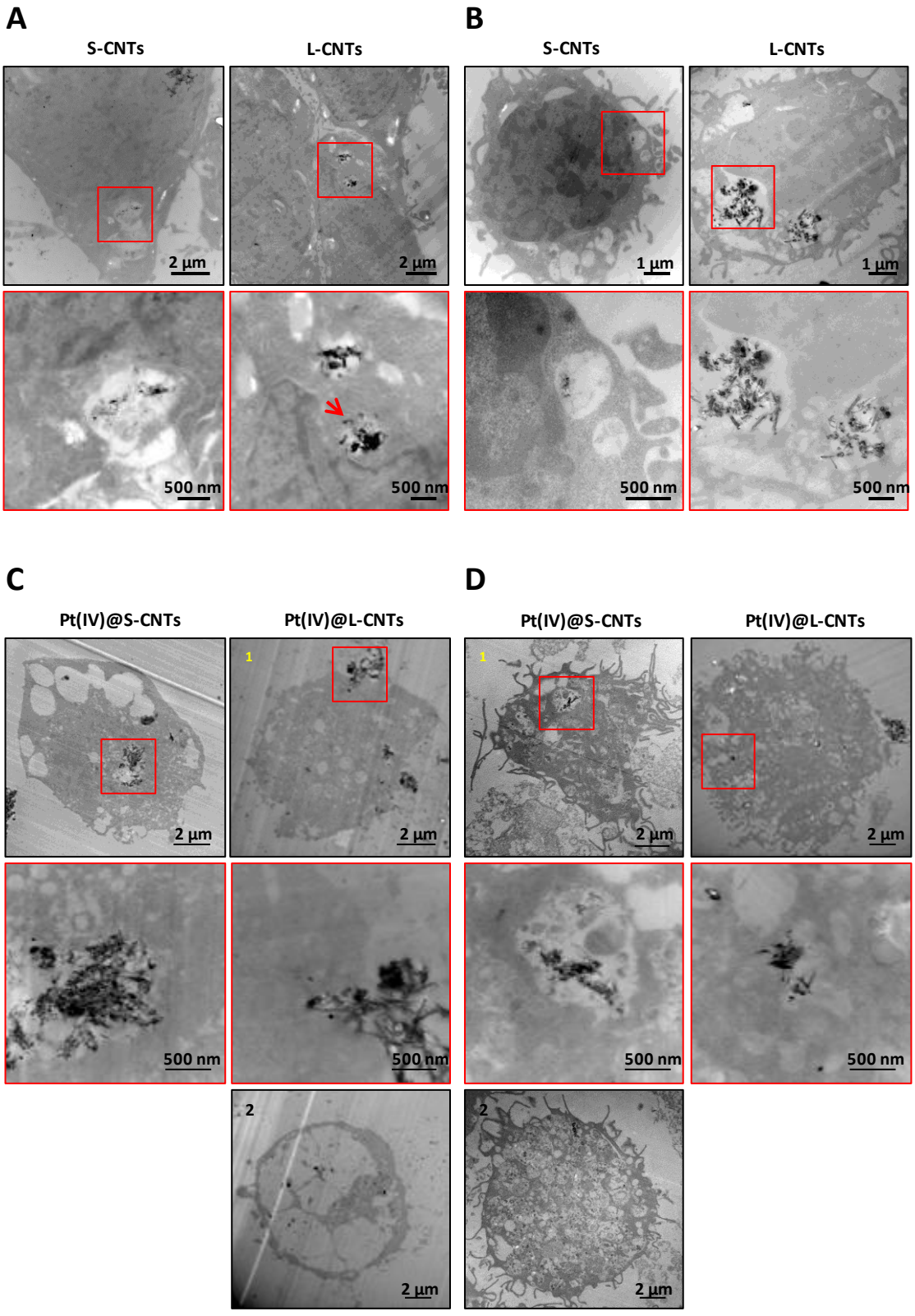

Figure 9. TEM images of HeLa (A) and RAW 264.7 (B) incubated with MWCNTs (10 µg/ml) during 6 h or with the same concentration of Pt(IV)@CNTs during 24 h (panels C and D for HeLa and RAW 264.7, respectively). When identified, the doted area in the top image is enlarged in the respective bottom picture.

The cellular uptake of Pt(IV)@CNTs was also followed by flow cytometry thanks to the functionalization with the Cy5 fluorophore (Figure 10). A fluorescence shift of HeLa (Figure 10A) or RAW 264.7 (Figure 10B) cell populations (corresponding to the Cy5 on the CNT surface) in comparison to the control was observed, thus confirming their intracellular uptake. We can assert that only a negligible amount of fluorescence could be derived from the CNTs interacting with the cellular surface as the samples were extensively washed before the analysis.

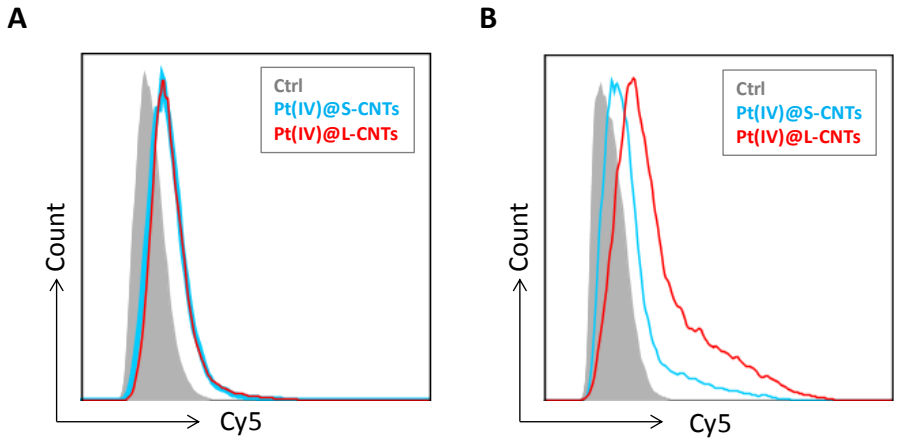

Figure 10. Flow cytometry analysis of Pt(IV)@CNTs (10 µg/ml) HeLa (A) or RAW 264.7 (B) cellular uptake. The histogram is relative to one of three representative experiments.

III.3.4 Analysis of the cellular platinum content

Flow cytometry analysis did not allow for a precise quantification of Pt(IV)@CNTs inside the cells as the occurrence of fluorescent quenching phenomena by CNTs could not be excluded (*Chiu et al. 2011*).

For this reason we used ICP/AES to quantitatively analyze the cellular content of platinum into HeLa and RAW 264.7 macrophages after a 6 h exposure to 1 µM of both free Pt(IV) and Pt(IV)@CNT samples. It is important to remark that almost equal concentrations of the two CNT types were utilized, as Pt(IV) loading inside S- and L-CNTs was rather similar (Table 1). As shown in Figure 11A and B, an increase in the cellular platinum content (both entrapped or released) compared to the free drug could be observed for both CNT conjugates in the two cell lines. In particular, the amount of platinum inside both HeLa and the macrophages was about two times higher compared to the free drug when the cells were exposed to Pt(IV)@S-CNTs. Concerning Pt(IV)@L-CNTs, the increase in the intracellular drug accumulation compared to free Pt(IV) was again more evident. In fact the platinum amount found inside HeLa and RAW 264.7 cells was about three and four times higher, respectively, compared to the free drug. Such results allow also quantifying the CNT cell internalization. Interestingly, not a great difference in the ability to

internalize the complexes between HeLa and RAW 264.7 cells was observed. In fact, as macrophages are phagocytic cells, a major CNT uptake compared to HeLa cells was expected. This was not the case, demonstrating the ability of non-phagocytic cells to internalize a considerable amount of Pt(IV)@CNTs by endocytosis or by passive diffusion (*Lacerda et al. 2012*). On the other hand, L-CNTs were able to enter both cell types more efficiently as compared to S-CNTs; this result is consistent with their higher cytotoxicity after 24 hours (Figure 3). However, although less internalized, Pt(IV)@S-CNTs showed a cytotoxicity comparable to Pt(IV)@L-CNTs in HeLa cells during the long–term cell viability experiment (Figure 4A). The latter observation evidences how the slower Pt(IV) release by CNTs having smaller diameter could be advantageous to achieve an enhanced long-lasting cytotoxicity against tumor cells, compared to CNTs with larger diameter.

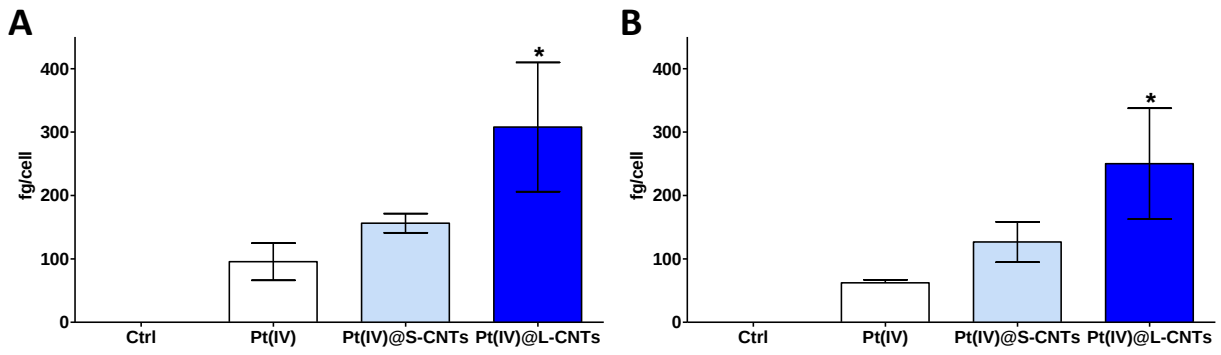

Figure 11. ICP/AES analysis of cellular platinum content in HeLa (A) and RAW 264.7 cells (B) exposed to Pt(IV) or to Pt(IV)@CNTs (1 μM) for 6 h. One-way ANOVA followed by Bonferroni's post-test was performed to determine the statistical differences versus control cells and to compare the two Pt(IV)@CNT samples to each other and to Pt(IV) (*$p<0.05$; **$p<0.01$; ***$p<0.001$).

The results obtained by the cell uptake experiments are encouraging, given the well-documented problems in cisplatin cancer therapy. In fact, despite being one of the most potent antitumor agents known, cisplatin's decreased intracellular accumulation is one of the main mechanisms of resistance to the drug (*Wang and Lippard 2005; Siddik 2003*). The results show that our Pt(IV)@CNTs complexes could promote the drug accumulation inside the cells. This, together with the slow drug release achieved by using S-CNTs as Pt(IV) carriers, could result in an enhanced drug cytotoxicity and retention into cancer cells compared to the free drug.

III.4 Conclusions

In this study, an hydrophobic Pt(IV) prodrug of cisplatin was entrapped within the cavity of two functionalized MWCNTs having different inner diameters. The complexes were tested for their activity on two different cellular models. The activity of the entrapped drug was preserved in both conjugates and the role of the CNT diameter in the release time of the encapsulated drug was demonstrated. Both Pt(IV)@CNT complexes induced negligible cell activation and no pro-inflammatory cytokine production on RAW 264.7 macrophages 72 h after the end of the treatment. Both samples were efficiently internalized by the two types of cells and higher platinum levels were found in the cells after Pt(IV)@CNT exposure, compared to the cells treated with the free drug. Our study shows that *f*-MWCNTs are promising nano-carriers to improve the accumulation of a chemotherapeutic drug inside the cells and demonstrates that the CNT diameter is an important parameter to consider in the preparation of the complexes. In particular, a smaller CNT diameter could be advantageous, allowing a slower drug release inside tumor cells compared to CNTs with larger diameter. This behavior could allow the drug to be retained in tumor cells and exert its function over a longer period of time. Future studies will include evaluation of the Pt(IV)@CNT constructs in both sensitive and Pt-resistant cell lines, to assess whether these nanocarriers are not only efficient transporters and delivery systems for chemotherapeutics, but they are also able to overcome the cisplatin-associated resistance due to P-glycoprotein efflux pump mechanisms. Pt(IV)@CNTs conjugates could be also tested *in vivo* in tumor-bearing mice cancer model after intra-tumoral injection. In addition, the CNT external surface could be further conjugated with a specific targeting moiety; this will allow targeting the tumor upon systemic administration in mice, exploiting also the enhanced permeability and retention effect. *In vivo* biodistribution experiments of Pt(IV)@CNTs are also currently under investigation.

CHAPTER IV

Graphene biological impact and possible use for cell targeting

IV.1 Introduction

As extensively described in the first chapter, graphene is considered the most promising new material to be exploited for various applications. In particular, some interesting works has been performed in the last few years; the main scope was to explore the use of graphene, especially in its oxidized form (GO), for widespread biomedical application, ranging from drug/gene delivery, bio-sensing and imaging, antibacterial activity and tissue engineering (*Shen et al. 2012; Liu et al. 2013; Goenka et al. 2014; Shi et al. 2014*).

In view of its possible use in biomedicine, studying the toxicity level of graphene is of fundamental importance. Being a quite new type of nanomaterial, limited data are present in literature on the impact of graphene on health and environment. Moreover, similarly to carbon nanotubes, graphene toxicity can be strongly dependent on the graphene form, size and grade of purity; the effects are also dependent on the particular cellular type tested or on the concentration used (*Bianco 2013*). Understanding the impact of this material on the immune cells is also a major goal. In fact, it has been proposed that nanomaterials could be used to directly modulate the immune system enhancing the efficacy of immune-based therapies against a variety of pathologies including also cancer proliferation. This applies to both graphene alone, or conjugated with specific molecule (*Orecchioni et al. 2014*). To investigate further the impact of graphene in a biological environment, we started with the comparison of the bioactivity of different graphene types towards two different cellular models. For this purpose, different experiments were performed exploiting the diverse techniques already described in the previous chapters. In particular, cell viability and activation were investigated in HeLa and RAW 264.7, for the reasons illustrated above, after exposure to non-purified or purified few layer graphene (FLG1 and FLG2, respectively) and to two commercial types of graphene oxide (GO-A and GO-N, respectively). Furthermore, the most promising GO material was also tested in murine intraperitoneal primary macrophages (mIPM).

On the other hand, graphene-based nanomaterials have been also used for targeted drug delivery purposes. In fact, one of the main goals in biomedicine is the design of therapies able to act specifically towards the diseased cell population without affecting the normal cells. This would avoid unwanted side effects. A good strategy to achieve efficient specificity is to conjugate drug carriers with specific ligands that can recognize molecular signatures: an over-expressed outer-membrane receptor is, for instance, a good candidate for drug targeting. This strategy may apply to

anticancer therapy and autoimmune diseases where specific therapies, depleting specific cell types, are unavailable. The ability of GO to target selectively tumor cells has been reported. One example is the work by Zhang et al. (*Zhang et al. 2010*) where GO was covalently conjugated with folic acid (FA) to target in a specific manner human breast cancer cells over-expressing FA receptors. The study showed an increased efficacy of FA-GO conjugates, carrying also two anticancer drugs, as compared to GO loaded with the drugs only. In the last part of my PhD work, the ability of the two types of commercial GO to target specifically a B cell model was investigated. For this purpose, the GO samples were non-covalently conjugated with Hen Egg Lysozyme (HEL). The ability to target A20 cells, genetically modified to over-express B cell receptor (BCR) recognizing the same enzyme, was examined.

IV.2 Experimental section

Materials

Few layer graphene samples were provided by I. Janowska (ICPEES, Strasbourg). The FLGs were generated through a simple, fast and low cost production protocol with high yield (*Janowska et al. 2012*). The procedure is a chemical-free method consisting of mechanical ablation of pencil lead on a harsh glass surface with simultaneous ultrasonication. The high purity sample (FLG1) was thermally treated to eliminate potentially adsorbed toluene between the graphene layers (FLG2). The average size of the FLG sheets was about 2 μm. FLG obtained by this method, consists mainly of 1 to 20 sheets that, occasionally, can go up to fifty sheets. The two samples of oxidized graphene (GO) were purchased as monolayer powder from Antolin Grupo (GO-A) or NanoInnova (GO-N). According to the manufacter's information, GO flake thickness was between 0.7-1.2 nm (corresponding to 1 to 2 flakes of GO), while they had an average size of few micrometers. GO samples were further characterized by dynamic light scattering, measurement of the zeta-potential and TEM observations. FLG samples were briefly sonicated in complete cell culture medium at a concentration of 100 μg/ml and diluted to the proper concentration prior to use (Figure 1A). Fresh FLG dispersions were prepared prior to each cellular exposure while GO solutions were prepared as 1 mg/ml stocks in deionized water (Figure 1B) and were properly diluted in complete culture medium before each cellular treatment.

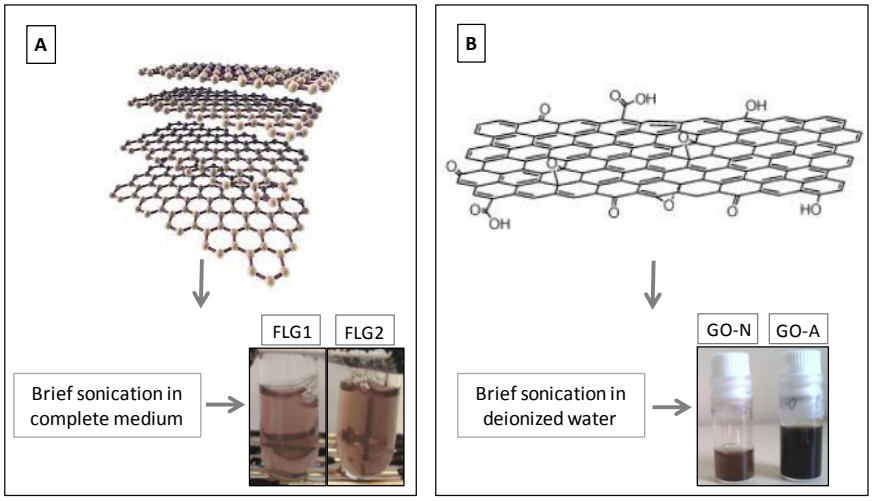

Figure 1. Scheme of preparation of the different graphene samples. FLG1 and FLG2 sample preparation is described in panel A while the two commercial GO samples (NanoInnova or Antolin) are shown in panel B.

Conjugation of graphene oxide with Hen Egg Lysozyme

Lysozyme has a strong and selective adsorption on graphene oxide (*Li S et al. 2014*). Aqueous dispersions of GO-A or GO-N (1 mg/ml) were obtained by adding 10 ml of deionized water to 10 mg of GO, followed by a 10 min sonication in a cold water bath. HEL (L6876, SIGMA) was added step-by-step following the adsorption on the GO surface by UV-Vis spectroscopy. In particular, after each addition of HEL to the GO solution, the complexes were left interact for at least 2 hours and then an aliquot was taken and centrifuged in order to precipitate GO. The supernatants were then analyzed in order to assess the presence of unbound HEL. HEL spectra were obtained analyzing the absorption in the wavelength range of 200-400 nm with a Varian Cary 5000 UV-VIS-NIR absorption spectrophotometer. Twelve mg of HEL were added in total obtaining a GO-HEL ratio of 1:1.2. The reaction was performed for 24 h, under stirring at 4 ºC. The samples were then filtered through a 0.1 µm pores membrane. The filtration process was repeated 3 times, washing the GO samples with deionized water between each step. The GO samples were then subjected to exhaustive dialysis through a 300 kDa MWCO. At the end of the dialysis GO-A and GO-N were lyophilized for 3 days. The filtration and dialysis membranes were purchased from Millipore and Spectrum Laboratories, Inc., respectively. To verify the HEL amount on the GO surface, the complexes were characterized by thermogravimetric analysis (TGA) on a TGA1 (Mettler Toledo). Briefly, by this technique the weight of a substance is monitored as a function of temperature or time as the sample specimen is subjected to a temperature program in a controlled inert atmosphere. Organic molecules have a specific degradation profile (weight loss) that is proportional to the amount of the given molecule.

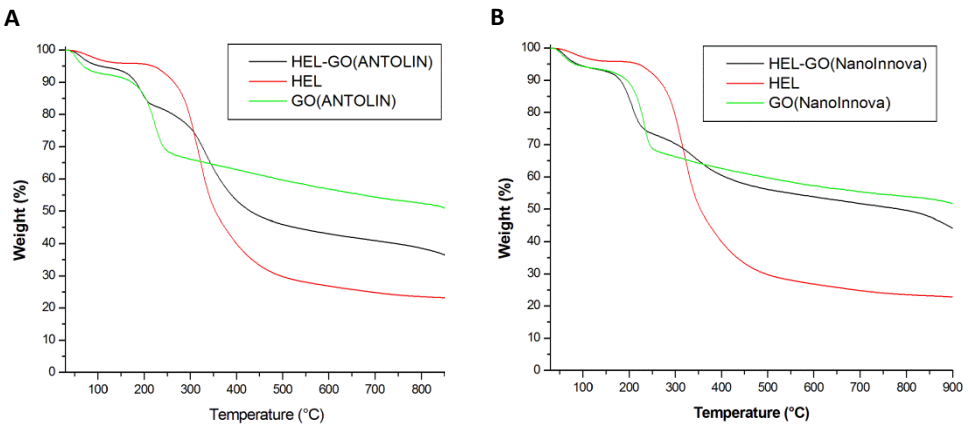

Figure 2. TGA profiles of GO-HEL conjugates (Antolin, panel A or NanoInnova, panel B). In each graph the weight loss of GO (green curve), GO-HEL (black curve) and free HEL (red curve) are shown.

Comparing GO-HEL profiles to the free GO profiles it was possible to determine the quantity of HEL adsorbed on GO surface. In particular, the estimated HEL loading was about 18.9 % w/w in GO-A (Figure 2A) and about 4.8 % w/w in GO-N (Figure 2B), measured at 600 °C. The difference in loading between the two samples could be easily explained by the fact that GO-A was better dispersed in water compared to GO-N, thus exposing a larger surface area for HEL binding. Dispersions were freshly prepared prior to cellular treatments by brief sonication of GO-HEL conjugates in complete medium, at a concentration of 500 µg/ml.

Cell cultures

Human cervix cancer cells and murine macrophages were chosen to compare the behavior of our various graphene samples (non-purified or purified FLG and commercial GO from Antolin or Nanoinnova) in non-phagocytic (HeLa) and in phagocytic (RAW 264.7) cells and to evaluate their proinflammatory effect. Cells were cultured as previously described (see chapter II for detailed protocol). Prior to graphene exposure, cells were detached, counted and reseeded in proper well size and density (see each particular experiment for details) and allowed to adhere overnight. The two commercial GO samples were further tested on a model of primary macrophages. In particular, mature and quiescent murine intraperitoneal macrophages (mIPM) were isolated from healthy untreated C57BL/6 mice (Charles River) by successive washes of the peritoneal cavity (Cohn A. 1978) with complete RPMI 1640 medium (medium supplemented with 10 % heat inactivated FBS and 100 U/ml gentamycin with the addition of 50 µM β-mercaptoethanol and 20 mM HEPES). Cells when then seeded in proper well size and density (see each particular experiment for details) and incubated overnight at 37 ºC in humidified air containing 5% CO_2 prior to graphene exposure. For cellular targeting purpose, mouse B lymphoma cells A20, wild type or over-expressing B cells

receptor (BCR) able to specifically recognize HEL, named A20 D1.3, were kindly provided by Helene Dumortier's group (IBMC, Strasbourg). Both cell lines were maintained in RPMI 1640 medium supplemented with 10 % heat inactivated FBS and 100 U/ml gentamycin with the addition of 50 μM β-mercaptoethanol and 20 mM HEPES incubated at 37 ºC in humidified air containing 5% CO_2. Cells were subcultured each 2-3 days and maintained between $1 \cdot 10^5$ and $1 \cdot 10^6$ cells/ml. Media and solutions were purchased from Lonza.

Flow cytometry analysis

Cell viability

The cytotoxicity of the various graphene samples towards human and murine cell lines was evaluated by flow cytometry. Hela and RAW 264.7 cells were seeded into 96-well culture plates at a density of $1 \cdot 10^5$ cells per well and allowed to adhere overnight. The total cells obtained from peritoneal washings were seeded into same culture plates at a density of about $1.5 \cdot 10^5$ and allowed to adhere overnight. Cells were then exposed for 24 h to different concentrations of the graphene samples ranging from 1 to 100 μg/ml. After incubation, HeLa and RAW 264.7 cells were stained with both FITC-Annexin V and propidium iodide as previously described (see chapter II for details) while the culture supernatants were collected and kept at -20 ºC for further investigations. The percentage of live, early apoptotic and late apoptotic/necrotic cells was determined by acquiring at least 30.000 events using a Gallios flow cytometer (Beckman Coulter, Villepinte-France) and analyzing the data with FlowJo software. Peritoneal cells were stained with FITC-AnnexinV/PI as previously described, and with APC-anti Mouse F4/80 antibodies (Clone BM8, eBioscience 17480182), cellular surface macrophages marker (*Zhang X et al. 2008*). At least 50.000 events were acquired using the same instrument and the percentage of live, early apoptotic and late apoptotic/necrotic cells were determined on both F4/80 positive and F4/80 negative gated populations by FlowJo software.

Cell activation

RAW 264.7 and mIPM cell activation was explored through CD86 expression as previously described. Briefly, after incubation with graphene, the cells were harvested and stained with PE-Rat anti-Mouse CD86 antibodies (Clone GL1, BD Pharmingen 553692), prior to flow cytometry acquisition. Lipopolysaccharide (LPS, 1 μg/ml) in combination with interferon γ (IFN γ, 1 ng/ml) was used as cell activation positive control. The CD86 associated fluorescence intensity in RAW 264.7 macrophages was determined by acquiring at least 30.000 events using a Gallios flow cytometer (Beckman Coulter, Villepinte-France) and analyzing the data on live cell gated population (AnnV-/PI-) with FlowJo software. CD86 levels in mIPM were determined acquiring

50.000 events using the same instrument and analyzing the CD86 fluorescence intensity on F4/80 positive and AnnV-/PI- cell population.

Targeting of A20 D1.3 cells with GO-HEL conjugates

For cellular targeting purpose, 50 µl of different concentrations of GO-HEL, free HEL or free GO (diluted in PBS 2 % FBS) were mixed with 20 µl of A20 wild-type or A20D1.3 diluted in the same buffer in a 96-well V-bottom plates ($0.5 \cdot 10^6$ cells/well) and incubated at 4 ºC during 30 min in order to avoid any protein internalization. Cells were then washed with PBS 2% FBS and stained with Biotin-Rabbit Anti-Mouse HEL antibodies diluted in the same buffer, at 4 ºC during 15 min. The antibody was provided by Helene Dumortier's group and it was produced in rabbit by the following protocol: upon injection of HEL soluble, the antibody was isolated by affinity chromatography Anti-IgG (DEAE Affi-Gel Blue Gel Biorad Ref 153-7307) and labelled with biotin-X-NHS (Calbiochem ref 203188). After washing the samples with PBS 2 % FBS, cells were further incubated with PE-Streptavidine (BD Pharmingen 554061), diluted in the same buffer, at 4 ºC during 15 min. Cells were then again washed and analyzed using a Gallios flow cytometer (Beckman Coulter, Villepinte-France) acquiring at least 30.000 events. Data were analyzed with FlowJo software.

Cytokine determination

RAW 264.7 or mIPM supernatants were collected after treatment for cell viability experiment and the levels of murine proinflammatory cytokines tumor necrosis factor alpha (TNF α), interleukine 6 (IL6) and interleukine-1β (IL1β) were detected by a double sandwich ELISA. LPS (1 µg/ml) in combination with IFN γ (1 ng/ml) was used as proinflammatory cytokine production positive control. Polyvinyl microtiter plates (Falcon) were coated overnight at 4 °C with 50 µl/well of purified Hamster Anti-Mouse/Rat TNF α (BD Pharmingen 557516) or purified Rat Anti-Mouse IL6 (BD Pharmingen 554400) or Purified Anti-Mouse IL1β (BD Biosciences 51-26661E from ELISA Set 559603) diluted in 0.05 M carbonate buffer, pH 9.6. After washings with PBS containing 0.05 % Tween (PBS-T), a saturation step was performed by adding 100 µl/well of PBS containing 10% FBS for 1 h at 37 °C. After washings with PBS-T, 50 µl/well of culture supernatants or Recombinant Mouse TNF (BD Pharmingen 554589) or Recombinant Mouse IL6 (BD Pharmingen 554582) or Recombinant Mouse IL1β (BD Biosciences 51-26666E from ELISA Set 559603), diluted in PBS-10% FBS, were added for 2 h at 37 °C. Plates were then washed with PBS-T and 50 µl/well of secondary Biotin Rabbit Anti-Rat/Mouse TNF (BD Pharmingen 557432) or Biotin Rat Anti-Mouse TNF (BD Pharmingen 554402) or Biotinylated Anti-Mouse IL1β (BD Biosciences 51-26662E from ELISA Set 559603), diluted in PBS-10% FBS, were incubated for 1 h at 37 °C. Plates

were washed with PBS-T, and 50 µl of streptavidin conjugated to horseradish peroxidase diluted in PBS 10% FBS were added per well. After 30 min incubation at 37 °C, plates were washed extensively and the enzymatic reaction, revealing the presence of cytokines in the tested supernatants, was visualized by adding 75 µl/well of 3,3',5,5'-tetramethylbenzidine diluted in 0.1 M citrate buffer, pH 5, in the presence of H_2O_2. The resulting absorbance was measured at 450 nm after the reaction was stopped with 25 µl/well of HCl 1 N.

Targeting of A20 D1.3 cells with GO-HEL conjugates

To follow HEL-BCR recognition, IL2 secretion was chosen as readout of B cells activation. For this purpose, 200 µl of A20 wild-type or A20D1.3 cells were seeded into 96-well cell culture plates at a density of $2 \cdot 10^6$ cells/ml in different concentrations of GO-HEL, free HEL or free GO. After 24 hours, the plates were centrifuged and supernatants were collected and kept at -20 °C until the ELISA test.

ELISA was performed with a mouse IL2 ELISA set (BD OptEIA™ 555148) according to the manufacturer protocol. Plates were washed extensively and the enzymatic reaction, revealing the presence of IL2 in the tested supernatants, was visualized by adding 75 µl/well of 3,3',5,5'-tetramethylbenzidine diluted in 0.1 M citrate buffer, pH 5, in the presence of H_2O_2. The resulting absorbance was measured at 450 nm after the reaction was stopped with 25 µl/well of HCl 1 N.

Transmission electron microscopy observations

For TEM observation, mIPM were seeded into 24-well plates on glass coverslips at a density of $3 \cdot 10^6$ cells per well and allowed to adhere overnight prior to exposure to 100 µg/ml of GO from Antolin or Nanoinnova (See chapter II for the detailed preparation protocol).

Sodium Dodecyl Sulphate-PolyAcrylamide Gel Electrophoresis (SDS-PAGE)

GO-A or GO-N, conjugated with HEL, were dispersed in water or in RPMI complete cell culture medium at concentration of 1.3 mg/ml or 5 mg/ml, respectively. The concentrations were chosen to have the same quantity of lysozyme in both samples, according to the loading of the enzyme on the GO surface (determined by TGA). Samples in RPMI were incubated for 2 h or 24 h at 37 °C. The same samples were then subjected to ultracentrifugation for 5 min to precipitate all GO and the supernatants were collected. Twenty µl amount of the obtained supernatants were then loaded in a 4–20% polyacrylamide gel (Mini-PROTEAN® TGX™, BIO-RAD), together with free HEL solution, complete RPMI alone and GO-A/GO-N-HEL in water (20 µl, corresponding to 25.4 µg or 100 µg of GO-A and GO-N, respectively). The HEL amount was the same in all samples (4.8 µg). Protein migration was performed at 180 V in a tris/glycine/SDS buffer (BIO-RAD) using an

electrophoresis apparatus (BIO-RAD). The gel was then stained over-night with Coomassie Brilliant Blue G-250 (BIO-RAD), prepared according to manufacturer's instructions.

Statistical analysis

The experiments shown (where it is not otherwise specified) are a summary of the data from at least three separate experiments run in triplicate for each cell line. Data are presented ± SEM. Statistical analyses were performed using a two-way ANOVA test followed by Bonferroni's post-test. All p values < 0.05 were considered significant.

IV.3 Results and discussion

IV.3.1 Assessment of the cell viability in response to different types of graphene

As a first step in our study, HeLa (non-phagocytic) or RAW 264.7 (phagocytic) cells were incubated for 24 hours with concentrations ranging from 1 to 100 µg/ml of the different graphene samples. At the end of the incubation, the cell viability was determined by flow cytometry. Results are shown in Figure 3. In the case of HeLa cells, no reduction of cell viability was observed for FLG1 and FLG2 (panel A); the sale result was also found for GO-A and GO-N samples (panel C). In the case of RAW 264.7 cells exposed to FLG1 or FLG2 (panel B), only a slight non significant decrease of cell viability (of about 5 %) was monitored. On the other hand, any cytotoxic effect was observed in the case of the two GO types (panel D). Furthermore, no difference between the effects of the two FLG samples or between the two commercial GO complexes was evidenced.

Since primary cells can show a different sensitivity to nanomaterials with respect to tumor cell lines and are a more representative model in view of a future bioapplication, the cytotoxicity of GO, subsequently used for the cellular targeting strategy, was further investigated using intraperitoneal murine primary macrophages (mIPM). Indeed, understanding the GO effect toward this immune cell population is of great interest as the material could be exploited in different biomedical contexts where macrophages are involved. In fact, macrophages are found in all tissues where they can exert a large number of different functions. They have roles in development, homeostasis, tissue repair and immunity. Despite their great role in maintaining the normal physiological condition, they can also be associated to several pathologies. For this reasons, macrophages have also emerged as important therapeutic targets in many human diseases such as neurodegenerative or autoimmune diseases, cancer and fibrosis (*Wynn et al. 2013*).

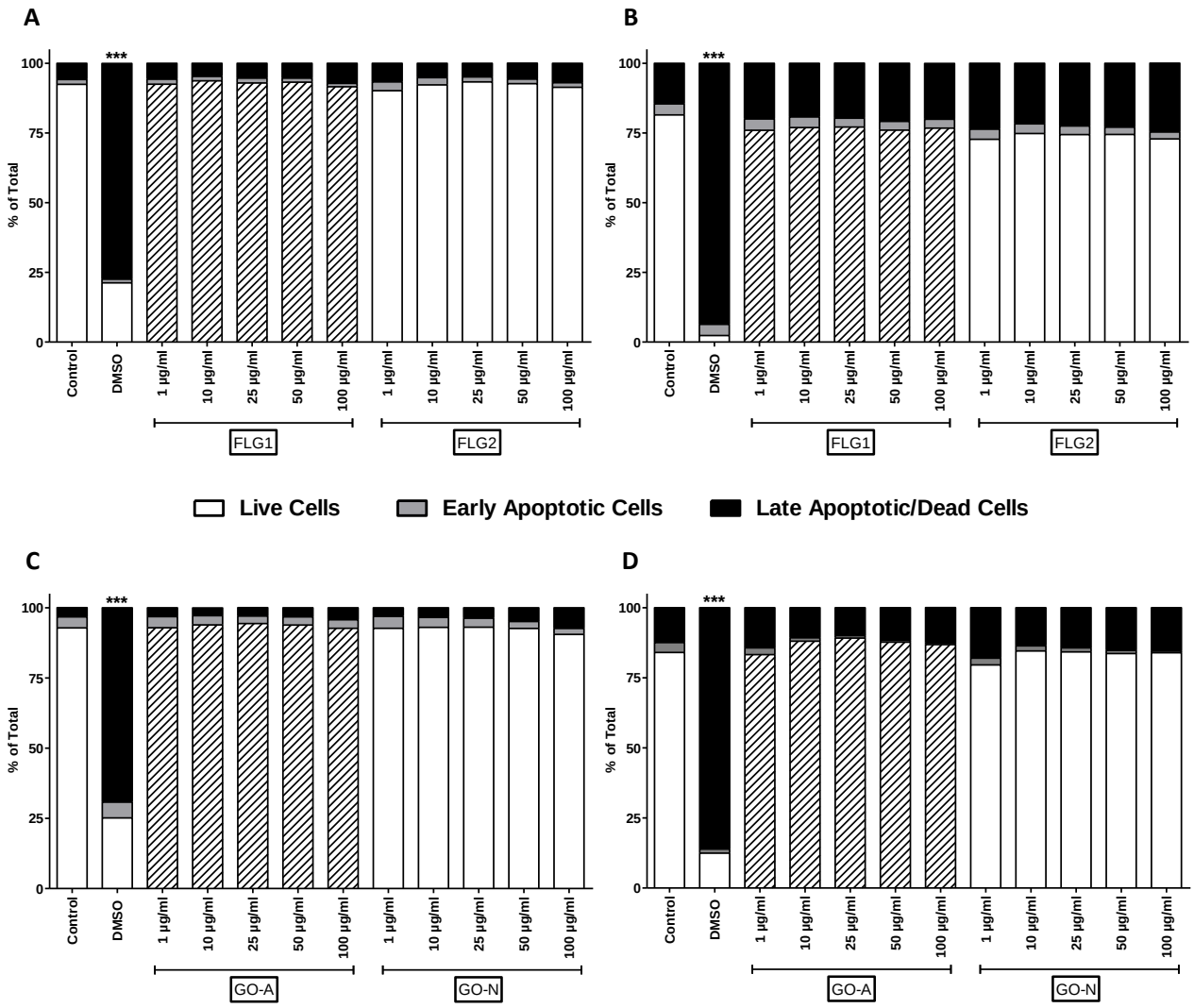

Figure 3. Flow cytometry analysis of cell viability in HeLa cells exposed to different concentrations of FLG1 and FLG2 (A) or GO-A and GO-N (C) during 24 h. Same analysis was performed in RAW 264.7 cells exposed to FLG1 and FLG2 (B) or GO-A and GO-N (D) during the same time. Two-ways ANOVA followed by Bonferroni's post-test was performed to determine the statistical differences *versus* control cells and to compare the different graphene samples to each other (*p<0.05; **p<0.01; ***p<0.001).

To investigate the behavior of GO toward mIPM, immune cells were collected from the peritoneal cavity of non-stimulated mice. Despite these fluids harbor a number of different immune cells including B cells and T cells, the presence of a high number of naive macrophages (about 30 %) makes the peritoneal cavity a preferred site for the collection of resident macrophages (*Zhang et al. 2008)*. The cells were therefore incubated for 24 hours with concentrations ranging from 1 to 100 µg/ml of GO-A or GO-N and analyzed by flow cytometry. Cell viability was determined on both F4/80 positive gated population (about 25-30 % of total) corresponding to macrophages (*Zhang et al. 2008*), and F4/80 negative gated population. It was clearly observed a selective cytotoxic effect towards the macrophage population concerning the two GO types (Figure 4). In fact, F4/80 negative cells (panel B) were absolutely not affected after exposure to these materials, while macrophages

displayed a decrease in cell viability after contact with both GO-A and GO-N (panel A). Going more in details, a concentration-dependent cytotoxicity was observed in the case of GO-N. In particular, mIPM showed a significant reduction of about 20 and 25 % in cell viability, after treatment with 50 or 100 µg/ml GO-N, respectively. This concentration-dependent trend was not observed in the case of GO-A. In fact, a reduction of about 15-20 % in cell viability was measured, to the same extent, from 10 to 100 µg/ml concentration. The selectivity of GO towards macrophages can be better appreciated in the corresponding dot plots of cell morphology (Figure 4C). In fact, despite the clear but not dramatic cytotoxic effect, the population corresponding to macrophages (evidenced by a circle in Figure 4C) seems to disappear selectively as GO-A or GO-N concentration increases.

Despite carbon nanomaterials can be internalized by both phagocytic and non-phagocytic cell types, the observed specific cytotoxicity toward mIPM could be interpreted as a preferential internalization of GO within phagocytic macrophages. This behavior could be adopted at different levels in therapeutic applications where an inhibition of macrophage functions would be used to modify the disease outcome. For example, it has been demonstrated that tumors are abundantly populated by macrophages (*Sica and Mantovani 2012*) where they can promote tumor initiation, progression and metastasis (*Qian and Pollard 2010*). It has also been shown that the targeted depletion of tumor-associated macrophages provides benefits in patients with diffuse-type giant cell tumor (*Ries et al. 2014*). The observed specific cytotoxicity toward this cell population makes GO a good candidate for the aimed depletion of tumor-associated macrophages (TAMs). On the other hand, it has been demonstrated that TAMs are able to capture nanoparticles and translocate them selectively from the periphery to the central hypoxic zone of the tumors (*Amoozgar and Goldberg 2014*). This behavior, together with the fact the GO can be functionalized to carry an anti-cancer drug, makes the material a good candidate for anticancer therapy. Finally, GO could be also employed in diseases such as fibrosis, which can arise after an exacerbated immune response and tissue injury driven by macrophages (*Duffield et al. 2005*).

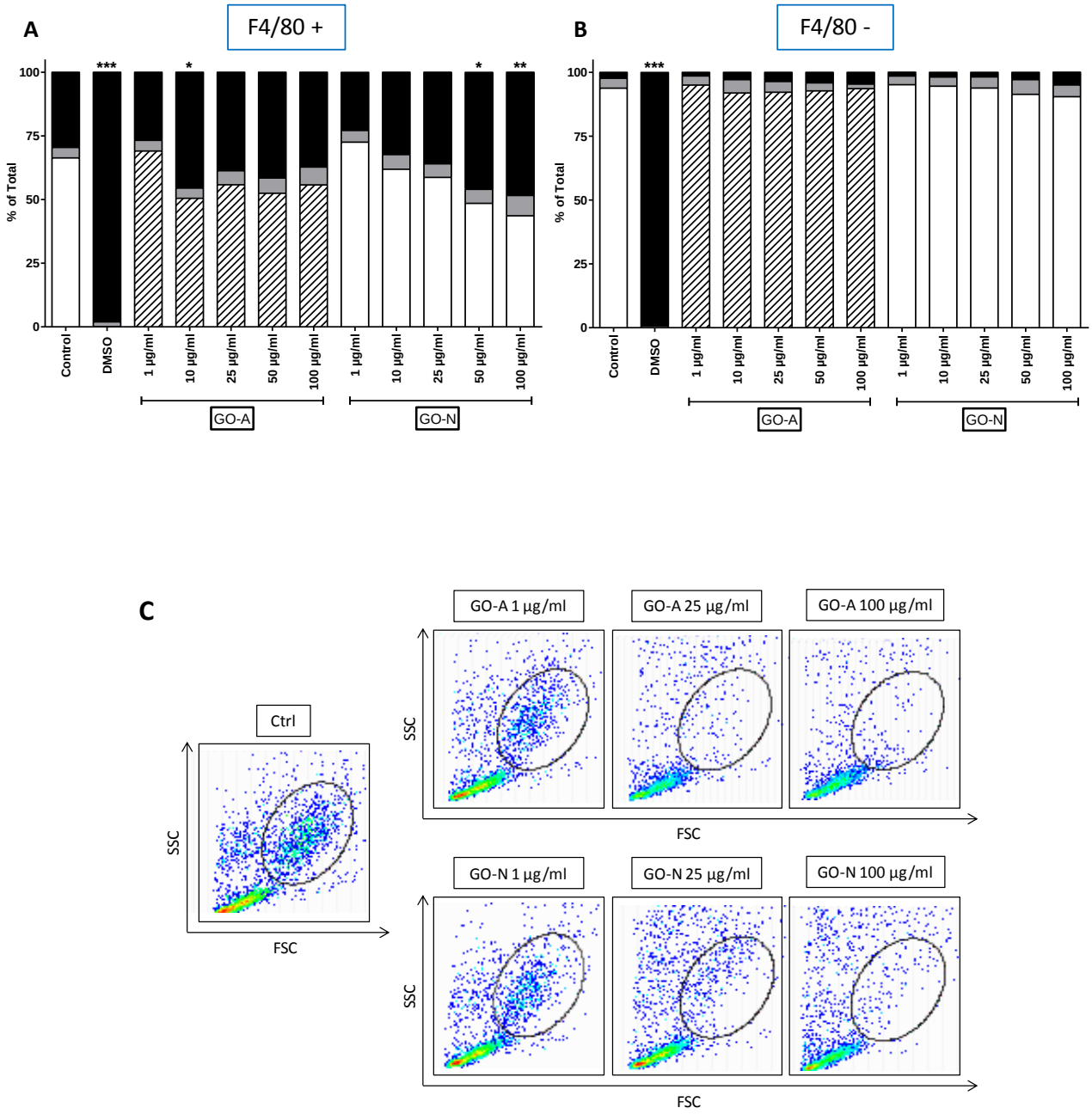

Figure 4. Flow cytometry analysis of cell viability in mIPM (F4/80 positive, panel A) or F4/80 negative cells (panel B) exposed to different concentrations of GO-A and GO-N during 24 h. Two-ways ANOVA followed by Bonferroni's post-test was performed to determine the statistical differences *versus* control cells and to compare the different graphene samples to each other (*p<0.05; **p<0.01; ***p<0.001). In panel C the corresponding FSC-SSC graphs are reported.

IV.3.2 Evaluation of a possible proinflammatory response

The literature about the impact of graphene on immune cells is rather limited (*Bianco 2013; Orecchioni et al. 2014*). Therefore, the effect on cell activation and cytokine production of the different graphene samples were compared on RAW 264.7 macrophages. As in the case of the viability experiments, GO putative induction of a proinflammatory response, was further

investigated in mIPM. Results obtained with FLG samples on RAW 264.7 cell line will be first described, while comparative results on GO effect on both RAW 264.7 and mIPM will be presented in a second moment.

RAW 264.7 cells were exposed for 24 hours to concentrations ranging from 1 to 100 µg/ml of FLG1 or FLG2, in the conditions described above (cell viability assessment). At the end of the incubation, the expression of the macrophage activation marker CD86 was analyzed by flow cytometry while the culture supernatants were collected to evaluate the levels of two proinflammatory cytokines, IL6 and TNF α, by ELISA. As shown in Figure 5, both FLG1 and FLG2 were not able to trigger RAW 264.7 activation (panel A) or pro-inflammatory cytokine production (panels B and C), contrarily to LPS/IFNγ used as positive activation controls. Similar investigation was carried out after exposing, for 24 hours, RAW 264.7 or mIPM to the same concentrations of GO-A or GO-N. The levels of IL6, TNF α and also of IL1β, another important proinflammatory cytokine, were also examined. Consistent with the results of FLG samples, no effect on RAW 264.7 cell activation (Figure 6A) or cytokine production (Figure 6C, E, G) was observed after exposure to both GO samples. Concerning mIPM, a concentration dependent increase in CD86 expression was evidenced after exposure to GO-A, but not to GO-N (Figure 6B). Despite this, the increase was significant only at 100 µg/ml GO-A concentration. This could be correlated to a lower purity grade of GO-A compared to GO-N (*Ali-Boucetta et al. 2013*). Analogous to RAW 264.7 macrophages, no proinflammatory cytokine production was found in mIPM supernatants after exposure to GO samples (Figure 6D, F, H).

In general, our results on cell activation and cytokine production revealed no induction of a proinflammatory effect by the two commercial GO types on RAW 264.7 cells on mIPM. In fact a slight increase in cell activation was observed only in the case of GO-A. Few studies are present in literature on the impact of GO on macrophage activation or cytokine production. A previous study was focused on the cellular impact of GO sheets having different sizes. The authors showed that only GO sheets with a lateral size of about 2 µm triggered strong mIPM activation, contrarily to sheets of about 300 nm (*Yue et al. 2012*). Another study showed cytokine secretion by RAW 264.7 cells in response to nano-sized or micro-sized GO (*Chen et al. 2012*). These apparently conflicting results with our study could be explained, for instance, by a different grade of purity of the materials that, in turn, could influence the immune cell response (*Ali-Boucetta et al. 2013*).

On view of these considerations, the results described in this chapter are consistent with a recent work of Bianco and collaborators which was focused on the effect of the lateral dimension of GO sheets on human and murine primary macrophages. In fact, the lateral size of our GO-A and GO-N flakes was about 1-2 µm. The GO of this size was not able to trigger macrophage activation as

evidenced in the mentioned study (*Russier et al. 2013*).

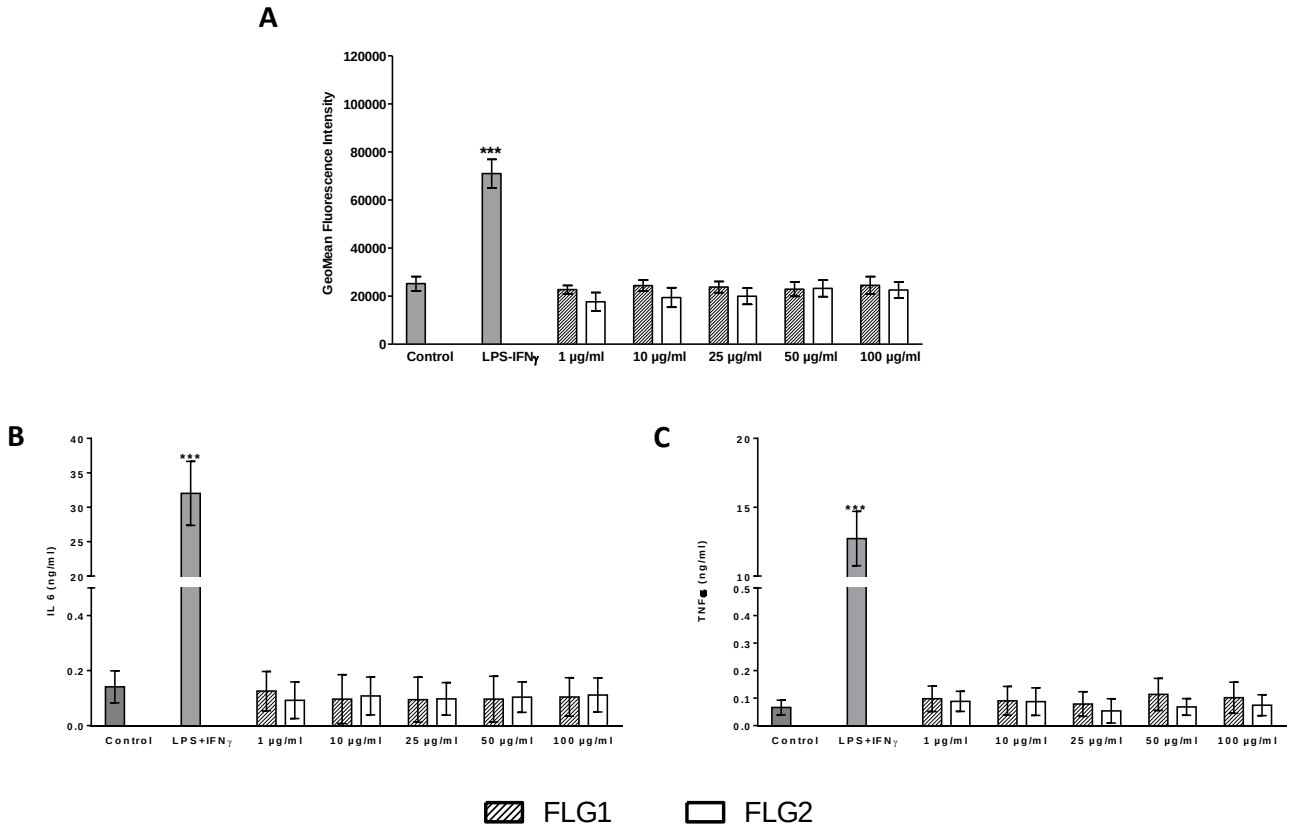

Figure 5. Flow cytometry analysis of CD86 expression (A) and cytokines production (IL6 panel B, TNF α panel C) in RAW 264.7 cells exposed to different concentrations of FLG1 and FLG2 during 24 h. Two-ways ANOVA followed by Bonferroni's post-test was performed to determine the statistical differences versus control cells and to compare the two graphene samples to each other (*$p<0.05$; **$p<0.01$; ***$p<0.001$).

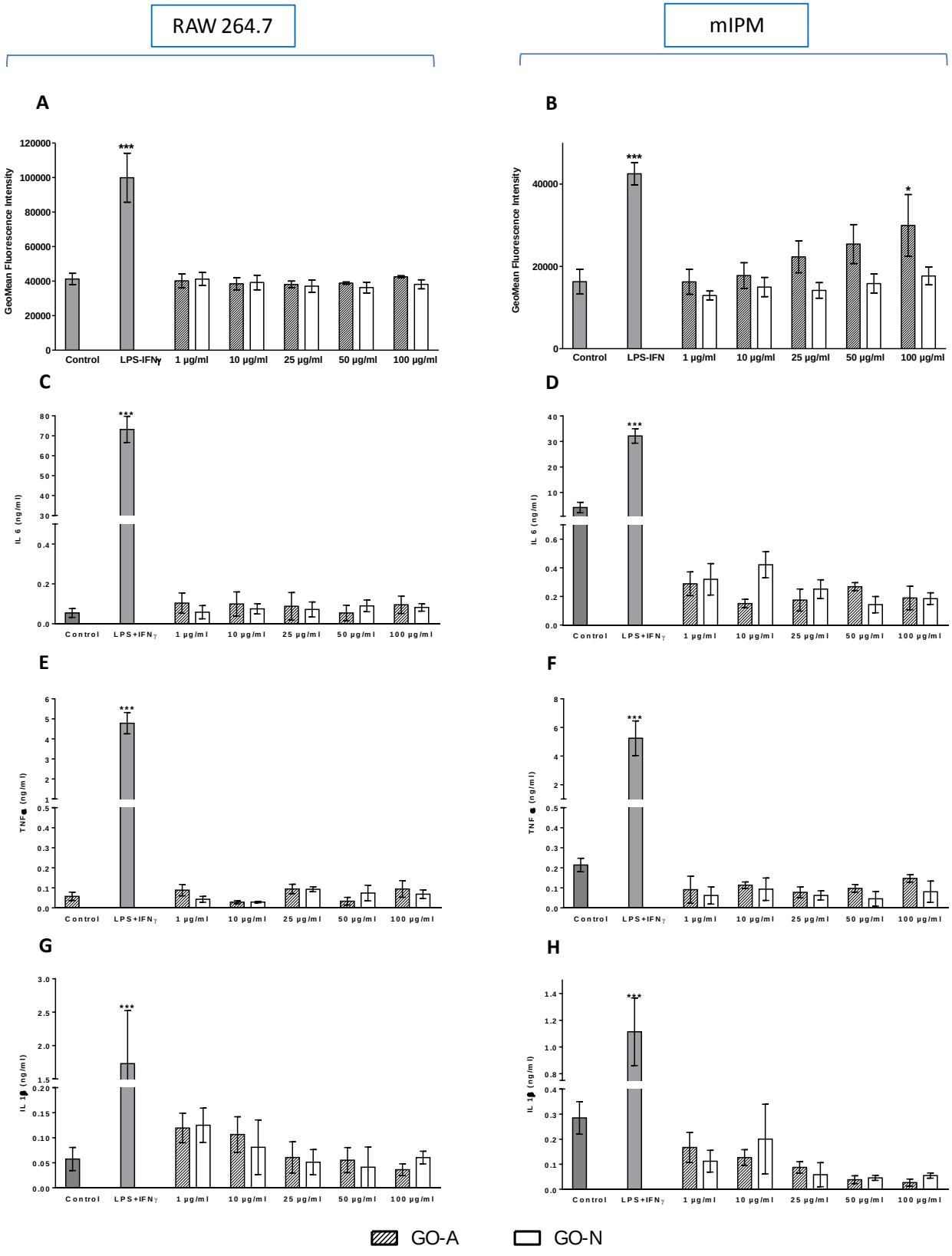

Figure 6. Analysis of RAW 264.7 (left panels) or mIPM (right panels) cell activation after exposure to different concentrations of GO-A or GO-N during 24 h. Flow cytometry analysis of CD86 expression is reported in panel A and B. In the bottom panels, IL6 levels (C and D), TNF α levels (E and D) and IL1β levels (G and H) are reported. Two-ways ANOVA followed by Bonferroni's post-test was performed to determine the statistical differences versus control cells and to compare the two graphene samples to each other (*p<0.05; **p<0.01; ***p<0.001).

IV.3.3 Interaction of graphene oxide with macrophages

In order to identify possible interactions and internalization mechanisms of GO-A and GO-N with cells, mIPMs were exposed for 24 hours to 100 µg/ml of both GO types. At the end of the incubation, cells were processed for TEM observations.

Even though the uptake mechanisms of GO are still not completely elucidated, some studies can be found in the literature suggesting both an active and a passive internalization pathway (*Yue et al. 2012; Mu et al. 2012; Peng et al. 2010*).

Concerning our study, it has worth noting that a high degree of GO internalization by mIPMs was observed concerning both GO types (Figure 7). In fact GO-A (panel A) and GO-N (panel B) were found inside almost all the cells under observation: expected behavior as macrophages are phagocytic cells. In the context of the identification of a possible internalization mechanism, GO was present inside large vesicles, suggesting a phagocytic internalization pathway; however, free GO flakes were also present in the cytoplasm. This could result from a passive translocation of GO sheets through the plasma membrane as it has been previously described for CNTs (*Pantarotto et al. 2004 A*) or suggested with dynamic membrane models (*Ly et al. 2013*). The free graphene flakes could be also the result of endosome disruption and/or evasion. None of the two GO types was found inside the nuclei despite their structure, in some cases, the nuclei seemed impaired as evidenced by a certain degree of nuclear condensation, typical feature of cells that are dying (*Ziegler et al. 2004*). Such observation can be correlated with the cytotoxicity evidenced after mIPM exposure to 100 µg/ml of GO. Moreover, cytoplasmic structures seemed to be impaired to a larger extent after cells were treated with GO-A compared to GO-N, as evidenced by the presence of big vacuoles, even though they gave similar results in the cell viability experiments. The phenomenon could be correlated to a higher dispersibility of GO-A (compared to GO-N) in aqueous media, which in turn could be more internalized by mIPM. On the other hand it was possible to evidence, very frequently, isolated GO sheets bound parallel to the plasma membrane, (black arrows in Figure 7). This is again consistent with the previous study by Russier et al. where a “mask effect” by GO, which could isolate cells from their environment, was observed; this could be responsible for GO impact on cellular parameters. It was also speculated that the mask effect could be used to modulate or deplete cells particularly sensitive to paracrine signals or cell-cell interactions (*e.g.* lymphocytes) (*Russier et al. 2013*). Moreover, some of the GO sheets enter the cell membrane sliding under it (red arrows in Figure 5). This was also simulated by a computer modelling (*Guo et al. 2013*). The possible internalization mechanism is illustrated in Figure 8.

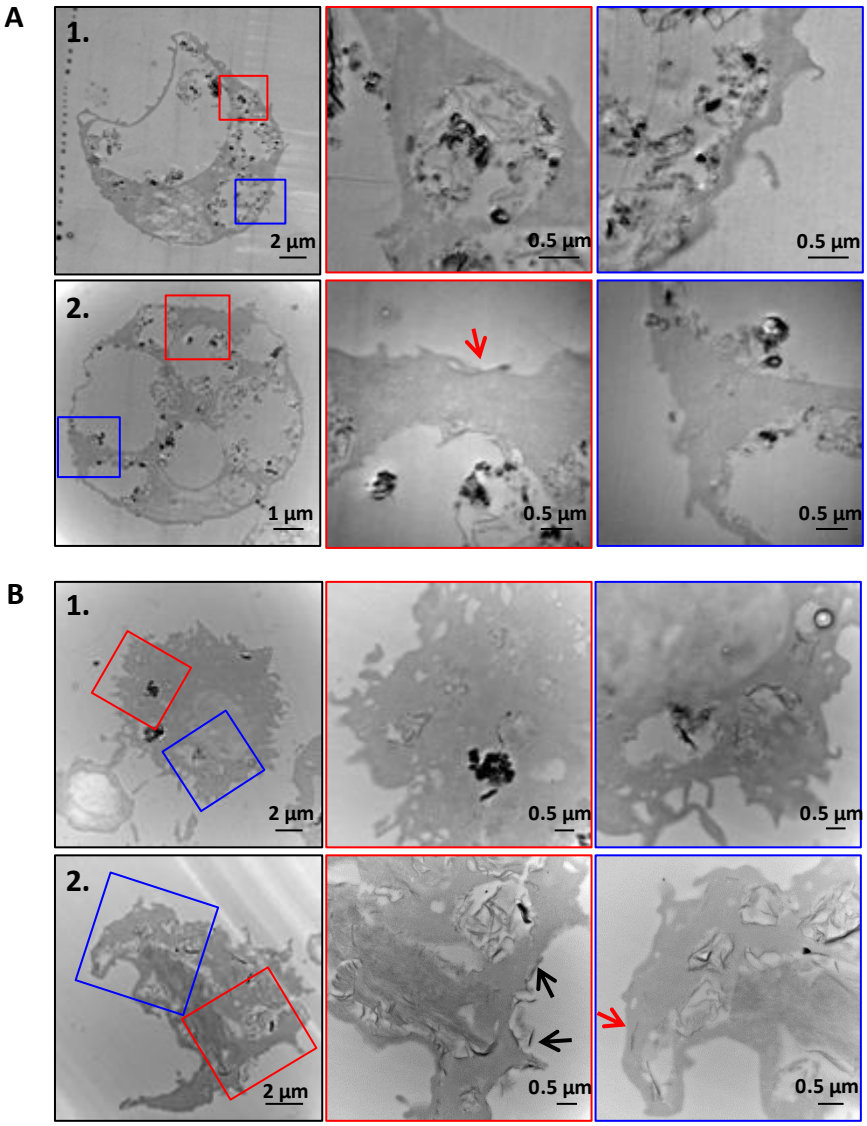

Figure 7. TEM images of mIPM incubated with 100 µg/ml of GO-A (A) or GO-N (B) during 24 h. The framed areas in the left images are enlarged in the respective right pictures.

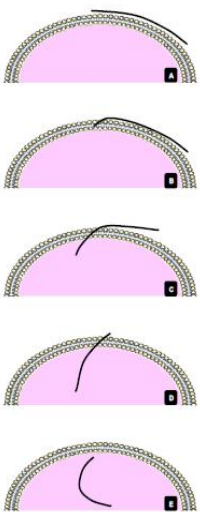

Figure 8. Hypothesized mechanism for GO passive internalization. First, the GO sheets dispose themselves parallel to the cellular membrane (A). Then, due to the tight interaction, the edge of the GO flake pierces the phospholipid bilayer (B), begins to passively enter the cellular membrane (C and D) and finally reaches the intracellular compartment (E). (*Russier et al. 2013*).

IV.3.4 B cell targeting with functionalized graphene oxide

As it was described previously in this thesis, one of the main goals of the researches in the biomedical field is the design drugs and vectors with specific activity toward a particular diseased cellular type without affecting the healthy components of the cell populations. We also described how both nanotube and graphene surfaces can be functionalized with specific moieties, which can recognize molecular signatures on the surface of the cells of interest, carrying in the same time a bioactive molecule (*e.g.* a drug).

After evaluating the impact of GO on different cell types in terms of cytotoxicity and proinflammatory response, my interests moved towards a possible application of the material in cell targeting. For this purpose, I used a model of B cells (A20 D1.3) genetically modified to over-express a BCR which specifically recognize HEL. The two commercial GO samples (GO-A or GO-N) were non-covalently conjugated with HEL. Non-covalent binding between GO and the lysozyme were previously described by Li et al. These authors have demonstrated the strong electrostatic interaction between the two molecules. Furthermore, GO-HEL association seemed selective when the reaction was performed in a mixture of proteins (*Li et al. 2014*).

As first step, it was important to determine whether the interaction between GO and the lysozyme was stable in complete (see experimental section) cell culture medium. In fact, its components as salts, amino acids and the abundant proteins present in the FBS, could disturb GO-HEL interaction, thus inducing the detachment of the enzyme. For this purpose, the two GO-HEL conjugates were dispersed in the medium in test tubes. The samples were then incubated for 2 or 24 hours. To mimic the conditions used for the cell treatment, the incubation was performed at 37 °C. After centrifugation (to precipitate GO), the supernatants were subjected to gel electrophoresis (SDS-PAGE). The free enzyme and the complete medium alone were used as controls. The two GO-HEL samples, dispersed in water, were also loaded into the gel, to confirm the presence of the enzyme on their surface. GO concentrations (in water or in cell culture medium) were calculated, according to the thermogravimetric analysis (see experimental section), to have in all the samples a HEL amount of about 5 µg. The low dimensions of lysozyme (compared to FBS proteins) allowed to visualize the enzyme by staining the gel with Coomassie blue. The results obtained confirmed the presence of lysozyme on the GO surface, as the denaturing conditions of SDS-PAGE make the enzyme detaching from the graphene (Figure 9, second and third lane). On the contrary, the enzyme was not detected in GO-A and GO-N supernatants after incubation in the cell culture medium, either after 2 hours or 24 hours (Figure 9, lanes 5-8). The results demonstrated that the complexes are stable also in complete RPMI, despite HEL and GO binding was performed via non-covalent interactions.

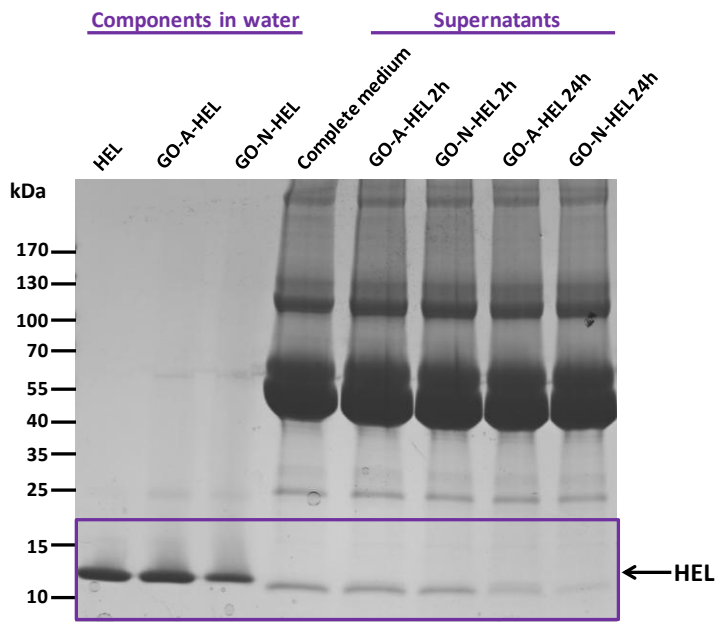

Figure 9. SDS-PAGE representative result. GO-A or GO-N conjugated with HEL and dispersed in water (second and third lane): the enzyme detaches from the GO surface, due to the denaturing conditions of the electrophoresis, and migrates. GO-A-HEL or GO-N-HEL supernatants after incubation in complete cell culture medium for 2 h or 24 h (lanes 5-8): the binding between the two molecules is stable as the enzyme is not detected in the supernatants.

Once proved their stability, HEL-GO conjugates were used to target the model B cells (A20 D1.3). Upon BCR-HEL binding, B cells produce IL2 (*Justement et al. 1989*), which could be revealed by ELISA. GO-HEL interaction with the BCR could be revealed also by flow cytometry using a specific biotinylated anti-HEL antibody (Figure 10).

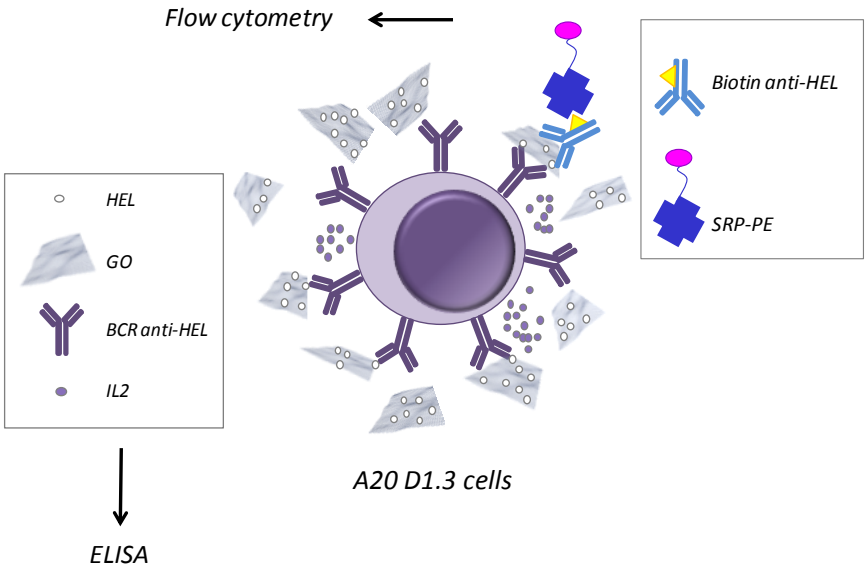

Figure 10. Targeting model: GO-HEL conjugates target B cells over-expressing a BCR specific for HEL protein. Upon GO-HEL-BCR binding, IL2 production by B cells is induced and can be detected by ELISA. The binding can be also revealed by flow cytometry using a specific biotinylated anti-HEL antibody.

Hence, A20 D.13 cells were exposed for 24 hours to concentrations ranging from 10 nM to 600 nM HEL of GO-A-HEL and GO-N-HEL. The free enzyme, as well as free GO, was used as control. The corresponding GO concentrations were back-calculated from lysozyme loading on GO surface (Table 1), accordingly to the termogravimetric analysis (see experimental section for details). At the end of the incubation, IL2 levels in the cellular supernatants were determined by ELISA.

Table 1. Concentrations of HEL, GO-A-HEL and GO-N-HEL used for the cell treatment. The corresponding GO concentrations were back-calculated from HEL loading onto GO surface.

HEL molar concentration (nM)	HEL (μg/ml)	GO-A-HEL (μg/ml)	GO-N-HEL (μg/ml)
10	0.22	0.77	3.00
30	0.43	2.30	9.00
100	1.43	7.60	29.90
300	4.30	22.75	89.60
600	8.60	45.50	179.2

Figure 11A shows the results obtained with both GO-HEL complexes and free HEL, which were able to induce IL2 production by A20 D1.3 cells. This demonstrates that the binding with BCR has occurred. The levels of IL2 were constant in all the concentration range in the case of HEL; on the contrary, these were higher as GO-HEL concentration increased. The phenomenon was observed with both GO samples up to a 100 nM HEL concentration suggesting an increased targeting ability by HEL when linked onto the GO-surface. This behavior was reversed in the concentration range between 100 nM and 600 nM HEL, even if IL2 levels were still higher as compared to the free protein. The latter observation could be explained by a saturation of the receptors and/or by a reduction in cell viability at these concentrations. The first hypothesis is the most reasonable as F4/80 negative cell population was not affected by GO (see Figure 4B). Finally, no IL2 production was monitored after the exposure of A20 D1.3 to free GO-A and GO-N (Figure 11B): therefore, the possibility of IL2 production induced by the free material was excluded. The specificity of GO-HEL conjugates towards A20 D1.3 cells was further confirmed performing the same experiments in A20 wild type cells (not expressing BCR against HEL). As expected, no IL2 production was detected in the supernatants of free HEL and GO-HEL samples. To further confirm the binding of the complexes to the BCR and thus the ability of the material to target specifically our cell model, flow cytometry analyses were performed. For this purpose both transgenic and wild type B cells were exposed to 30 nM or 100 nM of either free HEL or GO-A/ GO-N conjugated with the enzyme. Concentrations were chosen accordingly to the highest IL2 induction obtained in the previous experiment. The cells were left to interact with the molecules for 30 min. The treatment was

performed at 4 °C to avoid the internalization of the complexes by the cells. At the end of the exposure, cells were extensively washed and stained with a biotinylated antibody specific for HEL. GO-HEL binding to the BCR was revealed by flow cytometry after a second staining with streptavidin conjugated with phycoerythrin (PE) fluorophore.

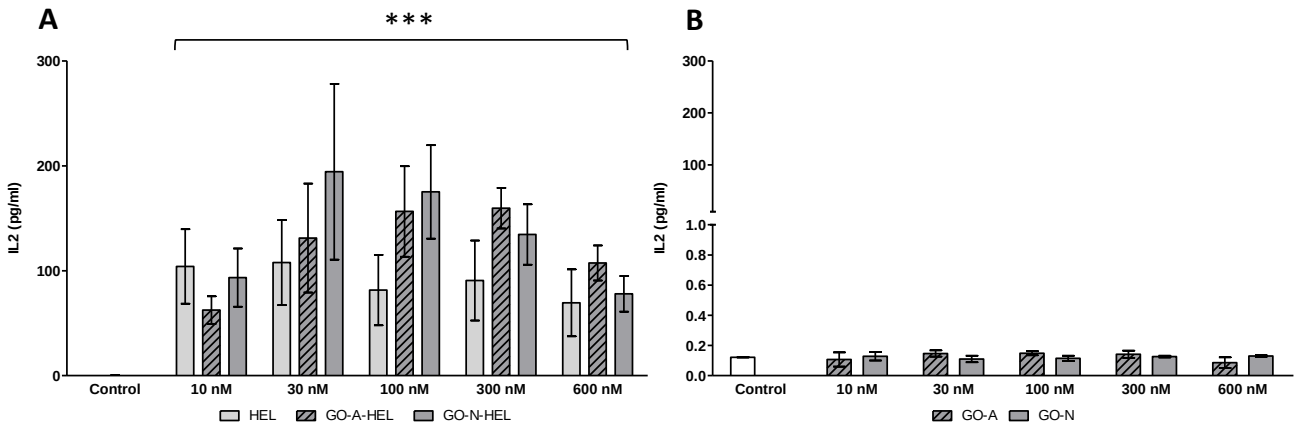

Figure 11. IL2 production by A20 D1.3 cells exposed to 30 nM or 100 nM concentrations of free HEL, GO-A-HEL and GO-N-HEL (A) during 24 h or incubated with the corresponding concentrations of free GO-A and GO-N as controls (B). Two-ways ANOVA followed by Bonferroni's post-test was performed to determine the statistical differences versus control cells. (*p<0.05; **p<0.01; ***p<0.001).

As expected from the ELISA results, both GO-HEL samples could efficiently target A20 D1.3 cells. In fact, a clear shift of the entire cell population, corresponding to PE-positive cells, was evidenced upon cellular exposure to the two GO-HEL samples confirming their ability to recognize the BCR, at the same extent of free HEL. The result is reported in Figure 12A (representative experiment with 30 nM HEL). Moreover, no difference compared to control cells was noticed in the case of the GO samples not conjugated with the enzyme, thus excluding the contribution of GO intrinsic fluorescence (*Shang et al. 2012*). The specificity of this binding towards our cellular model over-expressing a BCR anti-HEL was further confirmed by the results obtained with A20 wild-type cells. In this case, no positive cell population was detected after exposure to all graphene samples (Figure 12B). The result can be also visualized in Figure 12C and D where the mean fluorescence intensities (MFI) of A20 D1.3 and A20 wild-type exposed to 30 nM or 100 nM concentrations of free HEL, HEL-GO or free GO are reported. On the other hand, the slight increase in fluorescence in the case of A20 D1.3 control cells compared to A20 wild-type control cells could be due to a slight interaction of the biotinylated anti-HEL antibody with the BCR in the absence of HEL.

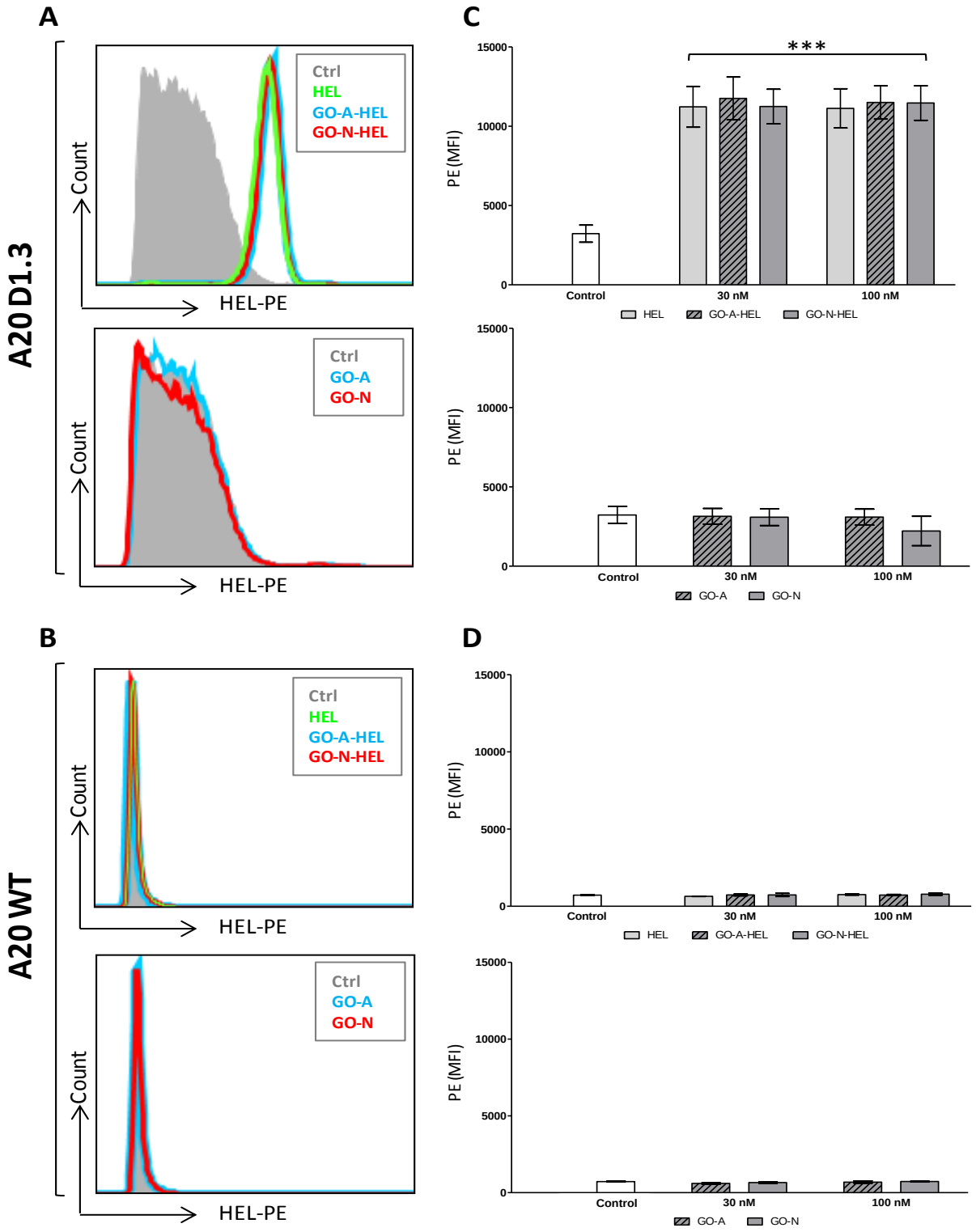

Figure 12. Flow cytometry analysis of B cell targeting with GO. PE fluorescence histograms (derived from HEL staining) of control cells *versus* cells exposed to 30 nM HEL, 30 nM GO-A-HEL and 30 nM GO-N-HEL or to the corresponding concentrations of free GO-A and GO-N (panel A for A20 D1.3, panel B for A20 wild type) during 30 min at 4 °C. PE mean fluorescence intensity in A20 D1.3 (C) or A20 wild-type cells (D) exposed to 30 nM or 100 nM HEL, GO-A-HEL, GO-N-HEL or to the corresponding concentrations of GO-A and GO-N as controls during 30 min at 4 °C. Two-ways ANOVA followed by Bonferroni's post-test was performed to determine the statistical differences versus control cells. (*$p<0.05$; **$p<0.01$; ***$p<0.001$).

The results obtained in the experiments illustrated above, demonstrate that functionalized graphene is able to target B cells in a selective fashion, thus suggesting its possible application in therapies where the specific elimination of B lymphocytes is required. In fact, GO can be further functionalized with a cytotoxic molecule. This can concern autoimmune diseases such as Systemic Lupus Erythematosus (SLE) or Rheumatoid Arthritis (RA) in which autoreactive B lymphocytes, the direct precursors of autoantibody-secreting cells are involved in the exacerbation of the disease (*Yanaba et al. 2008*). Recently an important progress has been made with the use of the chimeric antibody Rituximab, which specifically targets the CD20 molecule (*Gürcan et al. 2009*). CD20 is mainly expressed at the surface of B lymphocytes, which are then depleted upon recognition by anti-CD20 antibodies (*Anolik et al. 2004*). Despite Rituximab therapy has been reported to be successful for systemic autoimmune diseases such as RA (*Keystone et al. 2008*), trials with the same antibody gave variable results in other autoimmune diseases such as SLE (*Albert et al. 2008*). Furthermore, secondary side effects upon Rituximab administration were observed (*Carson et al. 2009*). These observations further confirm the fact that other strategies are necessary to achieve the specific depletion of autoreactive B cells involved in the pathogenesis. As we have demonstrated, graphene could be a promising candidate to reach this ambitious goal. In fact, new specific B-cell surface targets and appropriate cytotoxic molecules are currently under investigation and could be conjugated at the same time on GO surface; the conjugates could be then tested on murine models of SLE.

IV.4 Conclusions

In the third project in which I was involved during my PhD, the impact of different graphene samples toward different cellular types was investigated. Furthermore, the ability of graphene oxide to specifically target B cells was studied. This project started with the examination of the cytotoxicy of both few layer graphene and two types of commercial graphene oxide toward human cervix cancer cells and murine macrophages RAW 264.7 cell lines. In fact, being a promising material to be exploited in the biomedical field, a careful characterization of a possible negative impact on health is demanded and currently under investigation.

Reduction in cell viability was not observed after a 24 hour exposure to all materials even at high concentrations in both human and murine cellular lines. Moreover, the materials did not trigger RAW 264.7 activation or cytokine production. Since tumor cell lines showed an increased tolerance to death stimuli, graphene oxide was further tested on murine intraperitoneal primary macrophages. In this case, both commercial graphene types were able to reduce mIPM cell viability. Furthermore, it should be pointed out that this effect seemed to be macrophage-specific, since F4/80 negative

peritoneal cells were not affected by the exposure to GO-A or GO-N. These results suggest a possible utilization of GO in therapies in which the suppression of dangerous macrophages could be advantageous. This could be the case of cancer immunotherapy since it has been demonstrated that macrophages play an important role in cancer development and progression.

Despite the observed cytotoxicity, both commercial graphene samples did not elicit no proinflammatory response toward mIPM, a positive result in view of their possible application in biomedicine.

As expected, both GO samples were efficiently internalized by mIPM either by energy-dependent mechanisms and passive diffusion. In fact the nanomaterials were found inside vesicles but also free in the cytoplasm. Moreover GO sheets were observed also stacked parallel onto the plasma membrane surface, confirming the so called "mask effect" previously reported (*Russier et al. 2013*).

In the last part of the project, GO-A and GO-N were non-covalently conjugated with the lyzozyme. Both samples were able to target a B cell model genetically modified to over-express a BCR specific for HEL. The latter result suggests that GO could be a promising drug support to be exploited in specific targeted therapies in which the suppression of armful B-lymphocytes is demanded (e.g. SLE). This will be possible with the discovery of new specific surface targets and appropriate cytotoxic molecules that could be grafted onto GO surface. The conjugates could be then tested *in vitro* and *in vivo* in mouse models of SLE. Moreover, this approach can be applied to other diseases in which a specific cell population must be depleted such as lymphomas and cancer in general.

CHAPTER V

General conclusions and perspectives

Carbon nanotubes and graphene (the latter especially in its oxidized form) are among the most promising carbon-based nanomaterials used for widespread biomedical applications. In fact, the development of different chemical strategies to functionalize their surface or to fill the CNT inner cavity opened the doors for the conjugations of both materials with almost all the molecules of biological interest (*e. g.* DNA, proteins or small drugs). The functionalized materials have shown great promises in several context of the biomedical field, especially as nanocarriers for drugs.

However, a special issue concerns their toxicity as secondary side effects of the therapies must be avoided. Besides numerous efforts have been made to make both materials biocompatible and biodegradable, conflicting results are present in the literature and several factors interplay in determining CNT and graphene toxicity. Thus, further investigations in this context are demanded and better strategies to achieve a complete biocompatibility of the materials are still needed.

The first project carried out during my PhD internship was aimed at improving the solubility and the biocompatibility of pristine SWCNTs by non covalent functionalization. Bovine serum albumin was able to form a stable dispersion over the time. The materials were then tested on different cell lines, murine or human, phagocytic or non-phagocytic, to better elucidate the impact and the interactions of such materials with living systems. Interestingly, CNTs were less cytotoxic on murine macrophages when coated with BSA, as compared to the uncoated controls. On the other hand, both pristine and BSA-stabilized CNTs were not able to induce a proinflammatory response in macrophages. Thanks to the good dispersion quality, BSA-SWCNTs were able to penetrate non-phagocytic and phagocytic cell types by both passive diffusion and ATP-consuming mechanisms. Despite being able to interact and to be internalized by the cells, no changes in the dielectric parameters of fibroblast membrane were detected after exposure to BSA-CNTs. This is an innovative result as the effect of nanotubes on the plasma membrane dielectric characteristics and ion flux was very poorly investigated up to date.

Taken together, the results obtained by the first proof of concept study shed more light on the SWCNT impact and interaction with cells. First, we could create highly soluble and stable carbon nanotubes without the need of covalent functionalization, simply covering their surface with a biocompatible protein which interacts with their surface by hydrophobic interactions. SWCNTs showed to be less toxic in macrophages when coated with BSA thus suggesting also an increased biocompatibility. Further studies could be performed in mice to investigate the possible induction of

tissue damage and inflammation *in vivo*. Interesting could be also to examine the biodistribution of BSA-stabilized CNTs. In fact, it is generally assumed that non-covalently functionalized CNTs accumulate in the RES organs and in the lungs promoting *in vivo* toxicity; same materials showed a difficult excretion with urine and feces. However, the non-covalent coating of CNTs with some molecules as polymers (PEG) showed a reduced accumulation in the liver/spleen and an enhanced blood circulation (which is useful for the carriers to reach their target organs). Despite non-covalently functionalized CNTs seems to be not degradable, PEG-CNTs could be excreted via the bile and renal pathways (*Liu et al. 2008 A*). It would be of interest to investigate if our BSA-SWCNT complexes show the same behavior *in vivo*. Finally, the inner cavity of CNTs could be filled with a chemotherapeutic drug. Drug-filled and BSA-stabilized CNTs could be then used to passively target tumors by the EPR effect (*Iyer et al. 2006*).

In the second project, the anticancer activity of MWCNTs having different diameter and encapsulated with a cisplatin prodrug was investigated in a human cancer cell model. The CNTs efficently preserve the activity of the drug without inducing a high pro-inflammatory response on macrophages. In addition, cell viability experiments suggested a CNT diameter-dependent drug release. Moreover, cell internalization experiments and the intracellular platinum levels after Pt(IV)@CNT exposure demonstrate that they can promote the drug accumulation inside cells in comparison to treatment with the free complex.

Our study shows how, by tuning CNT diameter it is possible to control the release of a chemotherapeutic drug encapsulated inside their cavity. In particular, CNTs having a small diameter showed a slower drug release according to the cell viability tests. Such behavior could allow small Pt(IV)@CNTs to have an increased anticancer efficacy *in vivo*. Further investigations could be performed on Pt-resistant cells to assess whether it is possible to elude multi-drug resistance by the use of CNTs as carriers. The conjugates could be also tested *in vivo* in tumor-bearing mice after intra-tumoral or systemic injection. It would be of great interest to see how the different complexes influence the tumor growth according to their diameter and in comparison with the free drug. In addition, the Pt(IV)@CNTs external surface could also further functionalized to allow a specific tumor targeting. We are also currently investigating the *in vivo* biodistribution of our complexes to assess wether they could affect normal organs and tissues and their excretion profiles.

In the third and last project, the biological effect of various graphene types towards different cell types was examined. In particular, we focused on the impact of graphene oxide, which shows more promises in biomedical applications, on macrophages. We evidenced a selective cytotoxic effect of GO towards the primary macrophage population, as the viability of F4/80 negative cells (corresponding to the other immune peritoneal cells) was not affected by GO. Such behavior could

be exploited in therapies were the suppresion of macrophages could be advantageous. This can be the case of cancer, in which macrophages have shown to be responsible of tumor initiation, progression and metastasis (*Qian and Pollard 2010*). The mechanisms of GO interaction/internalization by primary macrophages were then better elucidated. The materials were internalized by both passive diffusion and phagocytosis. Moreover, GO sheets were observed also stacked parallel onto the plasma membrane surface, confirming the so-called "mask effect" previously reported. Isolating the cells from their environment, the mask effect could be useful to modulate or deplete cells particularly sensitive to paracrine signals or cell-cell interactions (*Russier et al. 2013*). In the last part of the project we were able to successfully target a B cell model overexpressing a lysozyme-specific B cell receptor (BCR), by functionalizing GO with this enzyme. The latter result suggests that GO could be a promising drug support to be exploited in specific targeted therapies in which the suppression of armful B-lymphocytes is demanded [*e.g*. systemic lupus erythematosus (SLE) and other autoimmune diseases]. Next step will be to conjugate GO with selective targeting moieties and specific cytotoxic drugs for *in vitro* and *in vivo* tests in murine models of SLE. This ambitious project is currently running at ICT in Strasbourg and promising results have been already obtained with CNTs. The group of Helene Dumortier and Sylviane Muller indentified the N-terminal region of histone H2B as preferential target of autoantibodies in SLE (*Dumortier et al. 2010*). This observation will allow the specific target of B lymphocytes expressing a BCR which specifically recognize that H2B region. In fact, the corresponding antigenic peptide can be grafted onto the surface of graphene oxide, together with a specific drug. Finally, this approach can be applied to other diseases in which a specific cell population must be depleted such as lymphomas and cancer in general.

All these examples evidence the potential use of carbon-based nanomaterials fot therapeutic purposes.

References

A

- Ajima K, Yudasaka M, Murakami T, Maigné A, Shiba K, Iijima S. Carbon nanohorns as anticancer drug carriers. *Mol Pharm* 2005;**2**:475-480.
- Ajima K, Murakami T, Mizoguchi Y, Tsuchida K, Ichihashi T, Iijima S, Yudasaka M. Enhancement of in vivo anticancer effects of cisplatin by incorporation inside single-wall carbon nanohorns. *ACS Nano* 2008;**2**:2057-2064.
- Al-Jamal KT, Nerl H, Müller KH, Ali-Boucetta H, Li S, Haynes PD, Jinschek JR, Prato M, Bianco A, Kostarelos K, Porter AE. Cellular uptake mechanisms of functionalised multi-walled carbon nanotubes by 3D electron tomography imaging. *Nanoscale* 2011;**3**:2627-2635.
- Al-Jamal KT, Nunes A, Methven L, Ali-Boucetta H, Li S, Toma FM et al. Degree of chemical functionalization of carbon nanotubes determines tissue distribution and excretion profile. *Angew Chem Int Ed Engl* 2012;**51**:6389-6393.
- Ali-Boucetta H, Kostarelos K. Pharmacology of carbon nanotubes: toxicokinetics, excretion and tissue accumulation. *Adv Drug Deliv Rev* 2013**;65**:2111-2119.
- Ali-Boucetta H, Bitounis D, Raveendran-Nair R, Servant A, Van den Bossche J, Kostarelos K. Purified graphene oxide dispersions lack in vitro cytotoxicity and in vivo pathogenicity. *Adv Healthc Mater* 2013*;***2**:433-441.
- Albert D, Dunham J, Khan S, Stansberry J, Kolasinski S, Tsai D, Pullman-Mooar S, Barnack F, Striebich C, Looney RJ, Prak ET, Kimberly R, Zhang Y, Eisenberg R. Variability in the biological response to anti-CD20 B cell depletion in systemic lupus erythaematosus. *Ann Rheum Dis* 2008;**67**:1724-1731.
- Allen BL, Kotchey GP, Chen Y, Yanamala NV, Klein-Seetharaman J, Kagan VE, Star A. Mechanistic investigations of horseradish peroxidase-catalyzed degradation of single-walled carbon nanotubes. *J Am Chem Soc* 2009;**131**:17194-17205.
- Amoozgar Z, Goldberg MS. Targeting myeloid cells using nanoparticles to improve cancer immunotherapy. *Adv Drug Deliv Rev* 2014; doi: 10.1016/j.addr.2014.09.007.
- Andón FT, Kapralov AA, Yanamala N, Feng W, Baygan A, Chambers BJ et al. Biodegradation of single-walled carbon nanotubes by eosinophil peroxidase. *Small* 2013;**9**:2721-2720.
- Anolik JH, Barnard J, Cappione A, Pugh-Bernard AE, Felgar RE, Looney RJ, Sanz I. Rituximab improves peripheral B cell abnormalities in human systemic lupus erythematosus. *Arthritis Rheum* 2004;**50**:3580-3590.
- Arnold WM and Zimmermann U. Electro-rotation: development of a technique for dielectric measurements on individual cells and particles. *J Electrostat* 1988;**21**:151–191.
- Azevedo AM, Martins VC, Prazeres DM, Vojinović V, Cabral JM, Fonseca LP. Horseradish peroxidase: a valuable tool in biotechnology. *Biotechnol Annu Rev* 2003;**9**:199-247.

B

- Bailey AM, Mao Y, Zeng J, Holla V, Johnson A, Brusco L, Chen K, Mendelsohn J, Routbort MJ, Mills GB, Meric-Bernstam F. Implementation of biomarker-driven cancer therapy: existing tools and remaining gaps. *Discov Med* 2014;**17**(92):101-114.
- Bakand S, Hayes A, Dechsakulthorn F. Nanoparticles: a review of particle toxicology following inhalation exposure. *Inhal Toxicol* 2012*;***24**:125-135.
- Belyanskaya L, Manser P, Spohn P, Bruinink A, Wick P. The reliability and limits of the MTT reduction assay for carbon nanotubes–cell interaction. *Carbon* 2007;**45**:2643-2648.

- Bertrand N, Wu J, Xu X, Kamaly N, Farokhzad OC. Cancer nanotechnology: the impact of passive and active targeting in the era of modern cancer biology. *Adv Drug Deliv Rev* 2014;**66**:2-25.
- Bhirde AA, Patel V, Gavard J, Zhang G, Sousa AA, Masedunskas A, Leapman RD, Weigert R, Gutkind JS, Rusling JF. Targeted killing of cancer cells in vivo and in vitro with EGF-directed carbon nanotube-based drug delivery. *ACS Nano* 2009;**3**:307-316.
- Bianco A, Kostarelos K, Partidos CD, Prato M. Biomedical applications of functionalised carbon nanotubes. *Chem Commun* 2005:571-577.
- Bianco A, Kostarelos K, Prato M. Making carbon nanotubes biocompatible and biodegradable. *Chem Commun* 2011;**47**:10182-10188.
- Bianco A. Graphene: Safe or toxic? The two faces of the medal. *Angew Chem Int Ed Engl* 2013;**52**:4986-4997.
- Burke AR, Singh RN, Carroll DL, Wood JC, D'Agostino RB Jr, Ajayan PM, Torti FM, Torti SV. The resistance of breast cancer stem cells to conventional hyperthermia and their sensitivity to nanoparticle-mediated photothermal therapy. *Biomaterials* 2012;**33**:2961-2970.

C

- Carson KR, Evens AM, Richey EA, Habermann TM, Focosi D, Seymour JF, Laubach J, Bawn SD, Gordon LI et al. Progressive multifocal leukoencephalopathy after rituximab therapy in HIV-negative patients: a report of 57 cases from the Research on Adverse Drug Events and Reports project. *Blood* 2009;**113**:4834-4840.
- Cepeda V, Fuertes MA, Castilla J, Alonso C, Quevedo C, Pérez JM. Biochemical mechanism of cisplatin cytotoxicity. *Anticancer Agents Med Chem* 2007;**7**:3-18.
- Cha C, Shin SR, Annabi N, Dokmeci MR, Khademhosseini A. Carbon-based nanomaterials: multifunctional materials for biomedical engineering. *ACS Nano* 2013;**7**:2891-2897.
- Chan CK, Peng H, Liu G, McIlwrath K, Zhang XF, Huggins RA, Cui Y. High-performance lithium battery anodes using silicon nanowires. *Nat Nanotechnol* 2008;**3**:31-35.
- Chen GY, Yang HJ, Lu CH, Chao YC, Hwang SM, Chen CL, Lo KW, Sung LY, Luo WY, Tuan HY, Hu YC. Simultaneous induction of autophagy and toll-like receptor signaling pathways by graphene oxide. *Biomaterials* 2012;**33**:6559-6569.
- Cherukuri P, Bachilo SM, Litovsky SH, Weisman RB. Near-infrared fluorescence microscopy of single-walled carbon nanotubes in phagocytic cells. *J Am Chem Soc* 2004;**126**:15638-15639.
- Chiu CF, Dementev N, Borguet E. Fluorescence Quenching of Dyes Covalently Attached to Single-Walled Carbon Nanotubes. *J Phys Chem A* 2011;**115**:9579–9584.
- Chou LY, Ming K, Chan WC. Strategies for the intracellular delivery of nanoparticles. *Chem Soc Rev* 2011;**40**:233-245.
- Cohn ZA. Activation of mononuclear phagocytes: fact, fancy, and future. *J Immunol* 1978;**121**:813-816.
- Colvin VL. The potential environmental impact of engineered nanomaterials. *Nat Biotechnol* 2003;**21**:1166-1170.
- Cui D, Tian F, Ozkan CS, Wang M, Gao H. Effect of single wall carbon nanotubes on human HEK293 cells. *Toxicol Lett* 2005;**155**:73-85.

D

- De Franceschi S, Kouwenhoven L. Electronics and the single atom. *Nature* 2002;**417**:701-702.

- De Volder MF, Tawfick SH, Baughman RH, Hart AJ. Carbon nanotubes: present and future commercial applications. *Science* 2013;**339**:535-539.
- Coussens LM, Werb Z. Inflammation and cancer. *Nature* 2002;**420**:860-867.
- Dhar S, Liu Z, Thomale J, Dai H, Lippard SJ. Targeted single-wall carbon nanotube-mediated Pt(IV) prodrug delivery using folate as a homing device. *J Am Chem Soc* 2008;**130**:11467-11476.
- Dhillon AS, Hagan S, Rath O, Kolch W. MAP kinase signalling pathways in cancer. *Oncogene* 2007;**26**:3279-3290.
- Di Giorgio ML, Di Bucchianico S, Ragnelli AM, Aimola P, Santucci S, Poma A. Effects of single and multi walled carbon nanotubes on macrophages: cyto and genotoxicity and electron microscopy. *Mutat Res* 2011;**722**:20-31.
- Dolcet X, Llobet D, Pallares J, Matias-Guiu X. NF-kB in development and progression of human cancer. *Virchows Arch* 2005;**446**:475-482.
- Duch MC, Budinger GR, Liang YT, Soberanes S, Urich D, Chiarella SE, Campochiaro LA, Gonzalez A, Chandel NS, Hersam MC, Mutlu GM. Minimizing oxidation and stable nanoscale dispersion improves the biocompatibility of graphene in the lung. *Nano Lett* 2011;**11**:5201-5207.
- Duffield JS, Forbes SJ, Constandinou CM, Clay S, Partolina M, Vuthoori S, Wu S, Lang R, Iredale JP. Selective depletion of macrophages reveals distinct, opposing roles during liver injury and repair. *J Clin Invest* 2005;**115**:56-65.
- Dumortier H, Lacotte S, Pastorin G, Marega R, Wu W, Bonifazi D, Briand JP, Prato M, Muller S, Bianco A. Functionalized carbon nanotubes are non-cytotoxic and preserve the functionality of primary immune cells. *Nano Lett* 2006;**6**:1522-1528.
- Dumortier H. When carbon nanotubes encounter the immune system: desirable and undesirable effects. *Adv Drug Deliv Rev 2013*;**65**:2120-2126.

E

- Elgrabli D, Floriani M, Abella-Gallart S, Meunier L, Gamez C, Delalain P, Rogerieux F, Boczkowski J, Lacroix G. Biodistribution and clearance of instilled carbon nanotubes in rat lung. *Part Fibre Toxicol* 2008;**5**:20.
- Etheridge ML, Campbell SA, Erdman AG, Haynes CL, Wolf SM, McCullough J. The big picture on nanomedicine: the state of investigational and approved nanomedicine products. *Nanomedicine* 2013;**9**:1-14.

F

- Fabbro A, Prato M, Ballerini L. Carbon nanotubes in neuroregeneration and repair. *Adv Drug Deliv Rev* 2013;**65**:2034-2044.
- Fabbro C, Ali-Boucetta H, Da Ros T, Kostarelos K, Bianco A, Prato M. Targeting carbon nanotubes against cancer. *Chem Commun* 2012;**48**:3911-3926.
- Feazell RP, Nakayama-Ratchford N, Dai H, Lippard SJ. Soluble single-walled carbon nanotubes as longboat delivery systems for platinum(IV) anticancer drug design. *J Am Chem Soc* 2007;**129**:8438-8439.
- Feynman R. There's plenty of room at the bottom (reprint from speech given at annual meeting of the American Physical Society). *Eng Sci* 1960;**23**:22–36.

G

- Gabizon A, Isacson R, Libson E, Kaufman B, Uziely B, Catane R, Ben-Dor CG, Rabello E, Cass Y, Peretz T, et al. Clinical studies of liposome-encapsulated doxorubicin. *Acta Oncol* 1994;**33**:779-786.
- Ge C, Du J, Zhao L, Wang L, Liu Y, Li D, Yang Y, Zhou R, Zhao Y, Chai Z, Chen C. Binding of blood proteins to carbon nanotubes reduces cytotoxicity. *Proc Natl Acad Sci U S A* 2011;**108**:16968-16973.
- Gillies ER, Fréchet JM. Dendrimers and dendritic polymers in drug delivery. *Drug Discov Today* 2005;**10**:35-43.
- Goenka S, Sant V, Sant S. Graphene-based nanomaterials for drug delivery and tissue engineering. *J Control Release* 2014;**173**:75-88.
- Gonzalez VM, Fuertes MA, Alonso C, Perez JM. Is cisplatin-induced cell death always produced by apoptosis? *Mol Pharmacol* 2001;**59**:657-63.
- Grant BD and Donaldson JG. Pathways and mechanisms of endocytic recycling. *Nat Rev Mol Cell Biol* 2009;**10**:597–608.
- Grivennikov SI, Greten FR, Karin M. Immunity, Inflammation, and Cancer. *Cell* 2010;**140**:883–899.
- Guo R, Mao J, Yan LT. Computer simulation of cell entry of graphene nanosheet. *Biomaterials* 2013;**34**:4296-4301.
- Gürcan HM, Keskin DB, Stern JN, Nitzberg MA, Shekhani H, Ahmed AR. A review of the current use of rituximab in autoimmune diseases. *Int Immunopharmacol* 2009;**9**:10-25.
- Guven A, Rusakova IA, Lewis MT, Wilson LJ. Cisplatin@US-tube carbon nanocapsules for enhanced chemotherapeutic delivery. *Biomaterials* 2012;**33**:1455-1461.

H

- Haddon RC. Carbon Nanotubes. *Acc Chem Res* 2002; **35**:997.
- Hafsi S, Pezzino FM, Candido S, Ligresti G, Spandidos DA, Soua Z, McCubrey JA, Travali S, Libra M. Gene alterations in the PI3K/PTEN/AKT pathway as a mechanism of drug-resistance (review). *Int J Oncol* 2012;**40**:639-644.
- Hampton MB, Kettle AJ, Winterbourn CC. Inside the neutrophil phagosome: oxidants, myeloperoxidase, and bacterial killing. *Blood* 1998;**92**:3007-3017.
- Hogan SP, Rosenberg HF, Moqbel R, Phipps S, Foster PS, Lacy P, Kay AB, Rothenberg ME. Eosinophils: biological properties and role in health and disease. *Clin Exp Allergy* 2008;**38**:709-750.
- Hollander MC, Blumenthal GM, Dennis PA. PTEN loss in the continuum of common cancers, rare syndromes and mouse models. *Nat Rev Cancer* 2011;**11**:289-301.
- Holt BD, Short PA, Rape AD, Wang YL, Islam MF, Dahl KN. Carbon nanotubes reorganize actin structures in cells and ex vivo. *ACS Nano* 2010;**4**:4872-4878.
- Holt BD, Dahl KN, Islam MF. Quantification of uptake and localization of bovine serum albumin-stabilized single-wall carbon nanotubes in different human cell types. *Small* 2011;**7**:2348-2355.
- Holt BD, Dahl KN, Islam MF. Cells take up and recover from protein-stabilized single-wall carbon nanotubes with two distinct rates. *ACS Nano* 2012;**6**:3481-3490.
- Hong H, Yang K, Zhang Y, Engle JW, Feng L, Yang Y, Nayak TR, Goel S, Bean J, Theuer CP, Barnhart TE, Liu Z, Cai W. In vivo targeting and imaging of tumor vasculature with radiolabeled, antibody-conjugated nanographene. *ACS Nano* 2012;**6**:2361-2370.

- Huang J, Zong C, Shen H, Liu M, Chen B, Ren B, Zhang Z. Mechanism of cellular uptake of graphene oxide studied by surface-enhanced Raman spectroscopy. *Small* 2012;**8**:2577-2584.
- Huang X, Qi X, Boey F, Zhang H. Graphene-based composites. *Chem Soc Rev* 2012;**41**:666-686.
- Huang X, Yin Z, Wu S, Qi X, He Q, Zhang Q, Yan Q, Boey F, Zhang H. Graphene-based materials: synthesis, characterization, properties, and applications. *Small* 2011;**7**:1876-1902.
- Hynes NE, Lane HA. ERBB receptors and cancer: the complexity of targeted inhibitors. *Nat Rev Cancer* 2005;**5**:341-354.

I

- Iijima, S. Helical microtubules of graphitic carbon. *Nature* 1991;**354**:56-58.
- Ishida S, Lee J, Thiele DJ, Herskowitz I. Uptake of the anticancer drug cisplatin mediated by the copper transporter Ctr1 in yeast and mammals. *Proc Natl Acad Sci U S A* 2002;**99**:14298-14302.
- Iyer AK, Khaled G, Fang J, Maeda H. Exploiting the enhanced permeability and retention effect for tumor targeting. *Drug Discov Today* 2006;**11**:812-818.

J

- Janowska I, Vigneron F, Bégin D , Ersen O, Bernhardt P, Romero T, Ledoux MJ, Pham-Huu C. Mechanical thinning to make few-layer graphene from pencil lead. *Carbon* 2012;**50**:3092-3116.
- Justement LB, Kreiger J, Cambier JC. Production of multiple lymphokines by the A20.1 B cell lymphoma after cross-linking of membrane Ig by immobilized anti-Ig. *J Immunol* 1989;**143**:881-889.

K

- Kagan VE, Tyurina YY, Tyurin VA, Konduru NV, Potapovich AI, Osipov AN, Kisin ER, Schwegler-Berry D, Mercer R, Castranova V, Shvedova AA. Direct and indirect effects of single walled carbon nanotubes on RAW 264.7 macrophages: role of iron. *Toxicol Lett* 2006;**165**:88-100.
- Kagan VE, Konduru NV, Feng W, Allen BL, Conroy J, Volkov Yet al. Carbon nanotubes degraded by neutrophil myeloperoxidase induce less pulmonary inflammation. *Nat Nanotechnol* 2010;**5**:354-359.
- Kam NWS, Jessop TC, Wender PA, Dai H. Nanotube molecular transporters: internalization of carbon nanotube-protein conjugates into Mammalian cells. *J Am Chem Soc* 2004;**126**:6850-6851.
- Kam NWS and Hongjie D. Carbon Nanotubes as Intracellular Protein Transporters: Generality and Biological Functionality. *J Am Chem Soc* 2005;**127**:6021-6026.
- Kam NWS, Liu Z, Dai H. Carbon nanotubes as intracellular transporters for proteins and DNA: an investigation of the uptake mechanism and pathway. *Angew Chem Int Ed Engl* 2006;**45**:577-581.
- Keystone E, Burmester GR, Furie R, Loveless JE, Emery P, Kremer J, Tak PP, Broder MS, Yu E, Cravets M, Magrini F, Jost F. Improvement in patient-reported outcomes in a rituximab trial in patients with severe rheumatoid arthritis refractory to anti-tumor necrosis factor therapy. *Arthritis Rheum* 2008;**59**:785-793.

- Kim ES, Tang X, Peterson DR, Kilari D, Chow CW, Fujimoto J, Kalhor N, Swisher SG, Stewart DJ, Wistuba II, Siddik ZH. Copper transporter CTR1 expression and tissue platinum concentration in non-small cell lung cancer. *Lung Cancer* 2014;**85**:88-93.
- Kinnula VL. Production and degradation of oxygen metabolites during inflammatory states in the human lung. *Curr Drug Targets Inflamm Allergy* 2005;**4**:465-470.
- Kolosnjaj J, Szwarc H, Moussa F. Toxicity studies of carbon nanotubes. *Adv Exp Med Biol* 2007;**620**:181-204.
- Kostarelos K, Lacerda L, Pastorin G, Wu W, Wieckowski S, Luangsivilay J, Godefroy S, Pantarotto D, Briand JP, Muller S, Prato M, Bianco A. Cellular uptake of functionalized carbon nanotubes is independent of functional group and cell type. *Nat Nanotechnol* 2007;**2**:108-113.
- Kostarelos K. The long and short of carbon nanotube toxicity. *Nat Biotechnol* 2008;**26**:774-776.
- Kotchey GP, Allen BL, Vedala H, Yanamala N, Kapralov AA, Tyurina YY, Klein-Seetharaman J, Kagan VE, Star A. The enzymatic oxidation of graphene oxide. *ACS Nano* 2011;**5**:2098-2108.
- Kraszewski S, Bianco A, Tarek M, Ramseyer C. Insertion of short amino-functionalized single-walled carbon nanotubes into phospholipid bilayer occurs by passive diffusion. *PLoS One* 2012;**7**:e40703.
- Kroto HW, Heath JR, O'Brien SC, Curl RF, Smalley RE. C60: Buckminsterfullerene. *Nature* 1985;**318**:162-163.
- Kruss S, Hilmer AJ, Zhang J, Reuel NF, Mu B, Strano MS. Carbon nanotubes as optical biomedical sensors. *Adv Drug Deliv Rev* 2013;**65**:1933-1950.

L

- Lacerda L, Russier J, Pastorin G, Herrero MA, Venturelli E, Dumortier H, Al-Jamal KT, Prato M, Kostarelos K, Bianco A. Translocation mechanisms of chemically functionalised carbon nanotubes across plasma membranes. *Biomaterials* 2012;**33**:3334-3343.
- Lacotte S, Dumortier H, Décossas M, Briand JP, Muller S. Identification of new pathogenic players in lupus: autoantibody-secreting cells are present in nephritic kidneys of (NZBxNZW)F1 mice. *J Immunol* 2010;**184**:3937-3945.
- Lajoie P, Nabi IR. Lipid rafts, caveolae, and their endocytosis. *Int Rev Cell Mol Biol* 2010;**282**:135-163.
- Lanone S, Andujar P, Kermanizadeh A, Boczkowski J. Determinants of carbon nanotube toxicity. *Adv Drug Deliv Rev* 2013;**65**:2063-2069.
- Law M, Greene LE, Johnson JC, Saykally R, Yang P. Nanowire dye-sensitized solar cells. *Nat Mater* 2005;**4**:455-459.
- Lee W, Sodek J, McCulloch CA. Role of integrins in regulation of collagen phagocytosis by human fibroblasts. *J Cell Physiol* 1996;**168**:695-704.
- Leslie EM, Deeley RG, Cole SP. Multidrug resistance proteins: role of P-glycoprotein, MRP1, MRP2, and BCRP (ABCG2) in tissue defense. *Toxicol Appl Pharmacol* 2005;**204**:216-237.
- Li J, Yap SQ, Chin CF, Tian Q, Yoong SL, Pastorin G, Ang WH. Platinum(IV) prodrugs entrapped within multiwalled carbon nanotubes: Selective release by chemical reduction and hydrophobicity reversal. *Chem Sci* 2012;**3**:2083-2087.
- Li J, Pant A, Chin CF, Ang WH, Ménard-Moyon C, Nayak TR, Gibson D, Ramaprabhu S, Panczyk T, Bianco A, Pastorin G. In vivo biodistribution of platinum-based drugs encapsulated into multi-walled carbon nanotubes. *Nanomedicine* 2014;**10**:1465-1475.

- Li S, Mulloor JJ, Wang L, Ji Y, Mulloor CJ, Micic M, Orbulescu J, Leblanc RM. Strong and selective adsorption of lysozyme on graphene oxide. *ACS Appl Mater Interfaces* 2014;**6**:5704-5712.
- Li R, Wu R, Zhao L, Wu M, Yang L, Zou H. P-glycoprotein antibody functionalized carbon nanotube overcomes the multidrug resistance of human leukemia cells. *ACS Nano* 2010;**4**:1399-1408.
- Li Y, Yuan H, von dem Bussche A, Creighton M, Hurt RH, Kane AB, Gao H. Graphene microsheets enter cells through spontaneous membrane penetration at edge asperities and corner sites. *Proc Natl Acad Sci U S A* 2013;**110**:12295-12300.
- Li Y, Feng L, Shi X, Wang X, Yang Y, Yang K, Liu T, Yang G, Liu Z. Surface coating-dependent cytotoxicity and degradation of graphene derivatives: towards the design of non-toxic, degradable nano-graphene. *Small* 2014;**10**:1544-1554.
- Liang F, Chen B. A review on biomedical applications of single-walled carbon nanotubes. *Curr Med Chem* 2010;**17**:10-24.
- Lim JP and Gleeson PA. Macropinocytosis: an endocytic pathway for internalising large gulps. *Immunol Cell Biol* 2011;**89**:836-843.
- Liu J, Cui L, Losic D. Graphene and graphene oxide as new nanocarriers for drug delivery applications. *Acta Biomater* 2013;**9**:9243-9257.
- Liu X, Hurt RH, Kane AB. Biodurability of Single-Walled Carbon Nanotubes Depends on Surface Functionalization. *Carbon* 2010;**48**:1961-1969.
- Liu X, Tao H, Yang K, Zhang S, Lee ST, Liu Z. Optimization of surface chemistry on single-walled carbon nanotubes for in vivo photothermal ablation of tumors. *Biomaterials* 2011;**32**:144-151.
- Liu Z, Sun X, Nakayama-Ratchford N, Dai H. Supramolecular chemistry on water-soluble carbon nanotubes for drug loading and delivery. *ACS Nano* 2007;**1**:50-56.
- (A) Liu Z, Davis C, Cai W, He L, Chen X, Dai H. Circulation and long-term fate of functionalized, biocompatible single-walled carbon nanotubes in mice probed by Raman spectroscopy. *Proc Natl Acad Sci U S A* 2008;**105**:1410-1415.
- (B) Liu Z, Chen K, Davis C, Sherlock S, Cao Q, Chen X, Dai H. Drug delivery with carbon nanotubes for in vivo cancer treatment. *Cancer Res* 2008;**68**:6652-6660.
- (C) Liu Z, Robinson JT, Sun X, Dai H. PEGylated nanographene oxide for delivery of water-insoluble cancer drugs. *J Am Chem Soc* 2008;**130**:10876-10877.

M

- Matsuura K, Saito T, Okazaki T, Ohshima S, Yumura M, Lijima S. Selectivity of water-soluble proteins in single-walled carbon nanotube dispersions. *Chem Phys Lett* 2006;**429**:497.
- Matsumura Y, Maeda H. A new concept for macromolecular therapeutics in cancer chemotherapy: mechanism of tumoritropic accumulation of proteins and the antitumor agent smancs. *Cancer Res* 1986;**46**:6387-6392.
- McMahon HT and Boucrot E. Molecular mechanism and physiological functions of clathrin-mediated endocytosis. *Nat Rev Mol Cell Biol* 2011;**12**:517-533.
- Milardi GL, Stringaro A, Colone M, Bonincontro A, Risuleo G. The cell membrane is the main target of resveratrol as shown by interdisciplinary biomolecular/cellular and biophysical approaches. *J Membr Biol* 2014;**247**:1-8.
- Mu Q, Su G, Li L, Gilbertson BO, Yu LH, Zhang Q, Sun YP, Yan B. Size-dependent cell uptake of protein-coated graphene oxide nanosheets. *ACS Appl Mater Interfaces* 2012;**4**:2259-2266.
- Muller PA, Vousden KH. Mutant p53 in cancer: new functions and therapeutic opportunities. *Cancer Cell* 2014;**25**:304-317.

- Murphy FA, Poland CA, Duffin R, Al-Jamal KT, Ali-Boucetta H, Nunes A, Byrne F, Prina-Mello A, Volkov Y, Li S, Mather SJ, Bianco A, Prato M, Macnee W, Wallace WA, Kostarelos K, Donaldson K. Length-dependent retention of carbon nanotubes in the pleural space of mice initiates sustained inflammation and progressive fibrosis on the parietal pleura. *Am J Pathol* 2011;**178**:2587-2600.
- Murphy FA, Schinwald A, Poland CA, Donaldson K. The mechanism of pleural inflammation by long carbon nanotubes: interaction of long fibres with macrophages stimulates them to amplify pro-inflammatory responses in mesothelial cells. *Part Fibre Toxicol* 2012;**9**:8.

N

- Nel A, Xia T, Mädler L, Li N. Toxic potential of materials at the nanolevel. *Science* 2006;**311**:622-627.
- Nepal D and Geckeler KE. pH-sensitive dispersion and debundling of single-walled carbon nanotubes: lysozyme as a tool. *Small* 2006;**2**:406-412.
- Nolan A, Weiden M, Kelly A, Hoshino Y, Hoshino S, Mehta N, Gold JA. CD40 and CD80/86 act synergistically to regulate inflammation and mortality in polymicrobial sepsis. *Am J Respir Crit Care Med* 2008;**177**:301-308.
- Novoselov KS, Geim AK, Morozov SV, Jiang D, Zhang Y, Dubonos SV, Grigorieva IV, Firsov AA. Electric field effect in atomically thin carbon films. *Science* 2004;**306**:666-669.
- Nunes A, Bussy C, Gherardini L, Meneghetti M, Herrero MA, Bianco A et al. In vivo degradation of functionalized carbon nanotubes after stereotactic administration in the brain cortex. *Nanomedicine (Lond)* 2012;**7**:1485-1494.

O

- Oberoi HS, Nukolova NV, Kabanov AV, Bronich TK. Nanocarriers for delivery of platinum anticancer drugs. *Adv Drug Deliv Rev* 2013**;65**:1667-1685.
- Ong LC, Chung FF, Tan YF, Leong CO. Toxicity of single-walled carbon nanotubes. DOI 10.1007/s00204-014-1376-6.
- Orecchioni M, Bedognetti D, Sgarrella F, Marincola FM, Bianco A1, Delogu LG. Impact of carbon nanotubes and graphene on immune cells. *J Transl Med* 2014;**12**:138.

P

- Pantarotto D, Partidos CD, Hoebeke J, Brown F, Kramer E, Briand JP, Muller S, Prato M, Bianco A. Immunization with peptide-functionalized carbon nanotubes enhances virus-specific neutralizing antibody responses. *Chem Biol* 2003;**10**:961-966.
- (A) Pantarotto D, Briand JP, Prato M, Bianco A. Translocation of bioactive peptides across cell membranes by carbon nanotubes. *Chem Commun* 2004:16-17.
- (B) Pantarotto D, Singh R, McCarthy D, Erhardt M, Briand JP, Prato M, Kostarelos K, Bianco A. Functionalized carbon nanotubes for plasmid DNA gene delivery. *Angew Chem Int Ed Engl* 2004;**43**:5242-5246.
- Park EJ, Zahari NE, Kang MS, Lee Sj, Lee K, Lee BS, Yoon C, Cho MH, Kim Y, Kim JH. Toxic response of HIPCO single-walled carbon nanotubes in mice and RAW264.7 macrophage cells. *Toxicol Lett* 2014;**229**:167-177.
- Patel NR, Pattni BS, Abouzeid AH, Torchilin VP. Nanopreparations to overcome multidrug resistance in cancer. *Adv Drug Deliv Rev* 2013;**65**:1748-1762.

- Peer D, Karp JM, Hong S, Farokhzad OC, Margalit R, Langer R. Nanocarriers as an emerging platform for cancer therapy. *Nat Nanotechnol* 2007;**2**:751-760.
- Peng C, Hu W, Zhou Y, Fan C, Huang Q. Intracellular imaging with a graphene-based fluorescent probe. *Small* 2010;**6**:1686-1692.
- Persidis A. Cancer multidrug resistance. *Nat Biotechnol* 1999;**17**:94-95.
- Pescatori M, Bedognetti D, Venturelli E, Ménard-Moyon C, Bernardini C, Muresu E, Piana A, Maida G, Manetti R, Sgarrella F, Bianco A, Delogu LG. Functionalized carbon nanotubes as immunomodulator systems. *Biomaterials* 2013;**34**:4395-4403.
- Piovesan S, Cox PA, Smith JR, Fatouros DG, Roldo M. Novel biocompatible chitosan decorated single-walled carbon nanotubes (SWNTs) for biomedical applications: theoretical and experimental investigations. *Phys Chem Chem Phys* 2010;**12**:15636-15643.
- Poland CA, Duffin R, Kinloch I, Maynard A, Wallace WA, Seaton A, Stone V, Brown S, Macnee W, Donaldson K. Carbon nanotubes introduced into the abdominal cavity of mice show asbestos-like pathogenicity in a pilot study. *Nat Nanotechnol* 2008;**3**:423-428.
- Prato M, Kostarelos K, Bianco A. Functionalized carbon nanotubes in drug design and discovery. *Acc Chem Res* 2008;**41**:60-68.

Q

- Qian BZ, Pollard JW. Macrophage diversity enhances tumor progression and metastasis. *Cell* 2010;**141**:39-51.
- Qu C, Wang L, He J, Tan J, Liu W, Zhang S, Zhang C, Wang Z, Jiao S, Liu S, Jiang G. Carbon nanotubes provoke inflammation by inducing the pro-inflammatory genes IL-1β and IL-6. *Gene* 2012;**493**:9-12.

R

- Rabik CA and Dolan ME. Molecular mechanisms of resistance and toxicity associated with platinating agents. *Cancer Treat Rev* 2007;**33**:9-23.
- Raffa V, Ciofani G, Vittorio O, Riggio C, Cuschieri A. Physicochemical properties affecting cellular uptake of carbon nanotubes. *Nanomedicine (Lond).* 2010;**5**:89-97.
- Rebucci M and Michiels C. Molecular aspects of cancer cell resistance to chemotherapy. *Biochem Pharmacol* 2013;**85**:1219-1226.
- Rice NA, Soper K, Zhou N, Merschrod E, Zhao Y. Dispersing as-prepared single-walled carbon nanotube powders with linear conjugated polymers. *Chem Commun* 2006;**21**:4937-4939.
- Ries CH, Cannarile MA, Hoves S, Benz J, Wartha K et al. Targeting tumor-associated macrophages with anti-CSF-1R antibody reveals a strategy for cancer therapy. *Cancer Cell* 2014;**25**:846-859.
- Ruiz-Garcia A, Bermejo M, Moss A, Casabo VG. Pharmacokinetics in drug discovery. *J Pharm Sci* 2008;**97**:654-690.
- Ruggiero A, Villa CH, Bander E, Rey DA, Bergkvist M, Batt CA et al. Paradoxical glomerular filtration of carbon nanotubes. *Proc Natl Acad Sci U S A* 2010;**107**:12369-12374.
- Russier J, Ménard-Moyon C, Venturelli E, Gravel E, Marcolongo G, Meneghetti M, Doris E, Bianco A. Oxidative biodegradation of single- and multi-walled carbon nanotubes. *Nanoscale* 2011;**3**:893-896.
- Russier J, Treossi E, Scarsi A, Perrozzi F, Dumortier H, Ottaviano L, Meneghetti M, Palermo V, Bianco A. Evidencing the mask effect of graphene oxide: a comparative study on primary human and murine phagocytic cells. *Nanoscale* 2013;**5**:11234-11247.

S

- Sasidharan A, Panchakarla LS, Chandran P, Menon D, Nair S, Rao CN, Koyakutty M. Differential nano-bio interactions and toxicity effects of pristine versus functionalized graphene. *Nanoscale* 2011;**3**:2461-2464.
- Sayes CM, Liang F, Hudson JL, Mendez J, Guo W, Beach JM, Moore VC, Doyle CD, West JL, Billups WE, Ausman KD, Colvin VL. Functionalization density dependence of single-walled carbon nanotubes cytotoxicity in vitro. *Toxicol Lett* 2006;**161**:135-142.
- Schinwald A, Murphy FA, Jones A, MacNee W, Donaldson K. Graphene-based nanoplatelets: a new risk to the respiratory system as a consequence of their unusual aerodynamic properties. *ACS Nano* 2012;**6**:736-746.
- Shah S, Yin PT, Uehara TM, Chueng ST, Yang L, Lee KB. Guiding stem cell differentiation into oligodendrocytes using graphene-nanofiber hybrid scaffolds. *Adv Mater* 2014;**26**:3673-3680.
- Shang J, Ma L, Li J, Ai W, Yu T, Gurzadyan GG. The origin of fluorescence from graphene oxide. *Sci Rep* 2012;**2**:792.
- Shen H, Zhang L, Liu M, Zhan Z. Biomedical Applications of Graphene. *Theranostics* 2012;**2**:283-294.
- Shi S, Chen F, Ehlerding EB, Cai W. Surface engineering of graphene-based nanomaterials for biomedical applications. *Bioconjug Chem* 2014;**25**:1609-1619.
- Shi Y, Liu SA, Kerwood DJ, Goodisman J, Dabrowiak JC. Pt(IV) complexes as prodrugs for cisplatin. *J Inorg Biochem* 2012**;107**:6-14.
- Shim M, Wong N, Kam S, Chen RJ, Li Y, Dai H. Functionalization of Carbon Nanotubes for Biocompatibility and Biomolecular Recognition. *Nano Lett* 2002;**2**:285-288.
- Shvedova AA, Kapralov AA, Feng WH, Kisin ER, Murray A et al. Impaired clearance and enhanced pulmonary inflammatory/fibrotic response to carbon nanotubes in myeloperoxidase-deficient mice. *PLoS One* 2012;**7**:e30923.
- Sica A and Mantovani A. Macrophage plasticity and polarization: in vivo veritas. *J Clin Invest* 2012;**122**:787-795.
- Siddik ZH. Cisplatin: mode of cytotoxic action and molecular basis of resistance. *Oncogene* 2003;**22**:7265-7279.
- Singh R, Torti SV. Carbon nanotubes in hyperthermia therapy. *Adv Drug Deliv Rev* 2013;**65**:2045-2060.
- Siu KS, Chen D1, Zheng X, Zhang X, Johnston N, Liu Y, Yuan K, Koropatnick J, Gillies ER, Min WP. Non-covalently functionalized single-walled carbon nanotube for topical siRNA delivery into melanoma. *Biomaterials* 2014;**35**:3435-3442.
- Sobhani Z, Dinarvand R, Atyabi F, Ghahremani M, Adeli M. Increased paclitaxel cytotoxicity against cancer cell lines using a novel functionalized carbon nanotube. *Int J Nanomedicine* 2011;**6**:705-719.
- Sozer N, Kokini JL. Nanotechnology and its applications in the food sector. *Trends Biotechnol* 2009;**27**:82-89.
- Spinato C, Ménard-Moyon C, Bianco A. Chemical Functionalization of Graphene for Biomedical Applications. *Functionalization of graphene* 2014, *Wiley-VHC, Weinnheim;***4**:95-139.
- Spyrou K and Rudolf P. An introduction to Graphene. *Functionalization of graphene* 2014 *Wiley-VHC, Weinnheim;***4**:95-139.
- Stefanutti E, Papacci F, Sennato S, Bombelli C, Viola I, Bonincontro A, Bordi F, Mancini G, Gigli G, Risuleo G. Cationic liposomes formulated with DMPC and a gemini surfactant traverse the cell membrane without causing a significant bio-damage. *Biochim Biophys Acta* 2014;**1838**:2646-2655.

- Sugiyama S, Okada Y, Sukhova GK, Virmani R, Heinecke JW, Libby P. Macrophage myeloperoxidase regulation by granulocyte macrophage colony-stimulating factor in human atherosclerosis and implications in acute coronary syndromes. *Am J Pathol* 2001;**158**:879-891.
- Sun X, Liu Z, Welsher K, Robinson JT, Goodwin A, Zaric S, Dai H. Nano-Graphene Oxide for Cellular Imaging and Drug Delivery. *Nano Res* 2008;**1**:203-212.

T

- Tan DS, Gerlinger M, Teh BT, Swanton C. Anti-cancer drug resistance: understanding the mechanisms through the use of integrative genomics and functional RNA interference. *Eur J Cancer* 2010;**46**:2166-2177.
- Taniguchi N. On the Basic Concept of Nano-Technology. *Proc Intl Conf Prod Eng Tokyo, Part II, Japan Society of Precision Engineering* 1974.
- Tardani F and Sennato S. Phase Behavior of DNA-Stabilized Carbon Nanotubes Dispersions: Association with Oppositely-Charged Additives. *J Phys Chem C* 2014;**118**:9268–9274.
- Thiebaut F, Tsuruo T, Hamada H, Gottesman MM, Pastan I, Willingham MC. Cellular localization of the multidrug-resistance gene product P-glycoprotein in normal human tissues. *Proc Natl Acad Sci U S A* 1987;**84**:7735-7738.
- Townsend MJ, Monroe JG, Chan AC. B-cell targeted therapies in human autoimmune diseases: an updated perspective. *Immunol Rev* 2010;**237**:264-283.

V

- Vashist SK, Zheng D, Pastorin G, Al-Rubeaan K, Luong JHT, Sheu F-S. Delivery of drugs and biomolecules using carbon nanotubes. *Carbon* 2011;**49**:4077–4097.
- Vettiger P, Cross G, Despont M, Drechsler U, Durig U, Gotsmann B, et al. The ‘millipede’ - nanotechnology entering data storage. *IEEE Trans Nanotechnol* 2002;**1**:39-55.
- Vieira AV, Lamaze C, Schmid SL. Control of EGF receptor signaling by clathrin-mediated endocytosis. *Science* 1996;**274**:2086-2089.
- Vlasova II, Sokolov AV, Chekanov AV, Kostevich VA, Vasil'ev VB. Myeloperoxidase-induced biodegradation of single-walled carbon nanotubes is mediated by hypochlorite. *Bioorg Khim* 2011;**37**:510-521.

W

- Wang B, He X, Zhang Z, Zhao Y, Feng W. Metabolism of nanomaterials in vivo: blood circulation and organ clearance. *Acc Chem Res* 2013;**46**:761-769.
- Wang D and Lippard SJ. Cellular processing of platinum anticancer drugs. *Nat Rev Drug Discov* 2005;**4**:307-320.
- Wang H, Wang J, Deng X, Sun H, Shi Z, Gu Z, Liu Y, Zhao Y. Biodistribution of carbon single-wall carbon nanotubes in mice. *J Nanosci Nanotechnol. 2004*;**4**(8):1019-24.
- Wang K, Ruan J, Song H, Zhang J, Wo, Y, Guo S. Biocompatibility of Graphene Oxide. *Nanoscale Res Lett* 2011;**6**:8.
- Wang Y, Li Z, Wang J, Li J, Lin Y. Graphene and graphene oxide: biofunctionalization and applications in biotechnology. *Trends Biotechnol* 2011;**29**:205-212.
- Wang P, Nie X, Wang Y, Li Y, Ge C, Zhang L, Wang L, Bai R, Chen Z, Zhao Y, Chen C. Multiwall carbon nanotubes mediate macrophage activation and promote pulmonary fibrosis through TGF-β/Smad signaling pathway. *Small* 2013;**9**:3799-3811.

- Wang X and Guo Z. Targeting and delivery of platinum-based anticancer drugs. *Chem Soc Rev* 2013;**42**:202-224.
- Widakowich C, de Castro G Jr, de Azambuja E, Dinh P, Awada A. Review: side effects of approved molecular targeted therapies in solid cancers. *Oncologist. 2007*;**12**(12):1443-55.
- Wynn TA, Chawla A, Pollard JW. Macrophage biology in development, homeostasis and disease. *Nature* 2013;**496**:445-455.

Y

- Yanaba K, Bouaziz JD, Matsushita T, Magro CM, St Clair EW, Tedder TF. B-lymphocyte contributions to human autoimmune disease. *Immunol Rev* 2008;**223**:284-299.
- Yang S, Guo W, Lin Y, Deng X, Wang H, Sun H et al. Biodistribution of Pristine Single-Walled Carbon Nanotubes In Vivo. *J Phys Chem C* 2007;**111**:17761–17764.
- Yang K, Zhang S, Zhang G, Sun X, Lee ST, Liu Z. Graphene in mice: ultrahigh in vivo tumor uptake and efficient photothermal therapy. *Nano Lett* 2010;**10**:3318-3323.
- Yang K, Wan J, Zhang S, Zhang Y, Lee ST, Liu Z. In vivo pharmacokinetics, long-term biodistribution, and toxicology of PEGylated graphene in mice. *ACS Nano* 2011;**5**:516-22.
- Yang K, Gong H, Shi X, Wan J, Zhang Y, Liu Z. In vivo biodistribution and toxicology of functionalized nano-graphene oxide in mice after oral and intraperitoneal administration. *Biomaterials* 2013;**34**:2787-2795.
- Yaron PN, Holt BD, Short PA, Lösche M, Islam MF, Dahl KD. Single wall carbon nanotubes enter cells by endocytosis and not membrane penetration. *Journal of Nanobiotechnology* 2011;**9**:45.
- Yue H, Wei W, Yue Z, Wang B, Luo N, Gao Y, Ma D, Ma G, Su Z. The role of the lateral dimension of graphene oxide in the regulation of cellular responses. *Biomaterials* 2012;**33**:4013-4021.

Z

- Zhang L, Xia J, Zhao Q, Liu L, Zhang Z. Functional graphene oxide as a nanocarrier for controlled loading and targeted delivery of mixed anticancer drugs. *Small* 2010;**6**:537-544.
- Zhang L, Chen H, Wang L, Liu T, Yeh J, Lu G, Yang L, Mao H. Delivery of therapeutic radioisotopes using nanoparticle platforms: potential benefit in systemic radiation therapy. *Nanotechnol Sci Appl* 2010;**3**:159-170.
- Zhang Y, Ali SF, Dervishi E, Xu Y, Li Z, Casciano D, Biris AS. Cytotoxicity effects of graphene and single-wall carbon nanotubes in neural phaeochromocytoma-derived PC12 cells. *ACS Nano* 2010;**4**:3181-3186.
- Zhang X, Goncalves R, Mosser DM. The Isolation and Characterization of Murine Macrophages. *Curr Protoc Immunol* 2008;Unit–14.1.
- Zhang X, Yin J, Peng C, Hu W, Li W, Fan C, Huang Q. Distribution and biocompatibility studies of graphene oxide in mice after intravenous administration. *Carbon* 2011;**49**:986–995.
- Zheng M, Jagota A, Semke ED, Diner BA, McLean RS, Lustig SR, Richardson RE, Tassi NG. DNA-assisted dispersion and separation of carbon nanotubes. *Nat Mater* 2003;**2**:338-342.
- Ziegler U, Groscurth P. Morphological features of cell death. *News Physiol Sci* 2004;**19**:124-128.

Publications

- Muzi L, Ménard-Moyon C, Russier J, Li J, Chin CF, Ang WH, Pastorin G, Risuleo G, Bianco A. The diameter of functionalized multi-walled carbon nanotubes filled with a cisplatin prodrug allows to control the release of the drug prolonging its anticancer efficacy. *Nanoscale*, submitted.

- Barbetta A, La Mesa C, Muzi L, Pucci C, Risuleo G, Tardani F. Cat-anionic vesicle-based systems as potential carriers in nano-technologies. *Nanobiotechnology* 2014, *W. Ahmed Ed, UK*;**7**:152-179.

Communications and National/International congress participation:

- *GDRI Graphene and Nanotubes Annual meeting 2014*
  Oral communication:
  Laura Muzi, Cécilia Ménard-Moyon, Julie Russier, Jian Li, Chee Fei Chin, Wee Han Ang, Giorgia Pastorin, Gianfranco Risuleo, Alberto Bianco.
  "A comparative study on the anticancer efficacy of two types of multi-walled carbon nanotubes filled with a cisplatin prodrug"
  21st-25th September 2014, Centre Culturel Saint Thomas, Strasbourg, France

- *MiniSymposium:* "Graphene: chemistry meets physics and biology"
  18th November 2013, Université de Strasbourg, France

- *International Workshop:* "Low-dimensional carbon nanostructures: graphene and nanotubes"
  18th March 2013, Accademia Nazionale dei Lincei, Roma, Italy

- *FISV National Congress*
  24th-27th September 2012, Sapienza Università di Roma, Italy